Analysis of Peroxynitrite-mediated Post-translational Modifications of Caveolin-1

By

Hemamali Jayampathi Warshakoon
B.Sc., University of Peradeniya, 1998

Submitted to the Department of Chemistry and the
Faculty of the Graduate School of the University of Kansas
in partial fulfillment of the requirements for the Degree of
Master of Science

_____
Chairperson

Committee members _____

_____

Date defended: October 10, 2005

The Thesis Committee for Hemamali Jayampathi Warshakoon certifies that this is the approved version of the following thesis:

Analysis of Peroxynitrite-mediated Post-translational Modifications of Caveolin-1

Committee:

_____

Chairperson

_____

_____

Date approved: October 10, 2005

Acknowledgements

First, I would like to convey my appreciation to my academic advisor, Dr. George S. Wilson for his support and guidance given to me throughout my graduate career. I give my sincere thanks to Dr. Christian Schöeneich, the co-advisor of my research project, for his invaluable guidance and support throughout this research. I also would like to express my thanks to the Wilson and Schoeneich group members for their cooperation and valuable input on my research.

My thanks to Dr. Rick Dobrowsky for providing me GST-caveolin gene construct. Thanks to Dr. Gerald Lushington for his assistance in simulating the structure of caveolin-1. I would like to express my appreciation and thanks to Dr. Heather Desaire for her input in developing my graduate career.

During my studies at the University of Kansas, I had the privilege of working with some fellow graduate students such as Dilusha Dalpathado, Luka Kapkiai, and Geetha Hewawasam who inspired me in many ways to keep trying when things didn't seem to work as expected. I thank you and I will always remember that you played a part in my life. I give sincere thanks and appreciation to Sue and Wayne Spellman for making Lawrence my second home through their continuous support.

I am greatly indebted to my mother, Mallika Madawala, for her sacrifices and hard work to provide me a good education. My sincere thanks to my brother, Namal, and sisters, Darshini and Deepika for their continuous love, encouragement and moral support that have made me who I am. My love and thanks to my precious little son Kevin for inspiring me to take on the future.

Abstract

Caveolin-1 is an important protein in caveolae, which plays a role in cholesterol transport, signal transduction, and transcytosis and tumor suppression. Caveolin-1 is found in endothelial cells, smooth muscle cells and adipocytes. The main focus of this study is to investigate the peroxynitrite-mediated *in vitro* post-translational modifications (PTMs) of caveolin-1.

Bovine brain was used to isolate caveolin-1 as an initial step for isolation method development. Density gradient centrifugation was used to isolate caveolin-1 from bovine brain. From the isolate, caveolin-1α**,** caveolin-1β isomers and caveolin dimer were identified by western blotting with anti-caveolin monoclonal antibody. Glutathione S-transferase (GST)-caveolin fusion protein was used to isolate caveolin-1 and used for *in vitro* experiments in this study.

During normal and pathological conditions, endothelial cells are subjected to locally generated reactive oxygen species such as peroxynitrite. Peroxynitrite is capable of modifying amino acids such as tyrosine, cysteine, tryptophan and methionine.

Peroxynitrite mediated tyrosine nitration of caveolin-1 was detected by SDS-PAGE followed by western blotting with anti-nitrotyrosine monoclonal antibody. The approach used to identify potentially modified peptide sequences of caveolin-1 was ESI-MS/MS. Fluorometry was used to detect formation of dityrosine.

Caveolin-1 was treated with different concentrations of peroxynitrite in caveolin- under the physiological conditions and found that caveolin-1 form dimer and oligomer under the physiological conditions. The stability of caveolin-1 dimer and oligomer suggests that the coupling mechanism could most likely be occurred via a covalent bond. Western blotting with anti-nitrotyrosine monoclonal antibody revealed the formation of nitrotyrosine upon the exposure to peroxynitrite.

In this study, we report the nitration of specific tyrosine residues of caveolin-1 for the first time. ESI-MS/MS analysis revealed that peroxynitrite can selectively nitrate Tyr^{6} and Tyr^{14} located in the tryptic peptide YVDSEGHLYTVPIR under physiological conditions. Caveolin-1 can form dityrosine upon exposure to peroxynitrite as shown by fluorometry. Oxidative and nitrative modifications due to the reaction of peroxynitrite with caveolin-1 may lead to several pathological conditions. Our study can provide authentic standards of modified proteins, which will be used to determine post-translational modifications of caveolin-1 *in vivo*.

Table of contents

Figures and tables

Tables

1. Introduction

1.a Caveolin and important characteristics of caveolin

Caveolae are flask shaped 50-100nm diameter cell membrane invaginations, which are abundant in endothelial cells, adipocytes, smooth muscle cells and fibroblasts. Caveolin is a major integral membrane component of caveolae *in vivo*. Caveolae are enriched in glycosylphospatidylinositol-anchored proteins, cholesterol and glycosphingolipids.[1,2] Caveolae are involved in several important functions including potocytosis, transcytosis and signal transduction.[1,2,3]

Caveolin was first identified as a major v-Src substrate that undergoes tyrosine phosphorylation in Rous sarcoma virus-transformed cells.[4,5] Caveolin is a 21-24kDa protein, consists of the sequence of 178 amino acids (figure 1a), where both the amino- and carboxyl- terminal domains remain entirely cytoplasmic[4] (figure1b). It is therefore accessible for cytoplasmic protein-protein interactions etc.[5] Caveolin has been re-named as caveolin-1 with the discovery of two other caveolins, caveolin-2 and caveolin-3.[5,6] Human caveolin-1 is 38% identical with and 58% similar to human caveolin-2. Caveolin-3 is 65% identical with and 85% similar to caveolin-1.[7] Caveolin-1 is expressed as caveolin-1α and caveolin-1β isoforms. The two isoforms have cytosolic N-terminal and C-terminal, and hydrophobic transmembrane domains whereas the N-terminal 31 amino acids are not found in caveolin-1β. The functional differences of these two isoforms are unknown.[8]

```
MSGGKYVDSE GHLYTVPIRE QGNIYKPNNK AMAEEMSEKQ
VYDAHTKEID LVNRDPKHLN DDVVKIDFED VIAEPEGTHS
FDGIWKASFT TFTVTKYWFY RLLSALFGIP MALIWGIYFA
ILSFLHIWAV VPCIKSFLIE IQCISRVYSI YVHTFCDPFF
EAVGKIFSNI RINMQKET
```

Figure 1a. Amino acid sequence of caveolin-1

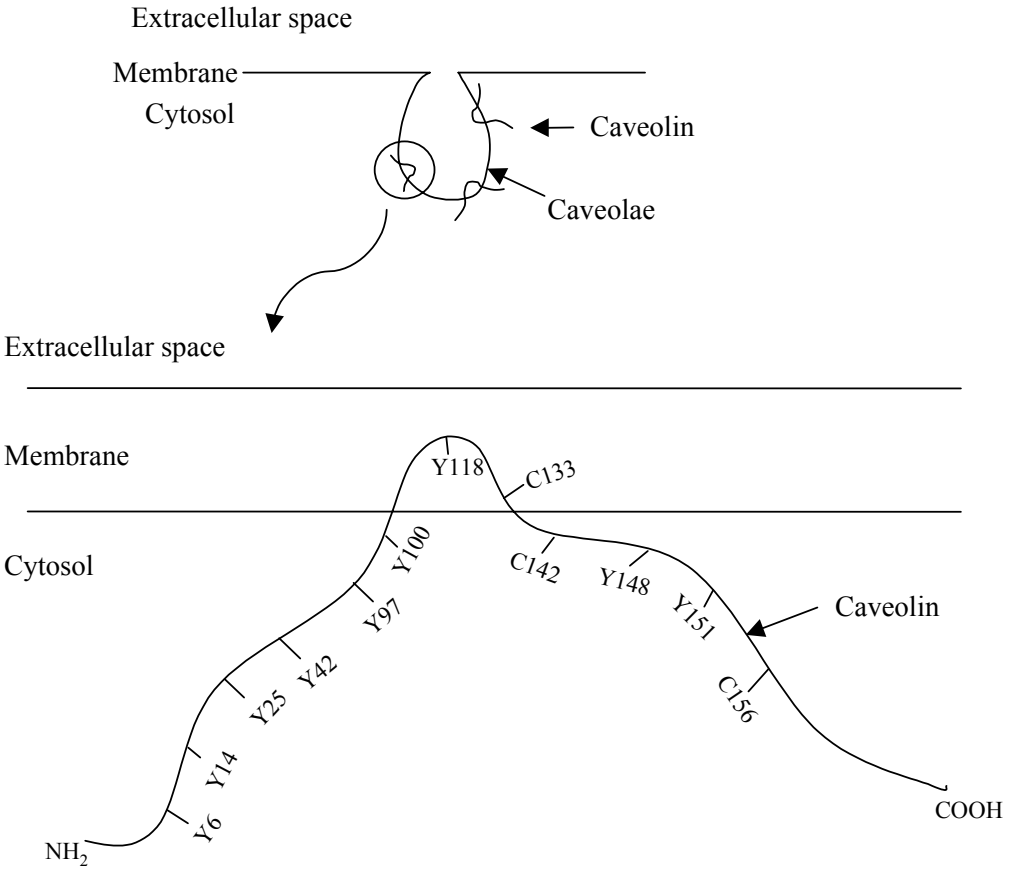

Figure 1b- Schematic representation of caveolin-1. Caveolin-1 is the principal component of caveolae. Both the N-terminal and C-terminal domains of caveolin-1 remain entirely cytoplasmic.

Caveolin-1 forms high molecular mass homo-oligomers of ~350kDa that have the capacity to interact with cholesterol and glycosphingolipids.[9,10] Li et al reported that recombinant overexpression of caveolin in caveolin-negative Sf21 insect cells is sufficient to drive the formation of caveolae sized vesicles.[11] Thus, it appears that the caveolin protein has the capability of interacting within itself and other proteins and can serve to orchestrate caveolae formation.

Caveolin co-purifies with a variety of signaling molecules, including G-proteins, Src-like kinases, H-Ras, epidermal growth factor receptor (EGF-R) and endothelial nitric oxide synthase (eNOS).[12,13] The caveolae signaling hypothesis states that caveolar localization of certain signaling molecules could provide a compartmental basis for their actions and explain cross talk between certain transmembrane signaling events.[14] Caveolin structurally and functionally interacts with wild-type C-terminal Src kinase. It interacts with G-protein α subunits and down-regulates their GTPase activity. Caveolin binds to wild-type H-Ras and it may be involved in other potential protein-protein interactions.[13,15]

Caveolae and rafts are plasma membrane subcompartments, which are enriched in cholesterol and glycosphingolipids. Due to the oligomerization of inserted caveolin molecules, caveolae are flask-shaped membrane invaginations of 50-100nm.[7,16] Rafts are flat membrane subdomains enriched in glycosyl phosphatidylinositol (GPI)-linked proteins.[7,9,16] Signaling molecules including endothelial nitric oxide synthase, GPI-linked proteins, and G-protein coupled receptors are segregated into caveolae microdomains after activation.[9] Caveolin-

1 actively contributes to the organization of cholesterol within caveolae. The association of cholesterol with caveolin and high cholesterol concentration in caveolae reflect that caveolin contributes to the influx and efflux of cellular cholesterol.[7] Fielding and Fielding assessed the relationship of cellular cholesterol efflux and caveolin using a series of pulse-chase experiments, which suggested that caveolin-1 is a major component of the cholesterol transport machinery.[17] Cholesterol trafficking between endoplasmic reticulum (ER) and caveolae is shown in figure 2. Recent reports on the function of caveolin-1 in the transport and storage of free fatty acids in lipid droplets, indicates caveolin as a major factor in hyperlipidemia and obesity. Caveolin-1 appears to be part of an intracellular lipid transport system capable of moving sterols between the ER and caveolae. Deficiency in caveolin-1 imparts resistance to diet induced obesity.[2,18]

Caveolae appear to mediate the selective uptake and transport of several molecules via transcytosis, endocytosis and protocytosis. In transcytosis, caveolae transport proteins from the luminal side of the endothelial cell to the interstitial compartment for subsequent uptake by underlying tissues. In caveolae-mediated endocytosis, caveolae bud off from the plasma membrane and fuse with various intracellular compartments through caveolae-caveosome-ER pathways. In protocytosis, caveolae mediate the uptake of small solutes less than 1kDa.[17] The underlying mechanism of invagination, budding, and vesicle trafficking differs significantly from the coated pit pathway. [2,19]

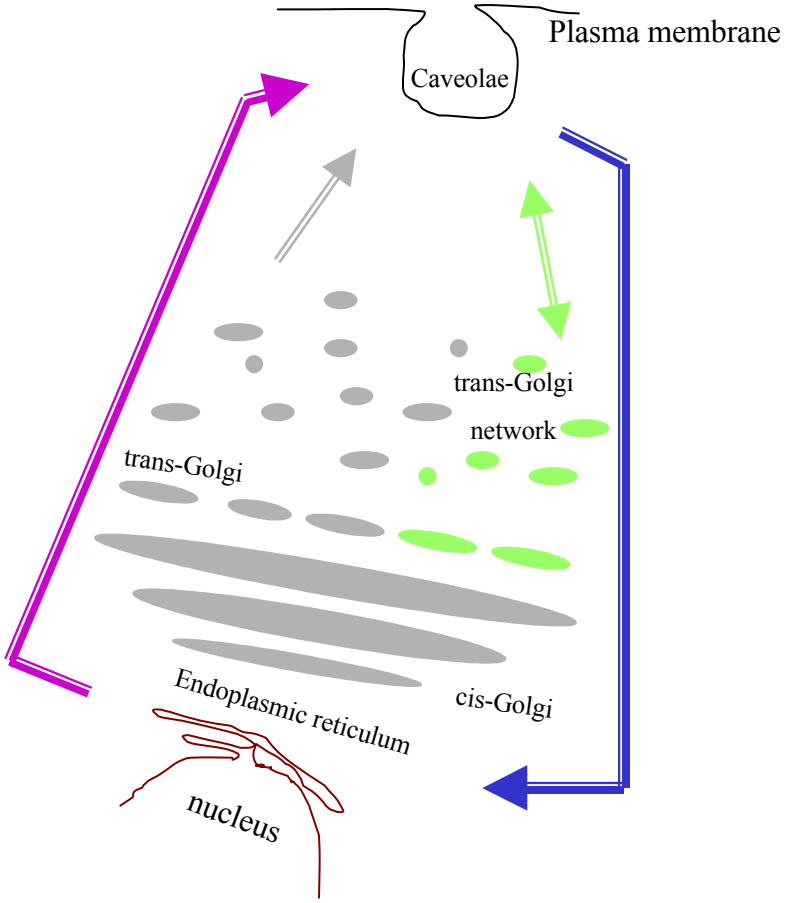

Figure 2. Trafficking of cholesterol between endoplasmic reticulum and caveolae. Different colors are used to show various routes caveolin-1 takes for cholesterol trafficking.Green arrow and vesicles-The cycling of caveolin-1 between the trans golgi and caveolae membranes. Grey color- the insertion of caveolin into the ER membrane, traffic through the ER, the Golgi complex, trans-Golgi network, and residence in caveolae vesicles.[9, 14] Purple arrow-caveolin-1 in complex with chaperone proteins in delivering newly synthesized cholesterol from the ER to caveolae.[7,9, 14] Blue arrow- translocation of caveolin-1 from caveolae membranes to the lumen of the ER in cells depleted of cholesterol

Caveolae are sites of calcium storage and entry. IP3 receptor and Ca^{2+} ATPase, which are key molecular components of calcium transport, have all been localized to caveolae. Caveolin-1 has been found in a complex with Ca^{2+} ATPase. Caveolae are the preferred sites of extracelluar Ca^{2+} entry in response to the depletion of Ca^{2+} in endoplasmic reticulum (ER).[20]

Human disease

Cancer

Invaginated caveolae are substantially reduced in many types of transformed cells.[21] Caveolin-1 may be a tumor suppressor because expression of the cDNA in transformed cells reverses anchorage-independent growth in soft agar. Caveolin-1 expression is essential for signal transduction from caveolae.[21,22] It has been reported that the D7S522 locus is the most commonly deleted region in primary breast cancers. Loss of the D7S522 locus (7q31.1) is strongly associated with systemic progression and death due to prostate cancers.[23] Caveolin-1 is co-localized at the D7S522 locus and caveolin-1 represents the tumor suppressor at the D7S522 (7q31.1) locus.[23,24,25]

Nitric Oxide (NO) is endogenously produced by a family of NO synthases (NOS) which includes three different isoenzymes, the inducible isoenzyme (iNOS), endothelial (eNOS), and neuronal (nOS) isoforms.[26] NOS expression and activity is linked to a number of human pathologies and particularly cancer, as

increased levels of NOS expression have been observed in central nervous system, colon and human breast tumors.[27,28] All NOS sequences contain caveolin-binding sequence (*ϕXϕXXXXϕXXϕ,* where*ϕ* is aromatic amino acid, Trp, Phe or Tyr and X is any amino acid), which leads to inhibition of their activity in association with caveolin-1.[26] Razani's group reported that eNOS activity is up-regulated in cav-1 null animals suggesting caveolin-1 is an endogenous inhibitor of eNOS.[29] Also, they reported that caveolin-1 mediates the caveolar endocytosis of specific ligands and caveolin-1 negatively regulates the proliferation of certain cell types.[29] Caveolin-1 functions as a tumor suppressor by blocking NOS function as down regulation of caveolin-1 would be expected to promote uncontrolled NOS activity and tumor development.[27,28,29]

Atherosclerosis

The elevation of serum cholesterol levels above the normal physiological range, hypercholesteromia, is the causal factor in the development of atherosclerosis.[24] Recent research suggests that decreased NO production is due to reduced activity of eNOS in response to elevated caveolin-1 levels during the hypercholesterolaemic state.[30] Bovine aortic endothelial cells were exposed to the serum obtained from hypercholesterolaemic individuals result in the increased expression of caveolin-1 in cultured cells.[30] NO release is reduced in these cells and observed the formation of the caveolin eNOS complex. Caveolin-1 is a negative regulator of eNOS.[30,31]

Alzheimer's disease

Alzheimer's disease (AD) is a neurodegenerative disease characterized by alterations of cholesterol homeostasis in both the periphery and the central nervous system.[7,19,24] Caveolin is involved in cellular cholesterol transport. In the hippocampus, caveolin protein levels are up-regulated by two-fold, as compared to age-matched control brains.[19] Caveolin mRNA in the frontal cortex of AD brains is elevated compared to control subjects. Several recent observations connect the emerging role of caveolin and cholesterol to the generation of amyloid beta (Aβ), the amyloidogenic peptide of amyloid precursor protein (APP). Caveolin-1 has been shown to physically associate with APP, which explains that caveolin-1 may play a pivotal role in the proteolysis of APP *in vivo*.[19,25] Up-regulation of caveolin-1 expression in AD brain could increase caveolae formation and amyloidogenesis, thereby modulating the disease pathogenesis.[33]

Over the last decade it has been confirmed that caveolin proteins are involved in the modulation of signal transduction events and cholesterol transport. Aberrations of such pathways will alter normal cell function and consequently lead to the induction of abnormal physiological conditions. Current evidence suggests that the altered expression of caveolin can contribute to disease conditions such as cancer, and Alzheimer's. Therefore, it is necessary to study the post-translational modifications of caveolin, which may create several

pathological conditions. The objective of this study is to analyze the post-translational modifications of caveolin-1 under oxidative stress, which may lead to several pathologies.

In the present thesis, only the *in vitro* reactions of caveolin with selected reactive oxygen species will be investigated. However, these studies serve to define authentic standards of modified protein, which will be used to determine oxidative modifications of caveolin *in vivo*.

1.b Post-translational modifications of caveolin-1 and the approaches used to study the post-translational modifications. Effects of post-translational modifications for the function of caveolin-1.

Most biological processes are regulated by post-translational modifications of proteins. Release of a completed polypeptide chain from a ribosome is often not the last chemical step in the formation of a protein. Various covalent modifications often occur, either during or after assembly of the polypeptide chain. Most proteins undergo co- and or post-translational modifications (PTMs). Knowledge of these modifications is extremely important because they may alter physical and chemical properties such as folding, conformation stability, activity and, consequently the function of the proteins. Prediction of protein PTMs is an important research tool for large-scale biological studies. The modification itself can act as an added functional group. Oxidation of particular amino acid residues of a protein, phosphorylation and glycosylation can affect protein-protein interactions, protein half-life, targeting and signal transduction. The analysis of proteins and their post-translational modifications is particularly important for the study of heart disease, cancer, neurodegenerative diseases and diabetes.[34]

The amount of protein in a single modification state can be a very small fraction of the total amount of the protein present. Isolation of the correctly processed protein in a sufficient amount for biochemical study is the tedious

fundamental step for successful PTM analysis. Analysis of PTMs is usually done by comparison of experimental data to a known amino acid sequence. Different analytical approaches such as antibody recognition or mass spectrometric (MS) techniques are used for correct identification of the protein of interest.[34,35] Sodium dodecyl sulfate-polyacrylamide gel electrophoresis (SDS-PAGE), separates proteins on the basis of molecular weight, two-dimensional gel electrophoresis separates protein populations on the basis of charge and molecular weight. Also, chromatographic purifications are commonly used to separate proteins for further analysis of PTMs. To identify the peptide and localize its modification, different mass spectrometric (MS) techniques such as electrospray mass spectrometry (ESI-MS), matrix assisted laser desorption ionization (MALDI-MS) mass spectrometry and fourier transform ion cyclotron mass spectrometry (FTMS) are used.[35]

The objective of this research project is analysis of post-translational modifications of caveolin-1, specifically introduced through peroxynitrite ($ONOO^-$). There is evidence for cytoplasmic modifications of caveolin-1. The C-terminus of caveolin-1 undergoes palmitoylation and the N-terminus of caveolin-1 undergoes tyrosine phosphorylation. Schlegel and co-workers found that caveolin-1 was phosphorylated on serine-80 by using a mutational approach and incorporation of [^{32}P] orthophosphate followed by autoradiography.[36] In exocrine cells, S80E mutation that mimics phosphorylation results in enhanced secretion while the S80A mutation blocks exocytosis. Caveolin-1 phosphorylation on

serine residue 80 is required for endoplasmic reticulum retention and entry into the regulated secretory pathway.[36]

The role of caveolin-1 in intracellular free cholesterol homeostasis has been described. Fielding and colleagues used site-directed mutagenesis and immunofluorescence microscopy to investigate phosphorylation level of caveolin-1 in response to platelet derived growth factor (PDGF). In smooth muscle cells, mutant S80A caveolin-1 bound significantly more sterol than the wild-type protein. The caveolin-1 level in response to PDGF is inversely related to the amount of caveolin-1 associated free cholesterol.[37]

Phosphoryation of caveolin on tyrosine is likely to be an intermediate step in a signaling cascade within caveolae. The caveolin family contains 8 conserved tyrosine residues that may serve as substrates for Src kinase. Li and co-workers used caveolin-derived synthetic peptides and site-directed mutagenesis to confirm that tyrosine 14 is the only tyrosine residue that bears any resemblance to the known recognition motifs for Src family tyrosine kinases.[38] Cao and colleagues screened a 3T3-L1 adipocyte cDNA library for proteins that interact with phosphorylated caveolin-1. The interaction of full-length caveolin and C-terminal Src kinase (Csk) was determined by both anti-phosphotyrosine (p14Y) and anti-phosphocaveolin western blotting. Csk association with caveolin-1 was completely dependent on phosphorylation of caveolin-1 in yeast fusion proteins and endogenous proteins in mammalian tissue culture cells.[39]

Vainonen and co-workers identified phosphorylation of serine 36 in caveolin-1α and homologous serine-5 in caveolin-1β in human adipocytes by nanospray quadrupole time-of-flight mass spectrometry. They enriched potentially phosphorylated peptides using an IMAC procedure, as the mass spectrometric fragmentation of major molecular ions was not enough to identify phosphorylated peptides.[40]

Caveolin-1 and many caveolae resident proteins are susceptible to modification by acylation. Palmitoylation is a 16 carbon saturated fatty acid (palmitic acid) attached to the thiol group of specific cysteine residue. Caveolin-1 is palmitoylated on cysteine 133, 143 and 156 residues. Palmitoylation of caveolin-1 is required for the transport of cholesterol from the site of synthesis in the endoplasmic reticulum to caveolae.[41] Uittenbogaard and Smart investigated caveolin palmitoylation using deletion mutagenesis, western blotting with anti-phosphocaveolin monoclonal antibody.[42]

It is evident that several different approaches have been successfully used to investigate post-translational modifications, phosphorylation and palmitoylation of caveolin. These approaches include site-directed mutagenesis, western blotting, immunofluorescence, IMAC (immobilized metal affinity chromatography) and mass spectrometry.

Mass spectrometry (MS) is an important tool in characterization of post-translational modifications due to its specificity, speed and sensitivity. The exact

location of the modification within the peptide cleavage fragment can be determined from the mass change of the peptide. The electrospray ion source is capable of producing multiply charged ions from large molecules and able to analyse biological analytes such as proteins and peptides. In this research project peroxynitrite mediated post-translational modifications of caveolin-1 have been investigated using SDS-PAGE, western blotting, fluorometry and ESI-MS techniques. Using this approach, for the first time we report nitration of specific residues of caveolin-1 under oxidative stress.

2. Peroxynitrite-mediated post-translational modifications of proteins

2.a Characteristics of peroxynitrite

The role of reactive oxygen species and reactive nitrogen species in biological aging has received considerable attention during the past two decades. The formation of $ONOO^-$ by the diffusion-limited reaction of $NO^{\cdot}$ with $O_2^{\cdot -}$ is of considerable biological interest.[43] Human neutrophils, endothelial cells and macrophages produce nitric oxide ($^{\cdot}NO$) from L-arginine.[44,45] Superoxide is produced by xanthine oxidase, NADPH oxidase or a non-enzymatic monoelectron reduction of oxygen. Reaction of $^{\cdot}NO$ and $O_2^{\cdot -}$ free radicals forms peroxynitrite which is a stronger oxidant than its precursor radicals.[45] The rate constant of the nonenzymatic reaction between $^{\cdot}NO$ and $O_2^{\cdot -}$ is 4.3-19 x 10^9 $M^{-1}s^{-1}$ under physiological conditions.[44]

$ONOO^-$ is a strong oxidant capable of modifying most biological molecules including amino acids such as tyrosine, cysteine, tryptophan and methionine.[43] Peroxynitrite can directly oxidize the prosthetic group of a protein, or directly react with the peptide chain leading to conformational and functional changes.[46,47]

When protonated, peroxynitrite forms peroxynitrous acid (ONOOH).[47,48] Peroxynitrite and peroxynitrous acid can cross the barrier of cell compartmentalization to reach their target molecules. Peroxynitrite anion diffuses through anion channels while peroxynitrous acid can diffuse across membranes.

Peroxynitrite has a half-life of less than 1s in phosphate buffer at pH 7.4. It is sufficiently stable under physiological conditions to react with target molecules such as protein sulfhydryl groups. Homolysis of peroxynitrous acid yields hydroxyl ($^{\cdot}OH$) and $^{\cdot}NO_2$ radicals. ONOOH-derived $^{\cdot}OH$ is a potent oxidant (reduction potential E= 2.3V)[44], which can oxidize amino acids such as tyrosine, methionine and cysteine. Nitrogen dioxide is an oxidant (E=0.99V) as well as a nitrating radical, which can nitrate tyrosine.[44,45,49]

The pH dependence study of the peroxynitrite reaction in carbonate buffer[50] confirmed that the actual reactant species are CO_2 and $ONOO^-$. Peroxynitrite reacts in carbon dioxide (CO_2) to form the nitrosoperoxycarbonate ($O=N-OOCO_2^-$) anion.[50,51] This reaction is the predominant pathway for peroxynitrite disappearance under physiological conditions as the rate constant of this reaction is 3×10^4 M^{-1} s^{-1}. Total carbonate concentration in physiological fluids is 25mM and the physiological concentration of CO_2 is 1.3mM that is sufficient to reduce the toxic effects of peroxynitrite.[51,52] Interactions of CO_2 with peroxynitrite play a central role in regulating various physiological effects.[51,52]

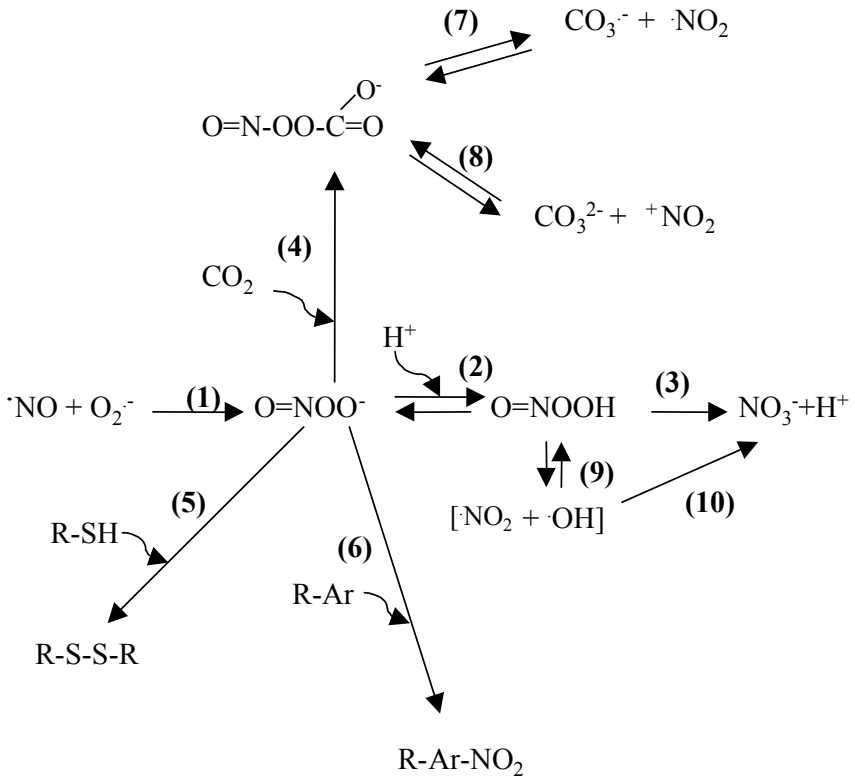

Figure 03. Reaction pathways of peroxynitrite

Reaction pathways of peroxynitrite are shown in figure 03.[49,52] Nitric oxide and superoxide form peroxynitrite (reaction 1), which is a strong oxidant. Under physiological pH (reaction 2) it rapidly protonates to peroxynitrous acid. Peroxynitrous acid can either decompose to nitrate (reaction 3) or can form $^{\cdot}NO_2$ and $OH^{\cdot}$ that can participate one-electron exchange reactions to produce corresponding oxidation products (reaction 9). Within the solvent cage, $^{\cdot}NO_2$ and $OH^{\cdot}$ radicals which do not participate in further oxidation to form nitric acid (reaction 10). In bicarbonate buffer peroxynitrite is unstable and reacts with CO_2 to produce nitrosocarbonate anion (reaction 4).[51] Peroxynitrite can directly oxidize sulfhydryl groups to disulfides (reaction 5). Peroxynitrite promotes nitration of tyrosine of proteins (reaction 6). Reaction 7 and 8 shows further reactions of nitrosocarbonate. Homolytic scission of nitrosocarbonate produces radicals $CO_3^{\cdot -}$ and $^{\cdot}NO_2$. $CO_3^{\cdot -}$ is more stable compared to $^{\cdot}OH$, and can diffuse from the site of origin and create oxidative damage. $^{\cdot}NO_2$ can abstract hydrogen from tyrosines. Heterolytic scission of nitrosocarbonate produces carbonate and NO_2^+ (reaction 8). Carbon dioxide scavenges peroxynitrite in aqueous environment preventing oxidative damage.[52]

2.b Nitration of tyrosine

In cardiovascular dysfunction, iNOS is induced in response to endotoxin (bacterial lipopolysaccharide). Induced iNOS produce large amount of $^{\cdot}NO$ which leads to the formation of reactive oxygen species or reactive nitrogen species capable of oxidizing biological molecules including protein tyrosine nitration.[53] Protein tyrosine nitration is a well-established post-translational modification occurring in diseases such as cardiovascular disease and atherosclerosis.[24,53] Figure 4 shows the mechanism nitrotyrosine formation. There is evidence that tyrosine nitrated proteins show a gain of function or less of function. It has also been shown that nitration of a tyrosine residue may prevent the subsequent phosphorylation of that residue.[54,55] Tyrosine nitration may change the rate of proteolytic degradation of nitrated proteins and favor either a faster clearance or the accumulation of nitrated proteins in cells. Cumulatively, this suggests that protein nitration may be involved in disease initiation and progression.[53,55,56]

It has been shown that nitration of tyrosine can be a fairly selective process. Tyrosine nitration could be protein specific or amino acid residue specific. All tyrosine residues of a protein are not nitrated and not all proteins are targets for nitration under physiological conditions.[57] It was previously reported that when equimolar concentrations of β-casein which contains 1.9mol% of tyrosine and phospholipase A2 which contains 7.9mol% of tyrosine were reacted under the same conditions with $ONOO^-$ in the presence of CO_2, β-casein showed

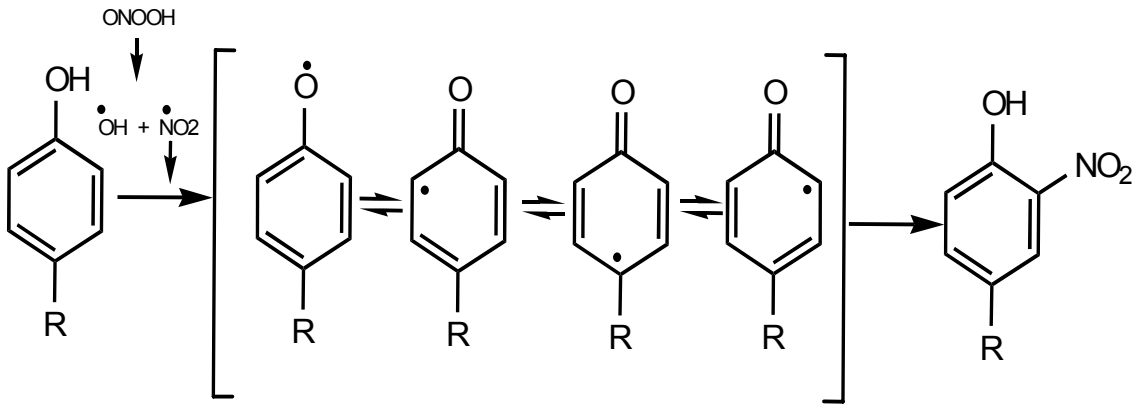

Figure 04. The mechanism of nitrotyrosine formation

nitration yield twice that of phospholipase A2.[57] This preference of tyrosine nitration could depend on sequence and structure of a given target protein and interaction with other surrounding molecules.[57,58,59] The Beckman group developed rabbit polyclonal antibody for nitrotyrosine in 1994, and reported the presence of nitrated protein in human atherosclerotic lesions. Western blotting using anti-nitrotyrosine antibodies as well as mass spectrometry techniques are used to detect nitrotyrosine at present.[60]

2.c Formation of dityrosine

Peroxynitrite reaction with tyrosine can form nitrotyrosine as well as dityrosines.[61] Dityrosine is a covalent cross-link between two proximal tyrosines (figure 5). Dityrosine cross-linking has been detected in human atherosclerotic plaques and Alzheimer diseased brains.[62,63] Dityrosine linkage can occur intramolecularly (between two tyrosine residues in the same molecule) or intermolecularly (between two molecules). Intermolecular dityrosine bridging leads to a high molecular weight product. High molecular weight oligomer formation due to dityrosine bridging in τ protein has been recently reported.[63] Dityrosine linkage is associated with insoluble and elastic properties of proteins that lead to several pathological conditions.[62,63] Dityrosine formation is detected by HPLC techniques, amino acid analysis, fluorometry and mass spectrometry.[63]

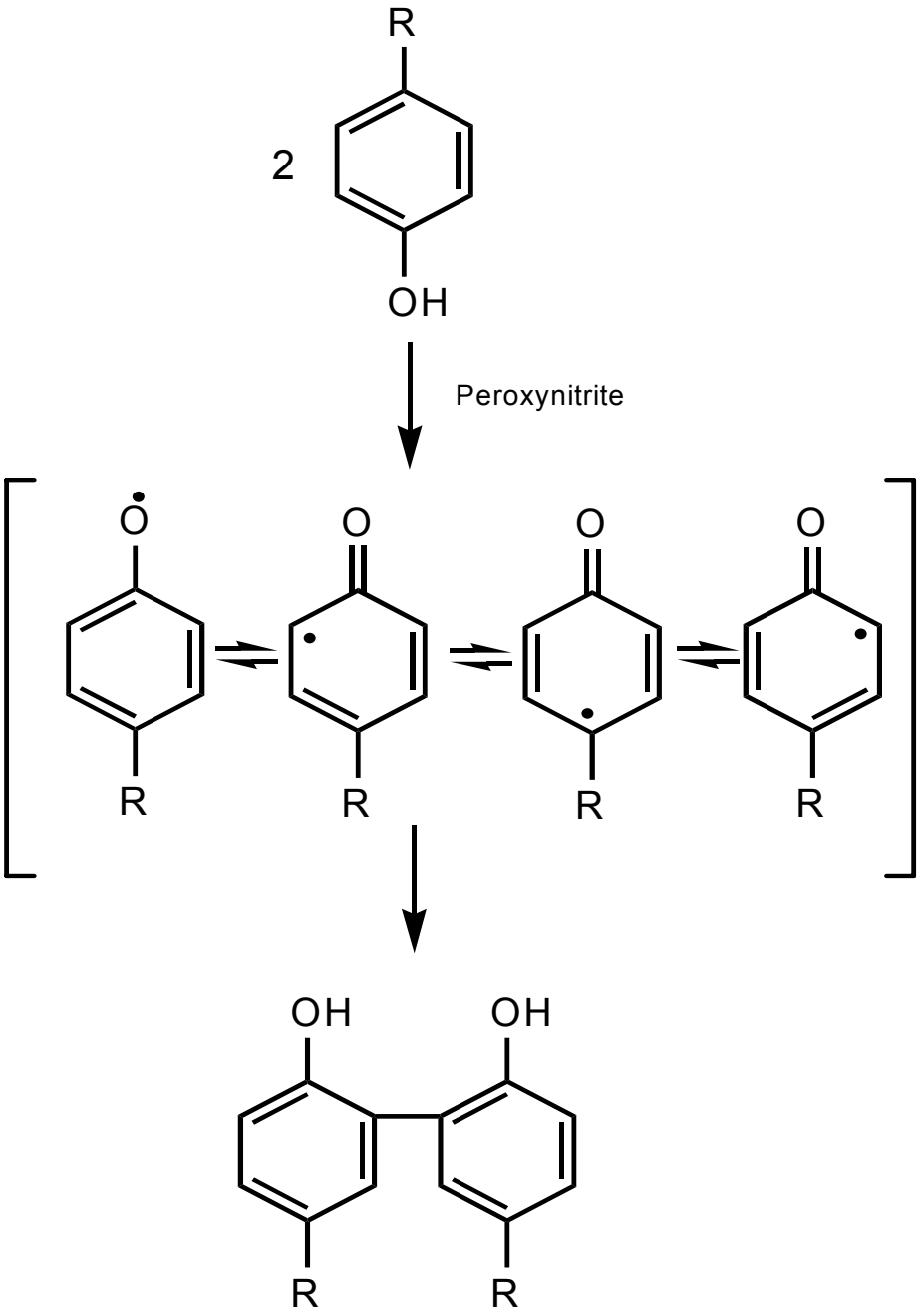

Figure 05. Formation of dityrosine

2.d Methionine oxidation

Oxidation of methionine residues or proteins by reactive oxygen species such as peroxynitrite generates methionine sulfoxide by the addition of an extra oxygen atom. Methionine oxidation can alter protein conformation and cause loss of biological activity.[64,65] In some cases, the presence of methionine sulfoxide is reported in native proteins. There are two kinds of methionine sulfoxide reductases (Msr) present *in vivo,* which can reduce methionine sulfoxide to methionine. Met/MetO cyclic interconversion of proteins may affect enzyme regulation and signal transduction.[64] The oxidation of methionine residues is associated with several diseases such as reperfusion injury and α-crystalline degeneration.[64,65]

In the presence of a strong oxidant methionine sulfone ($MetO_2$) can be formed which is found in pathological conditions. The specific oxidation of methionine residues in proteins can alter protein function as well as stability *in vivo*.[65,66] Post-translational modifications of methionine can be determined by mass spectrometry.

2.e Cysteine oxidation

The sulfur-containing side chain of cysteine is a prime target of reactive oxygen species. Oxidation of cysteine thiol group leads to the production of disulfide, sulfinic acid, and sulfonic acid formation.[65] Formation of thiyl radicals ($RS^{\cdot}$) by oxidation of cysteine sulfhydryl groups was shown recently by electron spin resonance (ESR) experiments.[67] The most common physiological consequence of cysteine oxidation is disulfide bond formation (figure 6). *In vitro*, disulfide bond formation can be reversed by using dithiothreitol (DTT).[65] Viner and colleagues reported that aggregation and enzyme inactivation of sarcoplasmic reticulum Ca–ATPase by peroxynitrite due to non-reversible intermolecular disulfide bond formation.[68] Disulfide bond formation can be detected by antibody immunoreactivity.

Figure 06. Disulfide bond formation

3. Methodology

3.1 Introduction

A variety of techniques can be used to determine the post-translational modifications of proteins. During the past two decades, SDS-PAGE has provided the ability to separate protein products in a single gel. Protein modifications are often separated by SDS-PAGE and identified by antibody recognition. For example, nitrated proteins are identified by SDS-PAGE followed by western blotting probed with anti nitro-tyrosine antibody.[69] Visualized protein bands can be used to determine the exact site and nature of the modification by mass spectrometry. However, very small protein amounts in SDS-PAGE gel bands may result in low sequence coverage and therefore a low probability of finding the modified peptides.[35]

Mass spectrometry (MS) is an important tool for the characterization of post-translational modifications due to its attractive performance characteristics such as specificity, speed and sensitivity.[70,71] A major goal of MS in proteomics is the identification and characterization of cellular proteins from extremely precise mass measurements. The technical characteristics of mass spectrometers are such that the value being measured is the mass-to-charge ratio m/z. The location of the modification within the peptide cleavage fragment can be determined from the mass change of the tandem mass spectrum, which involves two or more stages of mass analysis. For example the nitration of a tyrosine residue yields a characteristic mass increment of 45 units.[70] Antibody recognition to identify

nitration using antinitrotyrosine antibody will detect the presence or absence of nitration only. MS has the capability of detecting which amino acid is subjected to modification and accurately measure the mass increment from the native peptide. Electrospray-Ion trap mass spectrometry was used to analyze post-translational modifications in this study.

Major impact of electrospray in mass spectrometry is the capability of analyses of a wide range of analytes of biological interest such as peptides and proteins. Electrospray generates gas-phase ions of macromolecules by spraying a solution from the tip of an electrically charged capillary.[72] Electrospray is able to produce multiply charged ions from large molecules. Obtaining multiply charged ions is advantageous because it allows the analysis of high-molecular-weight molecules using analyzers with a low nominal mass limit.[72]

The ion trap mass spectrometer is known as a highly sensitive and extremely specific mass analyzer.[73] Commercially available ion traps have powerful software control of instrument operation.[73] The ion trap mass spectrometer is capable of performing multiple stages of mass spectrometry (MS^n). The other advantage of the ion trap analyzer is its ability to trap and accumulate ions to increase the signal-to-noise ratio of a measurement.

Caveolin-1 was isolated from glutathione S-transferase (GST)-caveolin-fusion protein, and bovine brain. SDS-PAGE was used to identify the isolated caveolin-1 and it was confirmed using antibody recognition (western blotting).

Isolated caveolin-1 was further analyzed using western blotting, fluorometry and ESI-MS/ MS in this study.

3.2 Materials

Sequence-grade trypsin was from Promega (Madison, WI), dithiothreitol (DTT), bovine Serum Albumin (BSA), sodium dodecyl sulfate and urea were purchased from Sigma (St. Louis, MO). The GST caveolin fusion gene construct was provided by Dr. Rick Dobrowsky. Precast Novex Tris-glycine-SDS gels, molecular weight standard and tris-glycine running buffers were obtained from Invitrogen (Carlsbad, CA). All other chemicals of highest available grade were obtained from Fisher (Pittsburgh, PA).

3.3 SDS-PAGE

The samples were separated on precast Novex 12% gels using Tris/Glycine running and Tris/SDS sample buffers. Protein separation was conducted for 1hour at 30mA at 12^{o}C using mini-gel electrophoresis unit (Hoefer Scientific instruments). The gels were stained for proteins by Coomassie Brilliant Blue (Pierce) for 2 hours and destained in 40% Methanol and 7.5% acetic acid solution.

3.4 Western Blotting

Samples were separated on precast Novex 12% gels using Tris/Glycine running and Tris/SDS sample buffers. Protein separation was conducted for 1h at 30mA at 12^0C using mini-gel electrophoresis unit (Hoefer Scientific instruments). The gels were electroblotted (400mA, 2h at 4^oC on to a 0.45uM PVDF membrane (Millipore). The membranes were incubated 2 hours at 4^oC in 5% (v/v) dry milk in T-TBS solution (20mM Tris, 150mM NaCl and 0.05% tween 20, pH 7.5). After blocking, the membrane was rinsed by T-TBS and exposed to primary antibody solution for one hour. The anti-caveolin mouse monoclonal antibody (BD Biosciences) 1:1000 dilution in T-TBS was used to probe the western blotting. Glutathione-S transferase was probed using anti-GST rabbit polyclonal antibody (BD biosciences) 1:10,000 dilution in TBS-T. After incubation, the membrane was washed with T-TBS and subjected to horseradish peroxidase conjugated anti-mouse monoclonal secondary antibody (Pierce) diluted 1:10,000 in T-TBS for 1h at room temperature. The spots were visualized by ECL detection kit (Amersham Biosciences) and the images were captured using a Kodak-developer/fixer kit (Fisher).

3.5 In-gel tryptic digestion of the gel bands

Protein bands were excised from the gels and incubated with 200mM NH_4HCO_3/MeCN 50/50 (v/v) solution for 90 minutes. 20mM of DTT was added to each sample and the samples were incubated with 25mM-iodoacetic acid for 30 min in the dark at room temperature. The samples were dried using 100% MeCN for 10 minutes and digested using 0.5µg of trypsin at 37^{o}C overnight.

3.6 Electrospray ionization tandem mass spectrometry (ESI-MS/MS)

In-gel tryptic digests of bands 1,2, and 3 (Figure 01) 7.5µl were submitted to ESI-MS/MS analysis in a Thermo Electron LCQ Duo mass spectrometer (San Jose, CA). Separation of tryptic peptides was achieved online before MS/MS analysis on a BioBasic C-18 nanoflow column (300 Å, 10cm x 75µm tip size; New Objective; Woburn, MA) with the following chromatographic conditions: mobile phase A, 0.1% formic acid in water, mobile phase B, 0.1% formic acid in MeCN; flow rate, 0.5µl/min (after 1:20 split delivered by a Micro Tech Scientific Ultra Plus II pump. The gradient profile used to increase mobile phase B linearly to the indicated fractions began with 0 to 5 min gradient held at 15% of phase B increased to 70% within 30 minutes and continued at 70% for 10 minutes. After each run, the column was allowed to re-equilibrate to the initial conditions for 30 min. The separation was followed by MS/MS analysis. Instrumental conditions used for mass spectrometric analysis included the following: number of

microscans, 3; length of microscans, 200 ms; capillary temperature, 150^0C; spray voltage, 1.8 kV; capillary voltage, 35 V. The mass spectrometer was tuned using the static nanospray setup with a 5μM solution of angiotensin I, mol. Wt. 1,296.5 (Sigma, St. Louis) infused by a picotip emitter (New Objective). A minimal signal of 2×10^6 was established for MS/MS acquisition. Thermo Electron Bioworks 3.1 software was used to achieve protein identification with the National Center for Biotechnology Information protein database downloaded from ftp:ncbi.nlm.gov. blast/db. The procedures used for SDS-PAGE, Western blotting, In-gel digestion and MS analysis were the same throughout the study unless otherwise mentioned.

3. Experimental

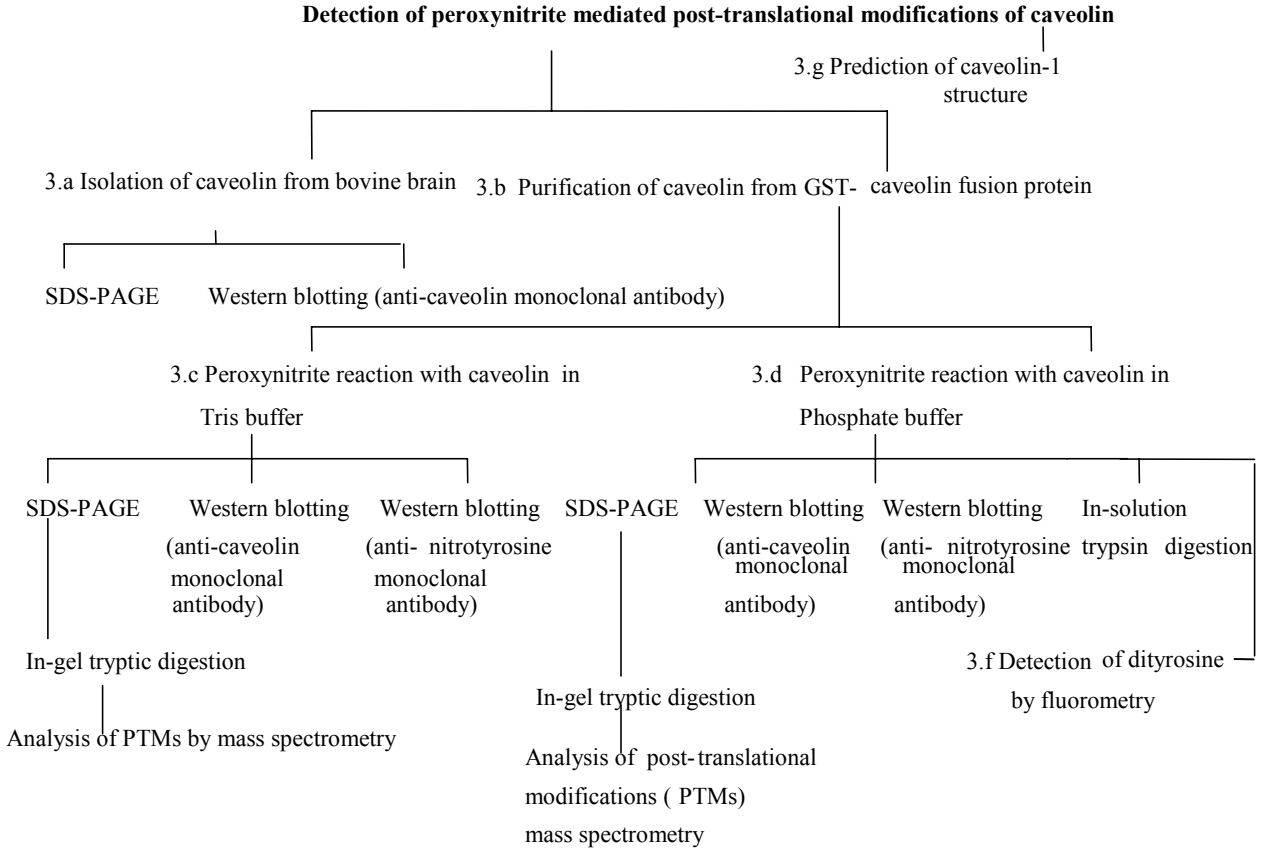

3.a Isolation of caveolin from bovine brain

Bovine brain (200mg) was homogenized in 2ml of 500mM sodium carbonate, pH 11.0. Homogenization was carried out in the polytron tissue grinder (Power Gen 700, Fisher Scientific) by three 15s bursts. Then the homogenate was adjusted to 45% sucrose by the addition of 2 ml of 90% sucrose prepared in MBS (25mM morpholine ethane sulfonate, pH 6.5, 0.15M NaCl) and placed at the bottom of an ultracentrifuge tube. A 5-35% discontinuous sucrose gradient was formed above (4 ml of 5% sucrose/4ml of 35% sucrose, both in MBS containing 250mM sodium carbonate)[12] and centrifuged at 39,000 rpm for 16h in an SW41 rotor (Beckman instruments). A light scattering band was confined to the 5-35% sucrose interface was observed that contained caveolin enriched membranes. Isolated caveolin-1 from bovine brain was further characterized by SDS-PAGE and western blotting probed with anti-caveolin monoclonal antibody.

3.b Expression and purification of caveolin-1

The clone of GST-canine caveolin cDNA in the PGEX4T vector, in the host strain *Escherichia coli* (*E.coli*) BL21 was used to purify caveolin. A 10ml of *E.coli* overnight culture was used to inoculate 1 liter of Luria-Bertani medium. The medium inoculated with 10ml of overnight culture was incubated at 37^{o}C in an absorbance A_{600}, until 0.6 was reached. *E. coli* cells which contain the

pGEX4T vector with GST-caveolin fusion gene construct were induced using isopropyl B-D-thiogalactoside and incubated at 37^0C for 5 hours. The cells were harvested by centrifugation at 5000g for 5 minutes, and re-suspended in 10 ml of ice-cold tris-buffer (STE) solution (pH 8.5) containing 7.5mM tris, 150mM sodium chloride (NaCl) and 3mM ethylene diamine tetraacetic acid (EDTA). Cells were incubated 15 minutes with lysozyme (0.1mg/ml) on ice followed by sonication in the presence of 1% (w/v) triton-X 100, 5mM dithiothreitol, 100uM PMSF (phenyl methyl sulfonyl fluoride) and 1mM benzamidine. The cell lysate was centrifuged at 20,000xg for 45 minutes at 4^oC to pellet the cellular debris. Glutathione-agarose beads were added to the supernatant and incubated at 4^oC with gentle rotation for 4h. After incubating with cell lysate for 4h, glutathione agarose beads were obtained by centrifugation of lysate at 5000xg for 5 minutes. The beads were washed 6 times with STET buffer (1% triton in STE) and once with STE. After incubation with 5 units of thrombin for 1h at room temperature, the cleaved proteins were eluted with 0.5ml of STE buffer. To 0.5ml elution fractions, 20ul of pre-washed thrombin-binding beads was added, followed by incubation for 30 min at 4^oC. Thrombin bound beads were removed by centrifugation at 6000g for 1minute. The protein concentration was measured by Coomassie Blue Plus protein reagent (Pierce), and this procedure yields approximately 125μg of caveolin from 1 liter of culture. Purified protein was characterized by SDS-PAGE, western blot analysis and ESI-ion trap mass spectrometry.

Optimization of caveolin purification from GST-caveolin fusion protein

Bacteria growth between absorbance A_{600} and OD 0.35-0.6 ranges to find the optimal bacterial growth for caveolin expression. Complete protease inhibitor cocktail tablet (Roche, cat. #1836170) was added to the cell lysate to inhibit protease activity. Thrombin cleavage was improved by increasing the incubation time of GST caveolin bound to glutathione agarose beads to 12h at room temperature.

3.c Reaction of different concentrations of peroxynitrite with caveolin in STE buffer (caveolin isolation buffer), pH 8.5

Peroxynitrite was prepared by the reaction of ozone with cooled aqueous sodium azide and the concentration of peroxynitrite stock was determined as described previously.[74] Dilutions of peroxynitrite were made in 0.1% NaOH from the peroxynitrite stock solution of 30mM and caveolin 14μM in tris buffered saline pH 8.5 was treated with 0, 100, 200 and 300μM of of final concentrations of peroxynitrite in the reaction. After nitration 200mM DTT, 4x-sample buffer contained 1M tris, 40% glycerol, 20% sodium dodecyl sulfate and 0.05% bromophenol blue were added to the samples. SDS-PAGE and SDS-PAGE followed by western blotting probed with anti caveolin mAb (1:10,000 dilution in T-TBS), and anti 3-nitrotyrosine mAb (1:5,000 in T-TBS) were carried out to detect the reaction of peroxynitrite with caveolin. Also, visualized gel bands in

SDS-PAGE was further analyzed by ESI-MS/MS to detect post-translational modifications.

3.d Reaction of different concentrations of peroxynitrite with caveolin in phospate buffer (physiological conditions) pH 7.5

The synthesis of peroxynitrite was done according to a method described previously.[74] The concentration of peroxynitrite stock solution was measured by absorbance (ε_{302} = 1670 M^{-1} cm^{-1}).[74] Dilutions of peroxynitrite were made in 0.1% NaOH from the peroxynitrite stock solution of 28mM. $NaHCO_3$ (25mM) was added to caveolin 14μM in phosphate buffer (NaH2PO4 25mM, NaCl 150mM, EDTA 3mM, pH 7.5) and treated with 0, 100, 200, 300 and 400μM of final concentrations of peroxynitrite in the reaction. Samples were left for 5 minutes at room temperature for equilibration. After nitration 200mM DTT and 4x-sample buffer were added to the samples. SDS-PAGE and SDS-PAGE followed by western blotting with anti caveolin mAb (1:10,000 dilution in T-TBS), and anti 3-nitrotyrosine mAb (1:5,000 in T-TBS) were carried out to detect the reaction of peroxynitrite with caveolin. Also, visualized gel bands in SDS-PAGE were further analyzed by ESI-MS/MS to detect post-translational modification.

Post-translational modifications of caveolin-1 under physiological conditions-peroxynitrite reaction with caveolin-1, detection by in-solution tryptic digestion and ESI-MS/MS

$NaHCO_3$ 25mM was added to caveolin (14μM) in phosphate buffer pH 7.5. Peroxynitrite was prepared by the reaction of ozone with cooled aqueous sodium azide and the concentration of peroxynitrite stock was determined as described previously.[74] Dilutions of peroxynitrite were made in 0.1% NaOH from the peroxynitrite stock solution of 28mM. Three samples were prepared by adding 0μM, 300μM and 400μM of peroxynitrite to 14μM 0f caveolin-1. Samples were vortexed vigorously for 30 seconds and left for 5 minutes for equilibration. Then 6M Guanidine-HCl, 50mM HCl (pH 8.0) and 2mM DTT were added and heated at 60^{o}C for 60 minutes. After denaturation, the samples were allowed to cool and were dialyzed against 50mM NH_4HCO_3 (pH 7.8). 200mM DTT was added and kept at 55^{o}C for 30 min. The samples were alkylated using 1M iodoacetamide for 1 hour at room temperature and digested at 37^{o}C overnight using trypsin. Residual guanidine-HCl in the 100μl digested sample was removed using ziptip (C18 column) method.

3.e Analysis of reducing effect of dithiothreitol (DTT) in caveolin-1 exposed to peroxynitrite by SDS-PAGE followed by western blotting probed with anti-caveolin monoclonal antibody

Three samples were made with caveolin 14μM in 25mM phosphate buffer. In sample 1, 25mM $NaHCO_3$ was added to caveolin-1 (14μM) in phosphate buffer and this reaction was not exposed to peroxynitrite. DTT (200mM) was added after equilibration of the reaction mixture for 5 minutes (sample 1). In sample 2, 25mM $NaHCO_3$ was added to caveolin-1 14μM in phosphate buffer and this reaction was exposed to 200μM of peroxynitrite. 200mM of DTT was added after equilibration of the reaction mixture for 5 minutes. The only difference in this sample from sample 1 is the exposure of caveolin-1 to 200μM of peroxynitrite. In sample 3, peroxynitrite 200μM was added to 14μM of caveolin-1 and equilibrated for 5 minutes. No DTT was added to the 3rd sample. Tris-SDS sample buffer was added to each sample and SDS-PAGE was carried out to observe possible reducing effects of DTT.

3.f Detection of dityrosine by fluorometry

Three samples were prepared for detection of dityrosine using a spectrofluorometer (Shimadzu, RF5000U). Sample A was prepared by adding 25mM $NaHCO_3$ and peroxynitrite 400μM to caveolin-1 14μM in phosphate buffer and equilibrating for 5 minutes. Fluorescence spectrum of dityrosine was obtained at an excitation wavelength 283nm and an emission wavelength 410

nm.[63] Same experiment was done by adding 2% SDS to see whether there is any change of the spectrum by disrupting non-covalent bonds by using SDS (Sample B). In sample C (control), peroxynitrite 200μM was added to phosphate buffer and equilibrated for 5 minutes and then caveolin-1 14μM was added. Fluorescence spectrum of dityrosine from all these three samples was obtained at an excitation wavelength 283nm and an emission wavelength 410nm.[63]

3.g Prediction of caveolin-1 structure

For the successful interpretation of post-translational modifications, which alter the protein function, an understanding of the 3-D structure of a protein is required. X-ray diffraction, and NMR based methods have been successfully used to determine protein structure and to study dynamic processes at the molecular level.[75,76]

The number of structurally characterized proteins is much less than the number of known protein sequences. Swiss-PROT and TrEMBL databases hold about 8,500,000 sequence entries whereas only about 20,000 experimental protein structures are deposited in the protein data bank (PDB).[77] As a benefit of structural genomics the gap between the protein of known amino acid sequences and those with known 3-D structures is narrowing down with time. To generate a 3-D model of a target protein from its amino acid sequence comparative modeling is used. An experimentally solved template 3-D structure that has a significant amino acid sequence homology to the target sequence is used to predict unknown

protein structure.[78] Caveolin-1 is one of the vast majorities of proteins that have an amino acid sequence with unknown 3-D structure. Thus, Dr. Gerald Lushington helped this project by predicting the cavoelin-1 structure using the comparative modeling method.

Caveolin-1 (PFAM accession number PF01146) has been characterized as a three-domain protein, with the middle domain (residues 75-106) entailing a transmembrane spanning hairpin.[79] It was ascertained from the Swiss Model database[77] that no suitable previously crystallized homologs (i.e., sequence identity greater than 25%) existed for either the full caveolin-1 structure or for any of its constituent domains. The Threader program was employed[80] to identify structural analogs based on common secondary structure elements, solvation free energy profiles, and other physicochemical attributes. Secondary structure predictions were made for each of the three Caveolin-1 domains using the PSIPRED program[81] at default settings, and a Threader search was run for each resulting sequence-structure file over the entire Threader database. Template models were determined from the Threader searches for each domain by retaining a) those structures with the top Z-score match relative to the target domain, and b) any other structures with Z-scores of at least 2.7 that showed relatively continuous alignment (i.e., minimal gaps) with the target. In the case of the N-terminal domain, the RNP domain of a human RNA-binding protein was used (PDB code: 1BNY[82]; Threader Z-score = 4.03) and a RNA-binding domain of the U1A spliceosomal protein (PDB code: 1URN[83]; Threader Z-score = 3.42; 86.5%

sequence coverage) as templates. For the C-terminal domain, we employed the II Alactose enzyme from Lactococcus lactis (PDB code: 1E2A[84]; Threader Z-score 4.58) and the rice non-specific lipid transfer protein (PDB code: 1RZL[85]; Threader Z-score 3.42; 97.2% sequence coverage) as templates. Finally, only a single template, the *E. coli* recA protein monomer (PDB code 2REB[86]; Threader Z-score 2.85; 96.9% sequence coverage), was deemed adequate (Threader Z-score greater than 2.7) for modeling the transmembrane domain.

Separate models for the N-terminal, C-terminal and transmembrane domains of Caveolin-1 were generated from the above list of templates via the Modeller program.[78] In all cases, the alignments generated from the Threader analysis were used as inputs for the sequence to structure mapping. Default restraint settings were retained and rigorous simulated annealing steps using the CHARMM force field and charges[87] were employed in order to permit reasonable co-integration of the structural features dictated by the different templates. Specifically, 5 simulated annealing cycles of 4.4 ps stepwise warming (0K→ 150K→ 250K→ 400K→ 700K→ 1000K) followed by 19.2 ps stepwise cooling (1000K→ 800K→ 600K→ 500K→ 400K→ 300K) were performed. The resulting domain models were evaluated for structural compatibility. Both the N- and C-terminal domain structures appeared to possess viable and intuitively reasonable folds. The resulting transmembrane domain model was found to possess the expected beta turn[88] in the approximate spatial center of its structure, however it also possessed two additional turns on either side of the central turn,

making a *W* type fold instead of the desired hairpin. Referring to the original PSIPRED secondary structure assessment, we found that the backbone in the region of these two peripheral turns was classified with low certainty as of an unstructured coil. To induce closer correspondence to known folding, we reset the backbone torsional angles within the four residues adjacent to each of the two spurious turns to correspond from their β-turn values instead to β-strand values and minimized the resulting structure with CHARMM (CHARMM force field; default convergence thresholds, permitting up to 10,000 steps). The resulting single hairpin structure attained a total energy that was 20.06 kcal/mol more stable than the comparably optimized *W* shaped structure.

The three domain models were finally combined into a unified structure via Modeller, using default restraint settings and the same simulated annealing refinement cycles as described above. The resulting model was visualized in SYBYL.[89] Secondary structure assignments were made according to standard α and β torsional angle ranges, and Connolly surfaces were generated with a 1.4 Å probe. Finally we were able to predict caveolin-1 structure.

4.a Isolation of caveolin-1 from bovine brain

4.a.1 Results

Bovine brain tissue was used to isolate caveolin-1 using a detergent free method[12] as described in the experimental section (3.a). The caveolin enriched membrane (CEM) fraction was visible as a light scattering band at the interface of the 5-30% sucrose layers. This fraction was separated from the bulk of the cellular protein content, which remained in the 45% sucrose layer at the bottom of the ultracentrifuge tube. The protein concentration of isolated caveolin-1 was measured using Coomassie Blue Plus protein reagent (Pierce) and this procedure yields approximately 90ug of caveolin from 200mg of brain tissue.

Isolated caveolin was subjected to SDS-PAGE and western blotting followed by anti-caveolin monoclonal antibody. Figure 07 shows the isolated caveolin enriched membranes (CEM) analyzed by SDS-PAGE. It shows the caveolin-1α, caveolin-1β isoforms between 20-25kDa. and caveolin-1 dimer around 44kDa. This result was further analyzed by western blotting with anti-caveolin monoclonal antibody.

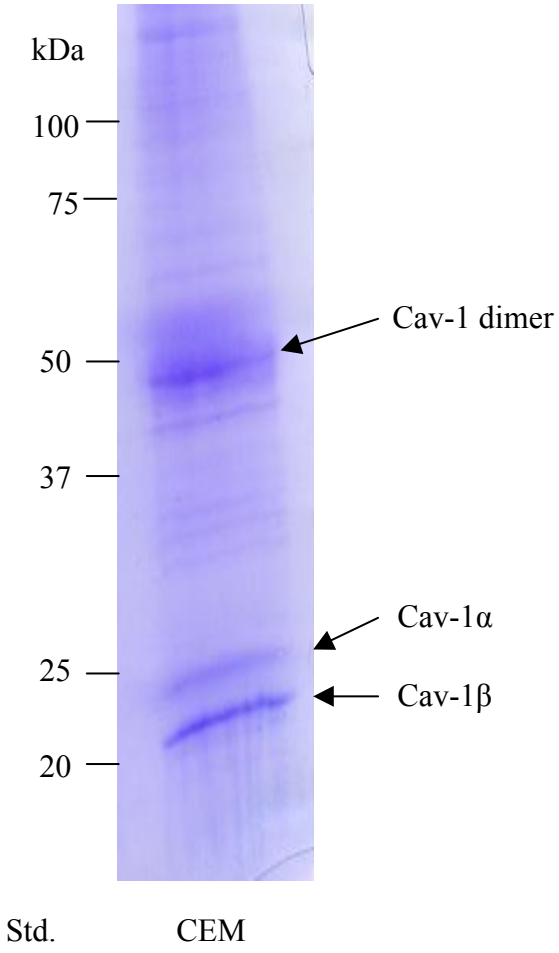

Figure 07. SDS-PAGE analysis of CEM (caveolin enriched membranes) isolated from bovine brain using density gradient centrifugation

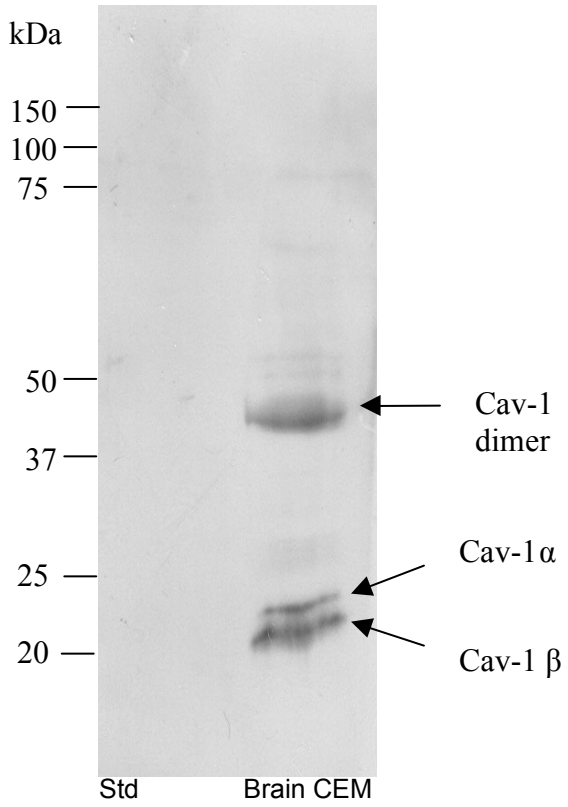

Figure 08. Western blotting - CEM (caveolin enriched membranes) isolated from bovine brain using density gradient centrifugation

Figure 08 shows the isolated CEM from bovine brain analyzed by SDS-PAGE followed by western blotting with anti-caveolin monoclonal antibody. The slower migrating band at 24-kDa the faster migrating 21kDa band and the band at 44kDa was recognized by the anti-caveolin monoclonal antibody.

4.a.2 Discussion

Detergent free sucrose gradient was used to isolate caveolin-enriched membrane fractions.[12] Sodium carbonate buffer is used to homogenize 200mg of bovine brain tissue. After homogenization bovine brain tissues were sonicated to obtain more finely disrupted cell membranes. After density gradient centrifugation, a light scattering band (caveolin enriched membranes) at 5-35% sucrose interface was obtained which contained caveolin but excluded most other cellular proteins.

Isolated caveolin enriched membranes were subjected to SDS-PAGE (figure 07) and we could observe bands at 21kDa, 24kDa and 44kDa. These were further analyzed by western blotting and anti-caveolin monoclonal antibody (2297, BD biosciences). Anti-caveolin monoclonal antibody was able to recognize caveolin-1α (24kDa), and caveolin1- 1β isoforms (21kDa) and caveolin 1 dimer at 44kDa.

Alternative mRNA splicing of caveolin-1 produces caveolin-1α and caveolin-1β isoforms, which have the molecular weights of 24kDa and 21kDa. The α and β isoforms start from methionine at positions 1 and 32, respectively.[8]

The two isoforms have a common hydrophobic amino acid stretch, a scaffolding domain, and the C-terminal region, whereas the N-terminal amino acids are only found in the α isoform. No detailed study concerning the functional diversity of these two caveolin-1 isoforms has been reported.[8]

4.a.3 Conclusion

Based on these results, the isolation of caveolin-1 from bovine brain tissue with the procedure adapted has been successful. Caveolin-1 has two isoforms, α and β and it can make a dimer at 44kDa. SDS-PAGE showed that we could isolate caveolin-1 isoforms and caveolin-1 dimer successfully. Anti-caveolin monoclonal antibody could recognize the caveolin-1 isoforms (bands at 24kDa, and 21kDa) and caveolin-1 dimer band at 44kDa. These results confirm that we could isolate caveolin-1 α and β isoforms and caveolin-1 dimer from bovine brain tissue successfully. Bovine brain tissue was used as to optimize the isolation procedure of caveolin-1 from tissues. Being able to isolate caveolin-1 will be useful in our future studies of in-vivo post-translational modifications of caveolin-1.

4.b Analysis of purification steps of caveolin-1 from GST-caveolin fusion protein

4.b.1 Results

The pGEX plasmids provide a multiple cloning site for fusing a gene of interest to the C-terminus of glutathione S-transferase (GST). GST (26kDa) enzyme binds reversibly and with high affinity to glutathione-containing affinity matrices.[90] In this study, we expressed GST-caveolin (canine) fusion protein in pGEX-4T-1 vector (figure 9) in *E. coli* (BL-21 strain).

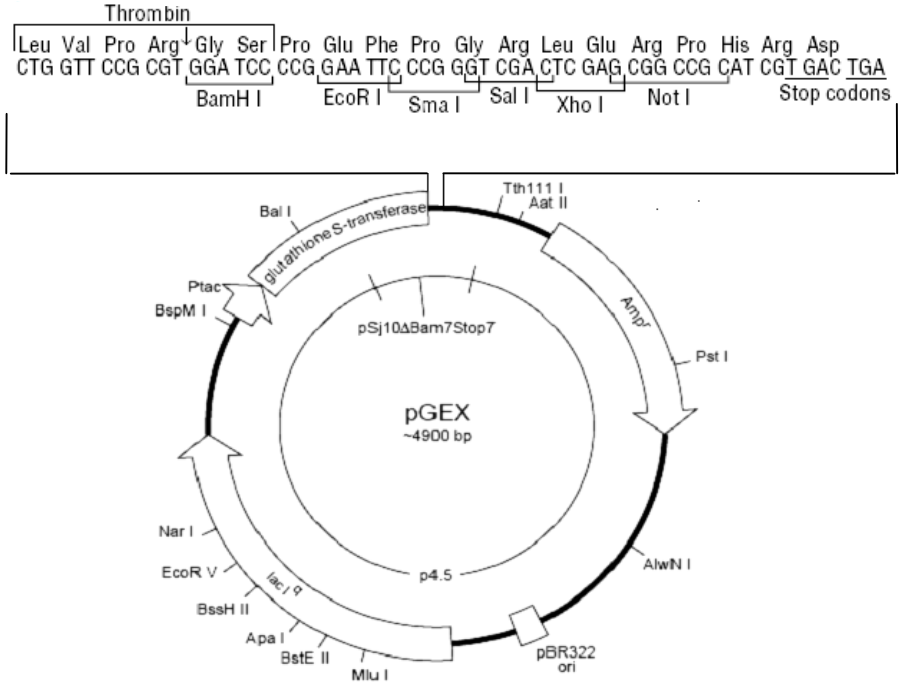

Figure 9. Structure of the pGEX 4T-1 plasmid vector.

After expressing the protein in *E. coli,* crude cell lysate was prepared and incubated with glutathione-agarose beads. Glutathione agarose-GST caveolin complex was centrifuged followed by extensive washing. After washing STE buffer was added to the beads containing GST caveolin (sample a) and caveolin was cleaved away from GST using thrombin since the sequence between GST and caveolin codes for a proteolytic cleavage site for thrombin. After incubating caveolin with thrombin GST-agarose beads were removed by centrifugation. The supernatant should contain purified caveolin-1 (sample c) and the agarose beads with immobilized GST (sample b) was removed by centrifugation. Figure 10 shows the analysis of samples a, b and c in sodium dodecyl sulfate polyacrylamide gel electrophoresis (SDS-PAGE) followed by Coomassie Brilliant Blue staining.

Figure 10, lane 2 shows the analysis of sample A. In this lane GST-caveolin was observed at 48kDa. The cell lysate, which contains GST-caveolin, was incubated with glutathione-agarose beads and cleaved using thrombin to isolate caveolin. The bands that appeared below 48kDa in lane 2 could be cleavage products of GST due to *E. coli* protease enzymes.

Lane 3, sample B (Figure 10) shows a band at 26kDa, which could be GST, remaining in agarose beads after thrombin cleavage. Lane 4, which was loaded from the supernatant after thrombin cleavage, shows a caveolin band at 22kDa. Western blotting with anti-caveolin antibody (Figure 11) and also with

Anti-GST antibody (Figure 12) was used to confirm these results using specific antibody recognition.

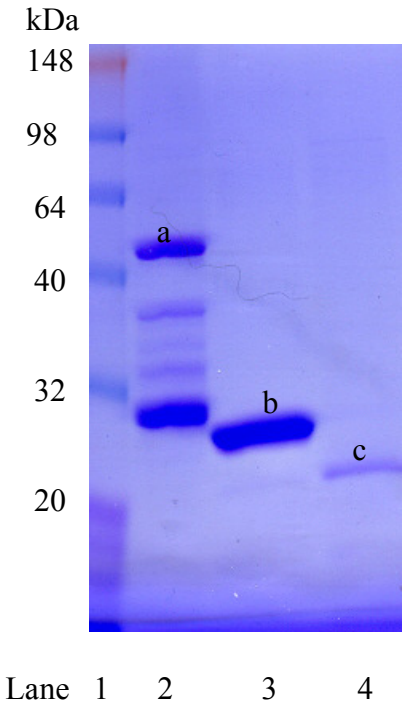

Band a- GST-caveolin, Band b- GST, Band c- purified caveolin

Figure 10. Isolation of caveolin from GST-caveolin fusion protein. SDS-PAGE followed by Coomassie Brilliant Blue staining, Lane 1- Protein standard, Lane 2- Lysate after incubation with GSH-agarose beads, Lane 3- GST remaining on GSH-agarose beads after thrombin cleavage, Lane 4- Supernatant after thrombin cleavage

Figure 11 shows the western blotting with α-caveolin mAb (BD Biosciences) in 1:1000 dilution in T-TBS. The α-caveolin mAb recognized the 48kDa band in lane 2, confirming that 48kDa band contains caveolin. Antibody recognition confirmed that the band at 22kDa in lane 4 is caveolin-1. 44kDa band in lane 4 that was recognized by the anti-caveolin antibody can be caveolin-1 dimer. Two less dense bands were appeared in lane 3 at 22kDa and 44kDa, that was loaded with glutathione-agarose beads after being cleaved by thrombin. This result suggests that there is some amount of caveolin still bound to glutathione agarose beads. Thrombin cleavage should be optimized to increase the caveolin-1 final concentration, which shows at 22kDa in lane 3.

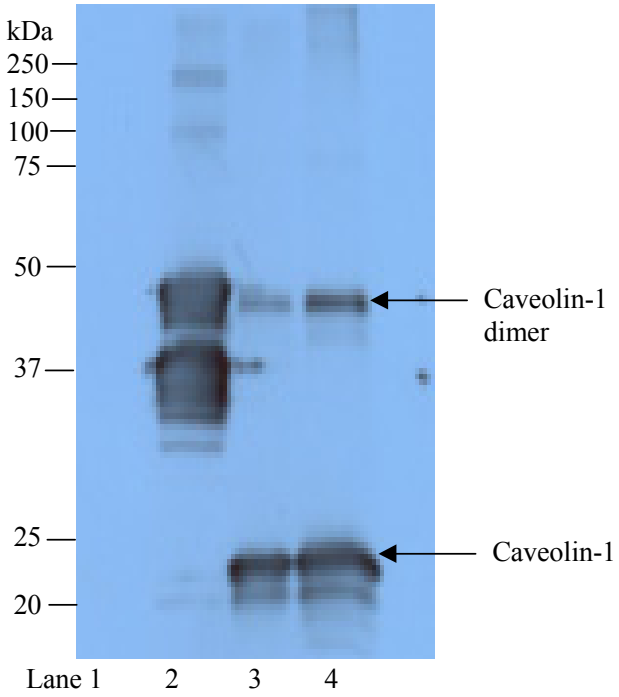

Figure 11. Isolation of caveolin from GST-caveolin fusion protein. Western Blotting with α-caveolin mAb (1:10,000 dilution in TBS-T), Lane 1- protein standard (no bands were shown in lane 1 as the protein standard was not recognized by the antibody), Lane 2-Lysate after incubation with GSH-agarose beads, The band at 48kDa shows GST-caveolin, The bands shown below 48kDa could be some cleavage products due to E.coli protease enzymes. Lane 3- caveolin (22kDa) remained in GSH-agarose beads after thrombin cleavage, Lane 4- Supernatant after thrombin cleavage which contains purified caveolin-1 (22kDa), 44kDa band shows caveolin-1 dimer

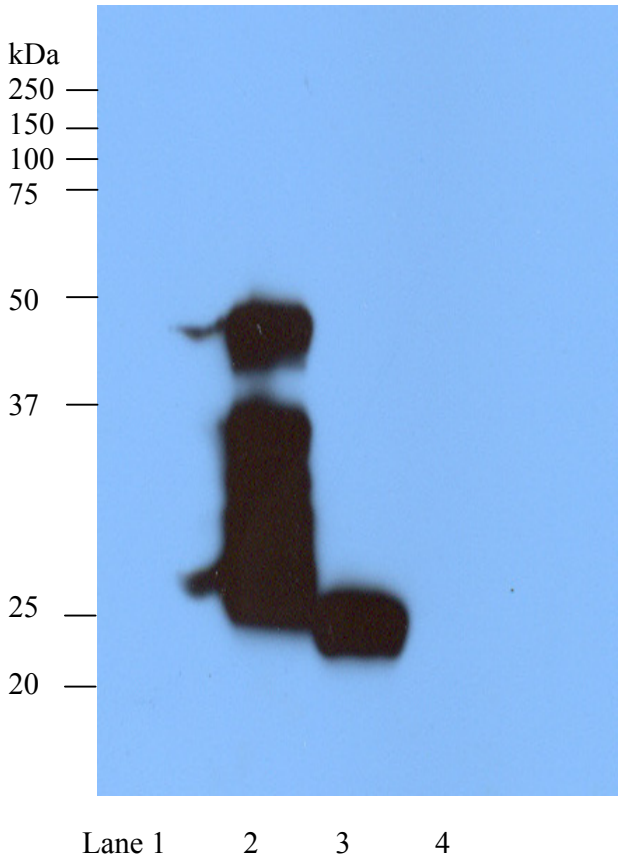

Figure12. Isolation of caveolin from GST-caveolin fusion protein. Western blotting with α–GST pAb, Lane 1- Protein standard, Lane 2- Lysate after incubation with GSH agarose beads, Lane 3- GST (26kDa) remaining in GSH agarose beads after thrombin cleavage, Lane 4- Supernatant after thrombin cleavage

Western blotting with anti-GST-pAb (BD Biosciences) 1:10,000 dilution in T-TBS is shown in figure 12. A protein band around 48kDa in lane 2 contains GST as it was recognized by anti-GST polycolonal antibody. A band at 26kDa in lane 3 was identified as GST by antibody recognition. The bands shown below 48kDa in lane 2 could be the cleavage products of GST due to *E. coli* protease enzymes. No protein bands showed in lane 4 suggesting that the supernatant of the cell lysate after thrombin cleavage is free from GST. This result confirms that the supernatant after thrombin cleavage contains purified caveolin-1.

MS analysis of the gel bands

ESI-MS/MS analysis (elecrospray ionization-tandem mass spectrometry) of in-gel tryptic digests was done. Peptides extracted from the 48kDa gel band (figure 10, sample A, lane2) were analyzed by ESI-ion trap-MS. A total of 9 peptides from caveolin-1 were detected, corresponding to 96 amino acids or 54% of the canine caveolin-1 sequence. Also a total of 10 peptides from GST were detected, corresponding to 97 amino acids or 42% of the GST sequence. A peptide should have minimum recommended values of XCorr and Delta Cn for reportable results. XCorr is abbreviated for the raw cross-correlation score of the top candidate peptide or protein for a given input data file and Delta Cn value is the difference or delta in cross-correlation score between the top two candidate peptides or proteins for a given input data file.

Table 1. Minimum recommended values

Charge	XC	Delta Cn
+1	1.0-1.5	0.1
+2	2.0-2.5	0.1
+3	2.5-3.75	0.1

Table 2. Peptides identified from caveolin-1 with reportable scores from MS analysis of 48kDa gel band (sample a, lane 2, figure 10)

Caveolin Peptides	Charge	XC	Delta Cn
EQGNIYKPNNK	1	1.596	0.466
ELDLVNR	1	1.601	0.510
YVDSEGHLYTVPIR	2	4.712	0.802
ASFTTFTVTK	2	3.029	0.641
VYSIYVHTFCDPFFEAVGK	3	2.821	0.546
IDFEDVIAEPEGTHSFDGIWK	3	3.748	0.390

Peptides from the MS analysis of 48kDa gel band revealed two proteins, caveolin-1 and GST. The peptides recovered from caveolin-1 with reportable scores from MS analysis of 48kDa gel band in figure 10, lane 02, sample A are shown in table 02. The MS/MS spectra of peptides identified from caveolin-1, YVDSEGHLYTVPIR and ASFTTFTVTK are shown in figure 13 and figure 14 respectively.

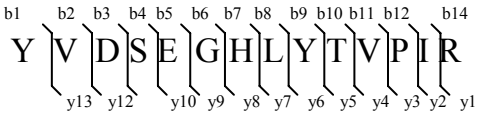

Charge	XC	Delta Cn
2	4.712	0.764

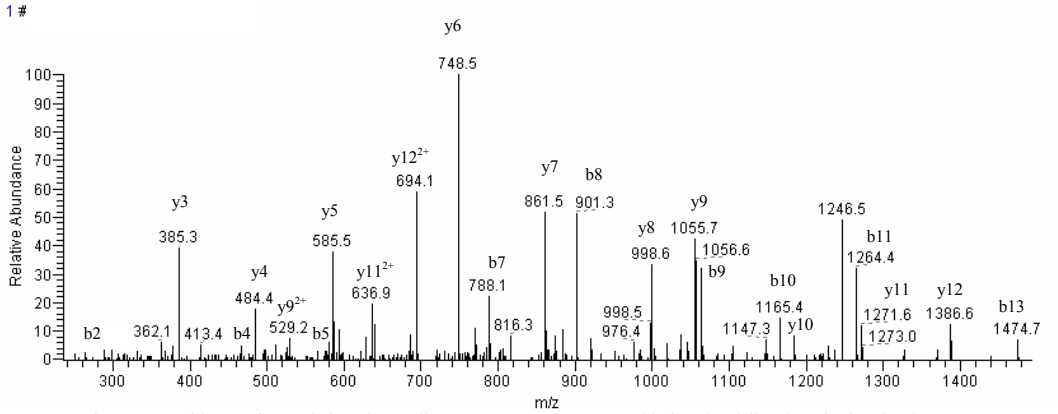

Figure 13. Peptide mass fingerprinting of caveolin-1YVDSEGHLYTVPIR peptide from ingel digestion of 48kDa band (sample a, lane 02)

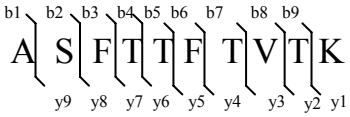

Charge	XC	Delta Cn
2	3.029	0.641

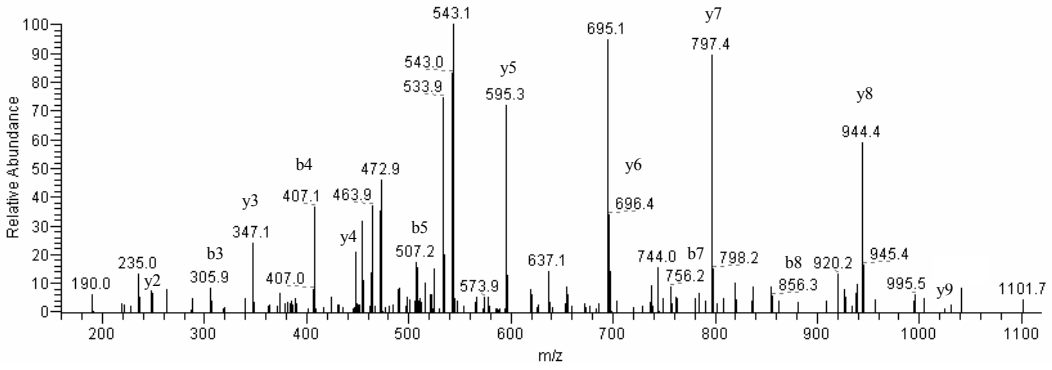

Figure14. Peptide mass fingerprinting of caveolin-1 ASFTTFTVTK peptide from ingel digestion of 48kDa band (sample a, lane 02)

The peptides recovered from GST with reportable scores from MS analysis of 48kDa gel band in figure 10, lane 02, sample a are shown in table 03. The MS/MS spectra of RIEAIPQIDK and LLLEYLEEK peptides identified from GST are shown in figure 15.

Table 3. Peptides identified from GST with reportable scores from MS analysis of 48kDa gel band (sample a, lane 2, figure 10)

GST Peptides	Charge	XC	Delta Cn
HNMLGGCPK	2	2.021	0.403
YEEHLYER	2	2.818	0.240
VDFLSK	1	1.759	0.111
RIEAIPQIDK	2	3.328	0.325
SPILQYWK	2	2.528	0.102
LLEYLEEK	2	3.241	0.211
YIAWPLQGWQATFGGGDHPPK	2	2.951	0.506
KFELGLEFPNLPYYIDGDVK	3	3.278	0.330

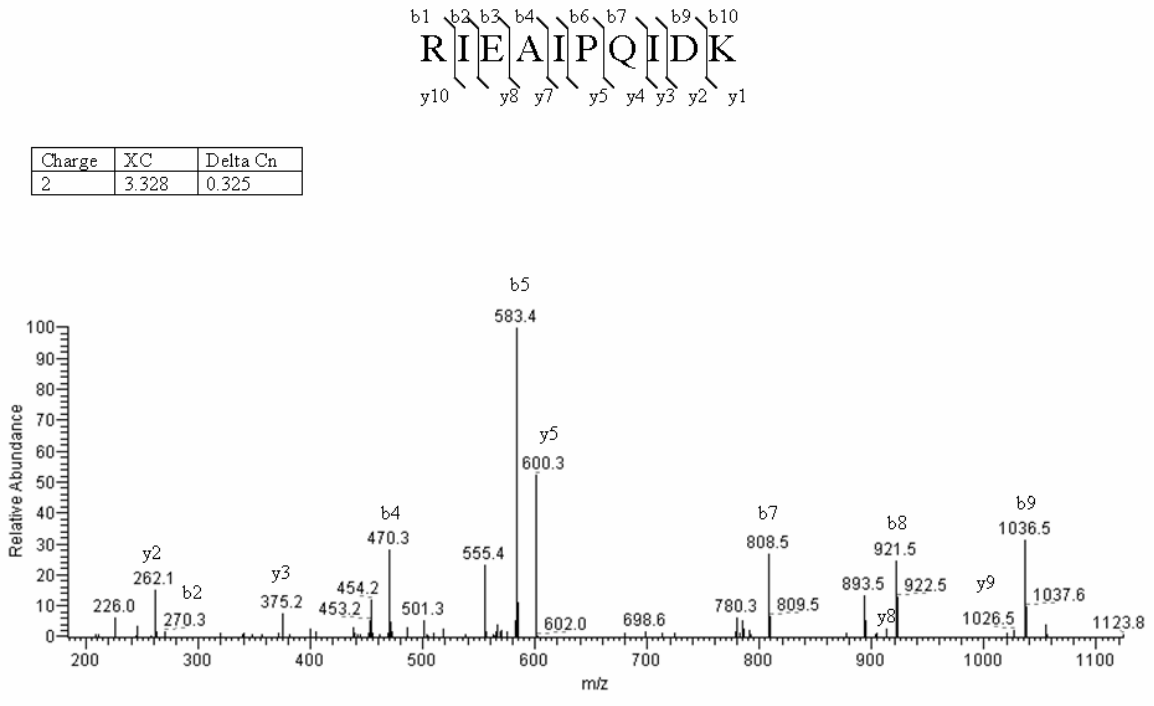

Figure 15. Peptide mass fingerprinting of glutathione S-transferase RIEAIPQIDK peptide from ingel digestion of 48kDa band (sample a, lane 02)

The peptides isolated from the 26kDa band (Fig.10, lane 3, sample b) provided positive identification of the isolated protein as glutathione S-transferase from LC-ESI-MS analysis. In this sample, caveolin was cleaved out by thrombin and only GST remains on the glutathione agarose beads. Eight peptides were detected covering 34% of human glutathione S-transferase sequence. MS/MS spectra of peptides RIEAIPQIDK and YIAWPLQGWQATFGGGDHPPK are shown in figures 16 and 17 respectively.

Table 4. Peptides with reportable scores from MS analysis of 26kDa gel band (sample b, lane 3)

Peptide	Charge	XC	Delta Cn
LPEMLK	1	1.647	0.146
RIEAIPQIDK	2	3.207	0.255
SPILGYWK	1	2.016	0.391
LLLEYLEEK	2	2.808	0.300
YIAWPLQGWQATFGGGDHPPKS	2	3.932	0.369

The peptides isolated from 22kDa (Figure 10, lane 4, sample c) band provided the identification of canine caveolin-1 from LC-ESI-MS analysis. The peptides YVDSEGHLYTVPIR, ELDLVNR, IDFEDVIAEPEGTHSFDGIWK and ELDLVNRDPK were detected with 25% canine caveolin-1 sequence coverage. The reason for not detection of 75% of the canine caveolin-1 could be the low protein recovery after thrombin cleavage of GST-caveolin fusion protein.

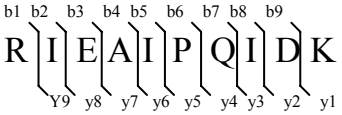

Charge	XC	Delta Cn
2	3.207	0.255

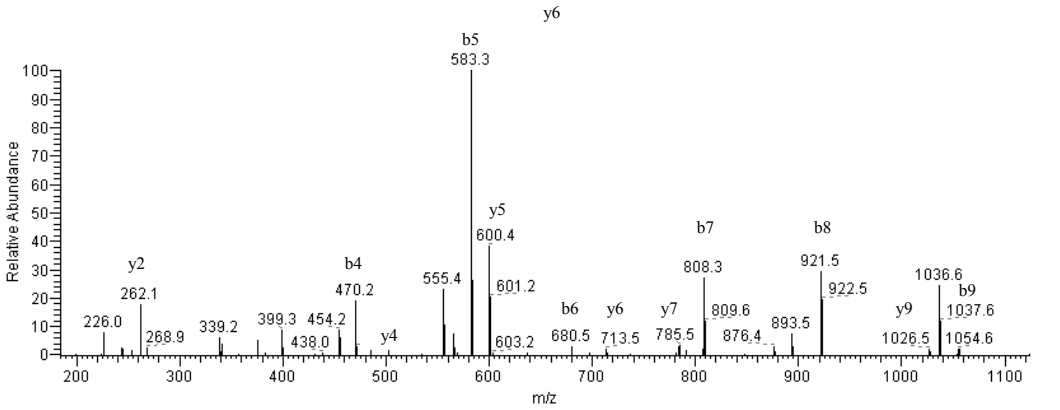

Figure 16. Peptide mass fingerprinting of glutathione S-transferase RIEAIPQIDK peptide from ingel digestion of 26kDa band (sample 0b, lane 03)

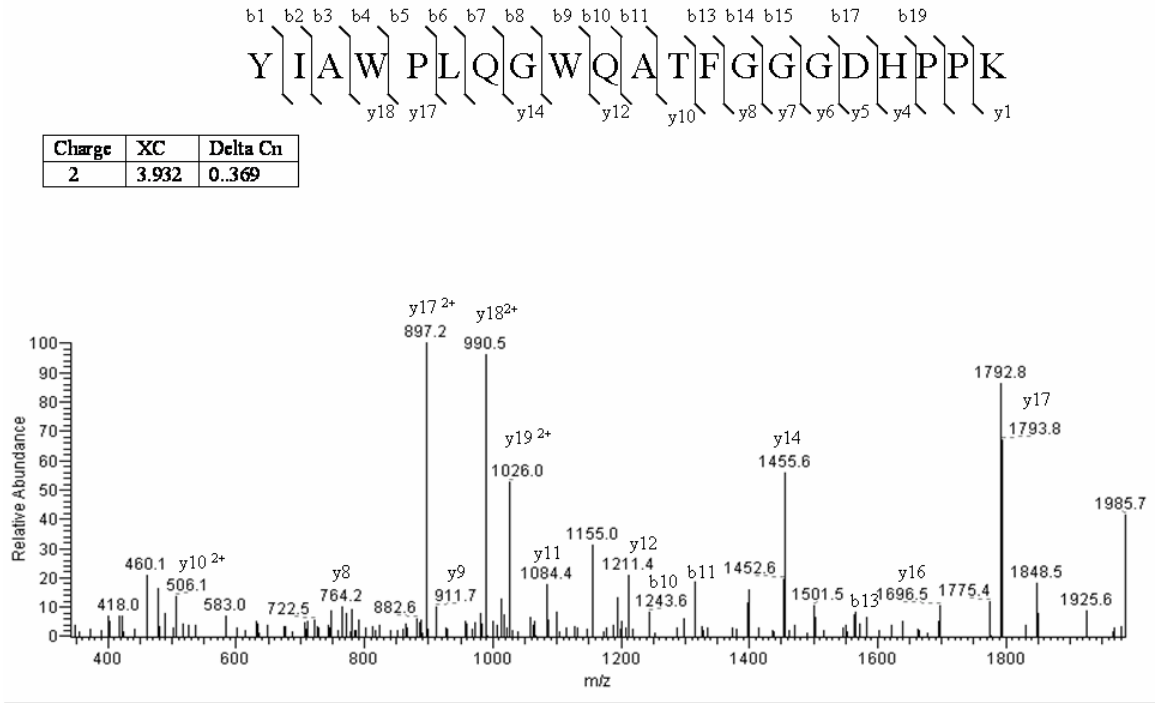

Figure 17. Peptide mass fingerprinting of glutathione S-transferase YIAWPLQGWQATFGGGDHPPK peptide from ingel digestion of 26kDa band (sample b, lane 03)

Optimization of caveolin purification from GST-caveolin fusion protein

The caveolin band obtained from SDS-PAGE (figure 10, sample c) is less dense and revealed only 25% of sequence coverage of canine caveolin-1. Purification of caveolin was optimized to obtain higher concentrations. Previously 10ml of overnight culture of *E. coli* bacteria, which express GST-caveolin, was further incubated at 37^0C until an absorbance A_{600} =0.6 was achieved. Overgrowth of bacteria can form inclusion bodies (GST caveolin purification handbook, Amersham Biosciences), which, in turn, could suppress protein expression. The bacteria growth between A_{600} in optical density 0.35-0.6 ranges was compared and it was found that the absorbance A_{600} 0.45 growth provided the highest concentration of caveolin-1. E. coli cells were grown at A_{600} 0.45 at 37^0C and cells were induced with 0.1mM isoprophyl β-D thiogalactoside and incubated at 30^0C for an additional 4h. Complete protease inhibitor cocktail tablet was added to the cell lysate to inhibit *E.coli* protease activity. Thrombin cleavage was improved by increasing the incubation time of GST caveolin bound to glutathione agarose beads to 12h at room temperature. After optimization the procedure, about 300ug (0.5ml of 0.6mg/ml solution in the STE buffer) of caveolin was obtained as measured by microassay with Coomassie Blue Plus protein reagent (Pierce).

After expressing the protein in *E. coli,* crude cell lysate was prepared and incubated with glutathione-agarose beads. Glutathione agarose-GST caveolin complex was centrifuged followed by extensive washing. After

washing STE buffer was added to the beads containing GST caveolin, vortexed and 20µl of GST-caveolin was loaded in lane 2 (sample a, figure 18). Caveolin was cleaved away from GST using thrombin since the sequence between GST and caveolin codes for a proteolytic cleavage site for thrombin. After incubating caveolin with thrombin GST-agarose beads were removed by centrifugation. The supernatant should contain purified caveolin-1 (sample b, 20µl loaded in lane 4, figure 18) and the agarose beads contained GST (sample C, 20µl was loaded in lane 3, figure 18) was removed by centrifugation.

After optimization, the samples were taken from GST caveolin purification steps were analyzed in SDS-PAGE followed by western blotting with anti-caveolin monoclonal antibody (1:10,000 dilution in TBS-T, which is shown in figure 18. In figure 18, lane 02, number of bands below 48kDa were reduced compared to the lane 1 in figure 11, showing that reduction of *E.coli* protease activity due to the addition of protease inhibitor.

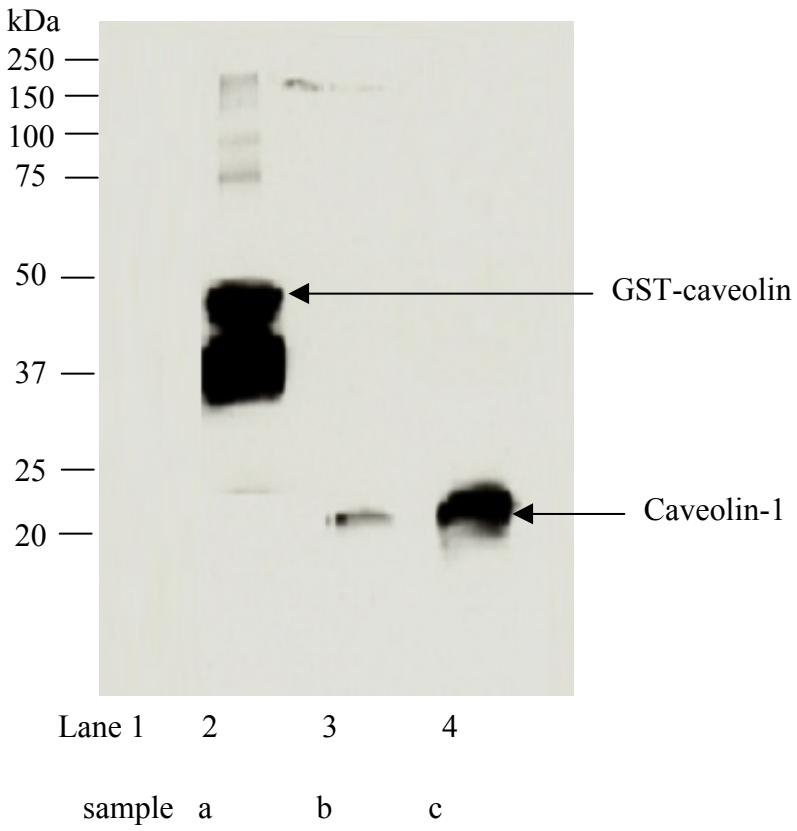

Figure 18. Western Blotting with α-caveolin mAb (1:10,000 dilution in TBS-T), Lane 1- Protein standard, Lane 2- Lysate after incubation with GSH-agarose beads (sample a), Lane 3- Caveolin left in GSH-agarose beads after thrombin cleavage (sample b), Lane 4- Supernatant after thrombin cleavage which contains purified caveolin (sample c)

4.b.2 Discussion

The pGEX-GST fusion protein system is used for high level expression and rapid purification of GST-caveolin fusion protein from *E. coli* cell lysate. Caveolin (canine) gene was inserted in to the C-terminus of glutathione S-transferase gene. Since isofoms of GST are not normally found in bacterial cells purification of GST fusion proteins is accomplished by expressing the appropriate plasmid in a bacterial host, preparing a crude cell lysate, and incubating with glutathione-agarose beads. The procedure is completed by centrifugation of the glutathione agarose-GST-caveolin fusion protein complex followed by extensive washing. When purified, caveolin is cleaved away using thrombin, as the sequence between GST and caveolin codes for a proteolytic cleavage site for thrombin. We could obtain 150μg (0.3mg/ml solution in the STE buffer) of purified caveolin as measured by microassay with Coomassie Blue Plus protein reagent (Pierce).

The samples a, b and c, obtained from the purification steps of caveolin from GST caveolin fusion protein, was analyzed by SDS-PAGE (figure 10), western blotting with anti-caveolin monoclonal antibody (figure 11), and also with anti-GST antibody (Figure 12) and ESI-MS/MS.

The anti-caveolin antibody recognized the band at 22kDa, (lane 4, figure 11) confirming that we could purify caveolin from GST-caveolin fusion protein. Lane-3 should have only the GST band at 26kDa. However, there is a caveolin band shown in lane 3 at 22kDa (figure 11). This result suggests the need of

improving the cleavage of caveolin from GST-caveolin by thrombin. The band at 48kDa in lane 2, (figure 11) was recognized by the anti-caveolin antibody and anti-GST antibody (lane 2, figure 12) confirming that this band contains GST and caveolin.

The gel bands a, b and c obtained from SDS-PAGE (figure 10) was subjected to in-gel trypsin digestion and analyzed by ESI-MS/MS. The band at 48kDa (sample a, GST-caveolin before thrombin cleavage) in lane 02 (figure 10) was analyzed by ESI-MS/MS. A total of 9 peptides from canine caveolin-1 were detected, corresponding to 96 amino acids or 54% of caveolin-1 sequence. A large peptide LLSALFGIPMALIWGIYFAILSFLHIWAVVPCIK (residues 102-147) and 5 small peptides, residues 1-5, 30-47, 58-65 and 172-178 could not be detected. As the dynamic mass range of ion-trap mass analyzer ranges between 400-2000Da, small tryptic fragments below 400Da could not be resolved by ion trap MS analysis. The peptide residues 102-147 originate from the hydrophobic domain of the transmembrane domain of caveolin that is from residue 101-135. The lack of detection could be due to poor extraction of peptides from the gel. Nevertheless, the coverage of 54% of the protein sequence provided positive identification of the isolated protein as caveolin-1. In fact, 7 of 9 Tyrosine residues are covered and only Y^{42} and Y^{118} are not detected. Also, from the analysis of the band at 48kDa (sample a), we could detect a total of 10 peptides from GST, corresponding to 97 amino acids or 42% of the human GST sequence.

The result of ESI-MS/MS confirms that the band at 48kDa contains GST-caveolin.

The band b at 26kDa (GST after thrombin cleavage) in lane 03 (figure 10) was analyzed by ESI-MS/MS. In this sample, caveolin was cleaved out by thrombin and only GST is remaining on glutathione agarose beads. From the band b, 8 peptides were detected covering 34% of human glutathione S-transferase sequence.

The peptides isolated from 22kDa (sample c, lane 04, figure 10) band provided the identification of canine caveolin-1 from LC-ESI-MS analysis. The peptides YVDSEGHLYTVPIR, ELDLVNR, IDFEDVIAEPEGTHSFDGIWK and ELDLVNRDPK were detected with 25% canine caveolin-1 sequence coverage. The reason for failing to detect the remaining fragments of caveolin-1 could be the low protein recovery after thrombin cleavage.

We could optimize the isolation procedure of caveolin-1 from GST-caveolin fusion protein by incubating bacteria at 37^0C up to an optical density A_{600} =0.45 and adding protease inhibitor cocktail tablet to the cell lysate. As we could see some caveolin was remaining in the lane 3 at 22kDa (figure 11), the thrombin cleavage was improved by increasing the incubation time of GST-caveolin bound to glutathione agarose beads with thrombin for 12h at room temperature. After optimization we could obtain about 300µg (0.5ml of 0.6 mg/ml solution in the STE buffer) of purified caveolin. After optimizing the isolation procedure, western blotting with anti-caveolin monoclonal antibody

(figure 18) was done for samples a, b and c. Sample b (Figure 18, lane 3), which contains GST/caveolin left in glutathione agarose beads after thrombin cleavage, shows a less dense caveolin band compared to the band shown in lane 03, figure 11 (western blotting with anti-caveolin monoclonal antibody) confirming that thrombin cleavage has been efficiently done. Sample c (figure 17, lane 4) shows a dense band at 22kDa confirming that we could increase the final concentration of purified caveolin-1.

4.b.3 Conclusion

The GST-caveolin fusion protein system was used for high level expression and rapid purification of GST-caveolin fusion protein to obtain sufficient protein concentration for our in-vitro studies of post-translational modifications of caveolin-1. The isolation of caveolin-1 from GST-caveolin fusion protein with an optimized procedure has been successful. After optimization of the procedure, we were able to obtain about 300ug (0.5ml of 0.6mg/ml solution in the STE buffer) of caveolin as measured by microassay with Coomassie Blue Plus protein reagent (Pierce).

4.c Reaction of different concentrations of peroxynitrite with caveolin in STE buffer (caveolin isolation buffer), pH 8.5

4.C.1 Results

Purified caveolin-1 14μM was reacted with peroxynitrite concentrations of 0, 100, 200 and 300μM respectively. This reaction was analyzed using SDS-PAGE followed by Coomassie staining as shown in figure 19. Lane1 is a protein molecular weight standard. Lanes 2, 3, 4 and 5 in SDS-PAGE gel (figure 19) show a clear band at 22kDa. It is clearly shown that the density of the 22kDa band is decreased with increasing concentrations of peroxynitrite. This suggests a reaction between peroxynitrite and caveolin-1. A less dense band shown around 44kDa could be caveolin-1 dimer. The reaction that is shown in SDS-PAGE (figure 19) was further analyzed by western blotting with anti-caveolin monoclonal antibody (figure 20), and also with anti-nitrotyrosine monoclonal antibody (Figure 21). The bands A, B, C, D, and E were analyzed by ESI-MS/MS to detect post-translational modifications.

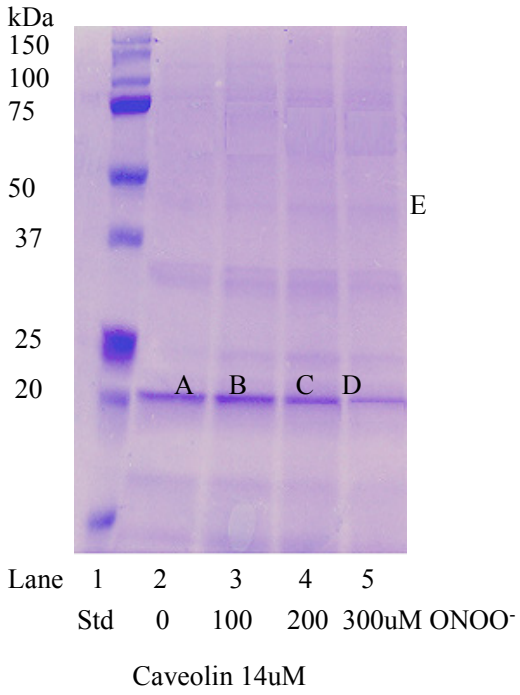

Figure 19. Reaction of different concentrations of peroxynitrite with caveolin-1 (14μM) in STE buffer pH 8.5 (caveolin isolation buffer), SDS-PAGE followed by coomasie staining. Lane 1- Protein standard, Lane 2- Caveolin-1 not treated with $ONOO^-$, Lane 3- Caveolin-1 treated with 100μM of $ONOO^-$, Lane 4- Caveolin-1 treated with 200μM of $ONOO^-$, Lane 5- Caveolin-1 treated with 300μM of $ONOO^-$. (Given peroxynitrite concentrations are the final concentrations of peroxynitrite in the reaction mixture).

Reaction Conditions: STE buffer pH 8.5 (7.5mM tris, 150mM NaCl, 3mM EDTA)

Figure 20 shows the western blotting with anti-caveolin monoclonal antibody (1:10,000). Lane 1 is the protein molecular weight standard. Untreated caveolin-1 is included in lane 2 as a negative control. Only the 22kDa band, which is caveolin-1 monomer, was shown in lane-1 not treated with peroxynitrite. In contrast the lanes 3, 4, & 5 which were treated caveolin-1 14μM with peroxynitrite 100μM, 200μM and 300μM showed 22kDa band as well as a band at 44kDa. Also caveolin-1 oligomers were shown between 88kDa and 250kDa.

The density of the band at 22kDa decreases as a function of increasing concentration of peroxynitrite explaining that there is an oxidation reaction occurring with the peroxynitrite treatment. This reduction of caveolin-1 immunoreactivity at 22kDa can be attributed to the loss of monomeric caveolin-1 and not to the artifactual loss of antibody, as confirmed by Coomassie Blue staining (figure 19) and immunodetection with anti-caveolin-1 monoclonal antibody (figure 20). Also we could observe reduction of the caveolin-1 dimer band at 44kDa as a function of increasing concentration of peroxynitrite. With increasing peroxynitrite concentration higher molecular weight bands are formed and the density of 22kDa and 44kDa bands are decreased. The reduction in the level of caveolin-1 monomer (band at 22kDa) and dimer (band at 44kDa) coincides with the appearance of caveolin-1 oligomer ranging from 88kDa (tetramer) to 250kDa.

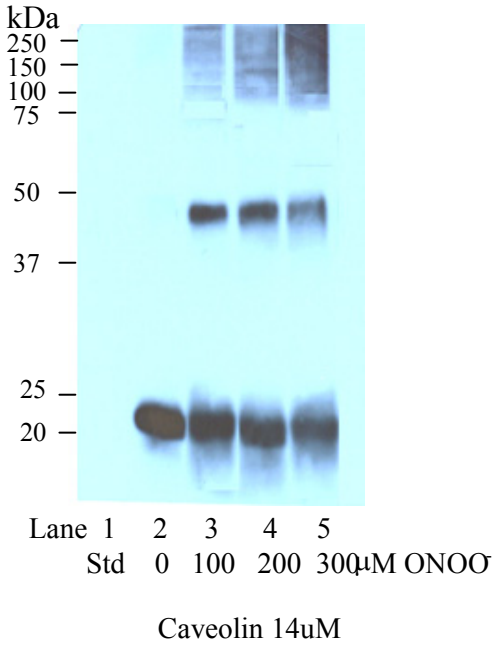

Figure 20. Reaction of different concentrations of peroxynitrite with caveolin-1 (14μM) in STE buffer pH 8.5 (caveolin isolation buffer), SDS-PAGE followed western blotting with anti-caveolin monoclonal antibody (1:10,000 dilution) Lane 1- Protein standard, Lane 2- Caveolin-1 not treated with $ONOO^-$, Lane 3- Caveolin-1 treated with 100μM of $ONOO^-$, Lane 4- Caveolin-1 treated with 200μM of $ONOO^-$, Lane 5- Caveolin-1 treated with 300μM of $ONOO^-$.

Reaction Conditions: STE buffer pH 8.5 (7.5mM tris, 150mM NaCl, 3mM EDTA)

Oxidative or nitrative role of peroxynitrite is responsible for caveolin-1 modifications upon peroxynitrite treatment. Nitration of tyrosine by peroxynitrite reaction with protein tyrosines is shown in figure 04. To detect nitrotyrosines, upon the treatment of caveolin-1 with peroxynitrite, western blotting with anti-nitrotyrosine monoclonal antibody was done (figure 21). Oxidative role of peroxynitrite could be responsible for caveolin-1 oligomer formation upon peroxynitrite treatment. Obviously peroxynitrite forms covalent bonds between peptides as we added 200mM dithiothreitol (DTT) in SDS-PAGE. SDS and DTT were not able to prevent oligomer formation of caveolin-1 upon the addition of peroxynitrite.

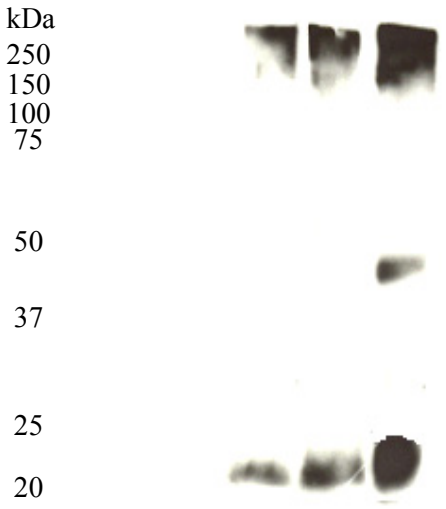

Figure 21. Reaction of different concentrations ofperoxynitrite with caveolin-1 (14 μM) in STE buffer pH 8.5 (caveolin isolation buffer), SDS-PAGE followed western blotting probed with anti-nitrotyrosine monoclonal antibody (1:5,000 dilution) Lane 1- Protein standard, Lane 2- Caveolin-1 not treated with $ONOO^-$, Lane 3- Caveolin-1 treated with 100μM of $ONOO^-$, Lane 4- Caveolin-1 treated with 200 μM of $ONOO^-$, Lane 5- Caveolin-1 treated with 300 μM of $ONOO^-$.

Reaction Conditions : STE buffer pH 8.5 (7.5mM tris, 150mM NaCl, 3mM EDTA)

Figure 21 shows the western blotting with anti-3-nitrotyrosine mAb (1:10,000) in the reaction of caveolin-1 (14μM) treated with increasing concentrations of peroxynitrite. There is no nitration shown in lane 2, which was not treated by peroxynitrite. Lane 3 and 4 show that upon nitration caveolin-1 oligomer is formed. The bands at 22kDa and between 100kDa to 250kDa show higher density than the same bands at lane 2 which explains that higher concentrations of 3-nitrotyrosine (3NY) are formed with increasing concentrations of peroxynitrite. Lane 5, which is caveolin (14μM) treated by peroxynitrite 300μM shows bands at 22kDa, 44kDa and between 100kDa to 250 kDa. Monomeric caveolin-1 appears to be consumed in figure 20, (lane 5), yet its presence is apparent in figure 21 (lane 5). The presence of 44kDa band in lane 5 (figure 21) suggests that with increasing nitration caveolin-1 dimer also can form 3-nitrotyrosine. The nitrated caveolin dimer at 48kDa is a less dense band compared to caveolin monomer. The appearance of caveolin-1 dimer in lane 5 indicates that the dimer forms more 3NY upon the reaction with increasing concentration of peroxynitrite. The reason for not detecting caveolin oligomer in SDS-PAGE (figure 19) could be higher detection limits of SDS-PAGE, higher sensitivity of western blotting (detection limit 1ng)[91] and/or the higher sensitivity of the antibody to the oligomer. These samples were further analyzed by mass spectrometry to detect possible sites of nitration.

MS analysis of the gel bands

ESI-MS/MS (elecrospray ionization-tandem mass spectrometry) analysis of in-gel tryptic digests of protein bands A, B, C, D and E (figure 19) was done. Protein bands were excised from the gels and incubated with 200mM NH_4HCO_3/MeCN 50/50V solution for 90 minutes and 20mM DTT was added. These samples were incubated with 25mM iodoacetic acid for 30 min in dark at room temperature. The samples were dried using 100% acetonitrile (MeCN) for 10 minutes and digested using 0.5μg of trypsin at 37^0C overnight. These samples were analyzed by ESI-MS/MS and searched the canine database from National Centre for Biotechnology Information (NCBI) using TURBOSEQUEST algorithm. The modifications searched were mass changes of Methionine +16kDa, Cysteine +58kDa, Cysteine+48kDa, Tyrosine+45kDa and Methionine+32kDa.

Sample A, lane 2. Protein band at 22kDa

Peptides extracted from the 22kDa gel band (band A, figure 19) were analyzed by ESI-ion trap-MS. This was resulted in positive identification of canine caveolin-1 with a total of 10 peptides corresponding to 76 amino acids or 43% of the canine caveolin-1 sequence.

Table 5. Peptides with reportable scores from MS analysis of sample A (Figure 19, lane 2, 22kDa,)

Peptide	Charge	XC	Delta Cn
EQGNIYKPNNK	2	2.373	0.495
ELDLVNR	1	1.199	0.280
YVDSEGHLYTVPIR	2	3.938	0.642
HLNDDVVK	1	2.969	0.609
AMAEEMSEK	2	2.2.472	0.576

Sample B, lane 3, Protein band at 22kDa

The peptides isolated from sample B (figure 19) provided positive identification of canine caveolin-1 from the analysis of ESI-Ion trap-MS recovering a total of 11 peptides corresponding to 122 amino acids or 68.54% of canine caveolin sequence. Within this protein sequence coverage, 7 tyrosines from the total of 9 tyrosines were detected. 3- nitrotyrosine (3NY) formation at Tyr^6 was located as shown in figure 22.

The nitration of Tyr^6 showed 3NY ion with m/z 209.16, which has increased mass of 45kDa in Y*VDSEGHLYTVPIR peptide confirming that peroxynitrite reaction selectively formed 3NY at Tyr^6. The nitrated Tyr residue, Tyr^6 is located in the cytosolic domain of caveolin-1.

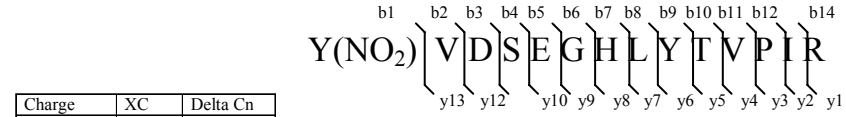

Charge	XC	Delta Cn
2	3.372	0.581

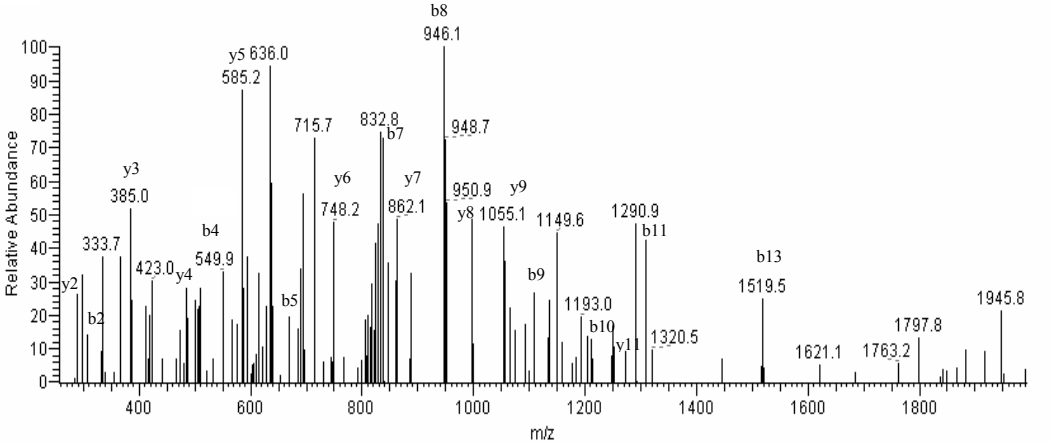

Figure 22. Peptide mass finger printing of caveolin-1 YVDSEGHLYTVPIR peptide from in-gel digestion of 22kDa (sample B, lane 03).

Table 6. Peptides with reportable scores from MS analysis of sample B (Figure 19, lane 3, 22kDa)

Peptide	Charge	XC	Delta Cn
EQGNIYKPNNK	2	2.912	0.351
ELDLVNR	2	1.651	0.491
Y*VDSEGHLYTVPIR	2	3.925	0.549
HLNDDVVK	2	2.979	0.610
IDFEDVIAEPEGTHSFDGWK	3	2.757	0.529
IFSNIR	2	1.656	0.380

Y* +45kDa (3-nitrotyrosine modification)

.

Sample C, lane 4. Protein band at 22kDa

LC-ESI-MS analysis of sample 3 (figure 19) provided the positive identification of canine caveolin-1 covering a total of 12 peptides corresponding to 118 amino acids or 66.29% of the caveolin-1 sequence. Within this protein sequence coverage, 8 tyrosines from the total of 9 tyrosines were detected.

Table 7. Peptides with reportable scores from MS analysis of sample C

(Figure 19, lane 4, 22kDa)

Peptide	Charge	XC	Delta Cn
EQGNIYKPNNK	2	1.656	0.437
YVDSEGHLY*TVPIR	2	3.384	0.564
Y*VDSEGHLYTVPIR	2	4.132	0.455
IFSNIR	1	1.475	0.360
SFLIEIQC$^{\#}$ISR	2	1.978	0.339
IDFEDVIAEPEGTHSFDGWK	3	2.846	0.330

Y* +45kDa (3-nitro-tyrosine modification)

C$^{\#}$ +58kDa (Cysteine carbamidomethylation)

3NY formation at Tyr^{6} and Tyr^{14} was located as shown in figure 23 and 24 (mass spectrum of Y*VDSEGHLYTVPIR and mass spectrum of YVDSEGHLY*TVPIR respectively. Y* showed 3NY ion with m /z 209.16, which has increased mass of 45kDa in Y*VDSEGHLYTVPIR peptide. Also, in Figure 24, YVDSEGHLY*TVPIR peptide shows 3NY at Tyr^{14} confirming that peroxynitrite reaction selectively formed 3NY at Tyr^{6} and at increased concentration of peroxynitrite can form another 3NY site at Tyr^{14}. The nitrated Tyr residues, Tyr^{6} and Tyr^{14} are located in the cytosolic domain of caveolin-1, which should be fairly accessible to peroxynitrite.

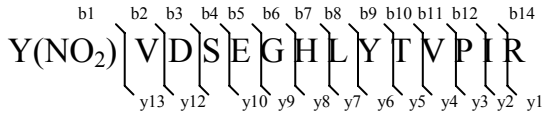

Charge	XC	Delta Cn
2	3.432	0.644

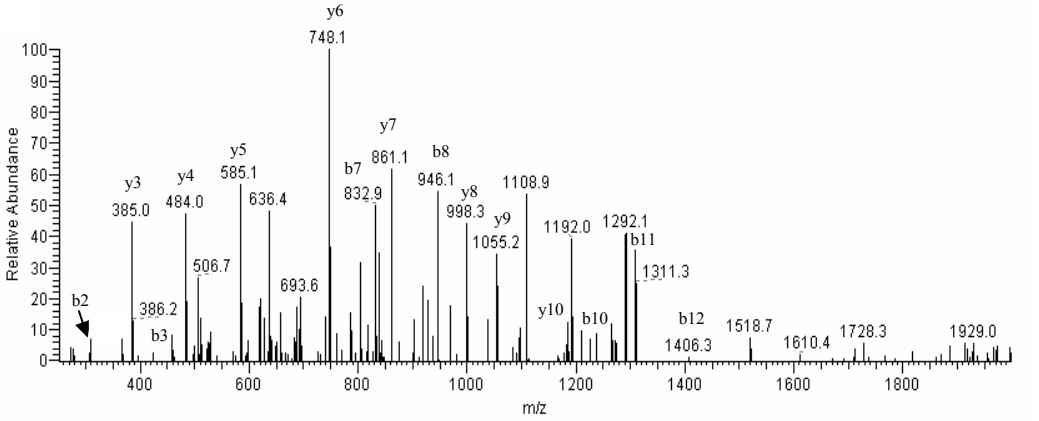

Figure 23. Peptide mass finger printing of caveolin-1 YVDSEGHLYTVPIR peptide from in-gel digestion of 22kDa band (sample C, lane 04). Nitration of Y^6

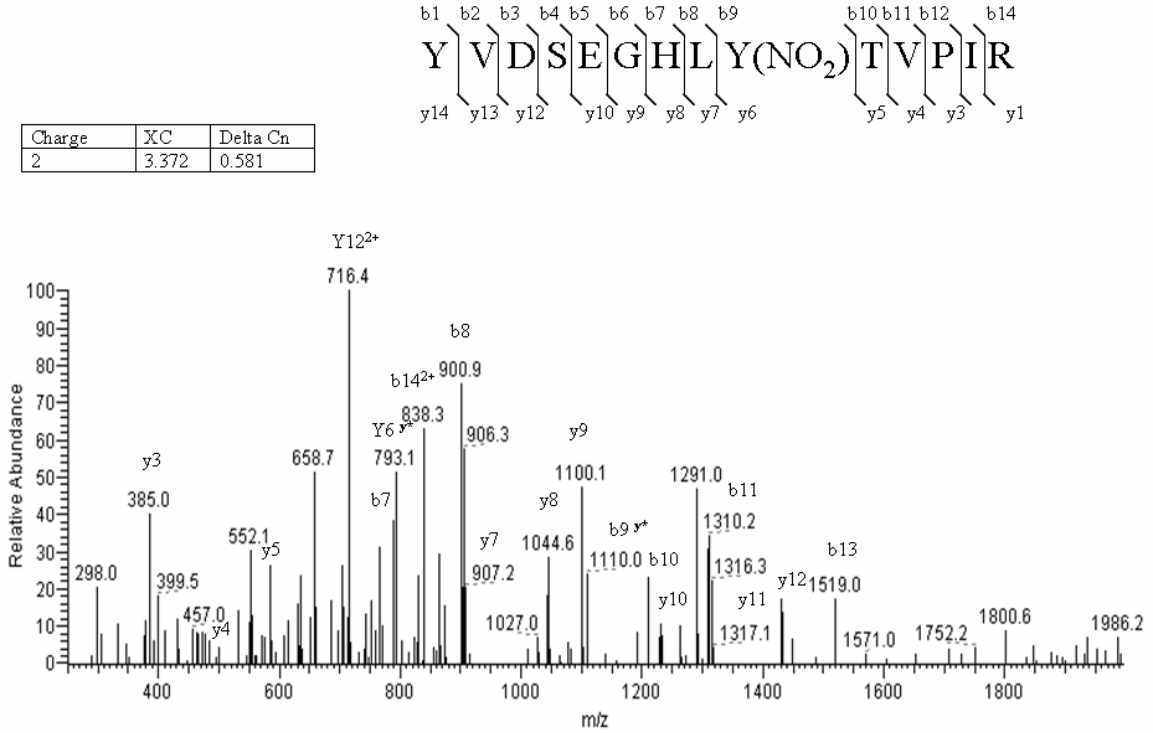

Figure 24. Peptide mass finger printing of caveolin-1 YVDSEGHLYTVPIR peptide from in-gel digestion of 22kDa (sample C, lane 04). Nitration of Y^{14}

Sample D, lane 5. Protein band at 22kDa

LC-ESI-MS analysis of sample D (figure 19) revealed the positive identification of canine caveolin-1 covering total of 13 peptides corresponding to 121 amino acids or 68% of caveolin-1 sequence. Within this protein sequence coverage, 6 tyrosines from the total of 9 tyrosines were detected.

From the ESI-MS analysis we could detect Tyr^{118} only in sample B. This could be due to its location in the hydrophobic transmembrane domain (between residues 110-131) of caveolin-1 sequence.

Table 8. Peptides with reportable scores from MS analysis of sample D

(Figure 19, lane 5, 22kDa)

Peptide	Charge	XC	Delta Cn
EQGNIYKPNNK	2	2.3	0.417
YVDSEGHLY*TVPIR	2	1.943	0.722
Y*VDSEGHLYTVPIR	2	3.638	0.466
HLNDDVVK	2	3.389	0.600
ELDLVNR	2	2.146	0.429
VYSIYVHTFTFC#DPFFEAVGK	3	2.590	0.413
IDFEDVIAEPEGTHSFDGWK	3	3.051	0.498

Y* +45kDa (3 Nitro-tyrosine modification)

C# +58kDa (Cysteine carbamidomethylation)

Figures 25 and 26 show the mass spectrum of Y*VDSEGHLYTVPIR and the mass spectrum of YVDSEGHLY*TVPIR peptides respectively. These results are

consistent with the results obtained from the samples B & C. Six tyrosine residues of canine caveolin sequence were detected and this result confirms that peroxynitrite selectively nitrates Tyr^{6} and Tyr^{14}.

The peptide, LLSALFGIPMALIWGIYFAILSFLHIWAVVPCIK (residues 102-147) was detected only in sample B. This peptide is located in the hydrophobic domain of caveolin and contains Y^{118}. As Y^{118} is in the hydrophobic transmembrane domain of caveolin-1, the accessibility for oxidative agents could be limited.

In sample A, which was not treated with peroxynitrite, we could detect Y^{6}, Y^{14}, Y^{25}, Y^{42} and nitration of tyrosines was not observed from ESI-MS analysis. In sample B, which was treated with peroxynitrite 100μM we could detect Y^{6}, Y^{14}, Y^{25}, Y^{42}, Y^{118}, Y^{148} and Y^{151} and nitration was detected in Y^{6}.

In sample C, treated by peroxynitrite 200μM, we could detect Y^{6}, Y^{14}, Y^{25}, Y^{42}, Y^{97}, Y^{100} and Y^{148}, Y^{151} from C-terminal of caveolin-1. The analysis of sample C from ESI-MS showed that peroxynitrite selectively nitrated Y^{6} and Y^{14} from the detected 6 tyrosines with the concentration of peroxynitrite was increased from 100μM to 200μM.

In sample D, treated by peroxynitrite 300μM, Y^{6}, Y^{14}, Y^{25}, Y^{42} from the N-terminal domain and Y^{148}, Y^{151} from C-terminal of caveolin-1 was detected. It was confirmed that only Y^{6} and Y^{14} were nitrated with increasing amounts of peroxynitrite. These 2 tyrosines are located in a single peptide in the N-terminal hydrophilic domain of caveolin-1.

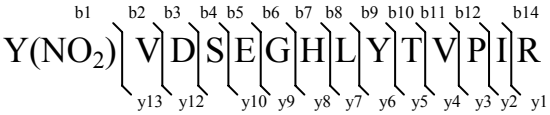

Charge	XC	Delta Cn
2	3.146	0.452

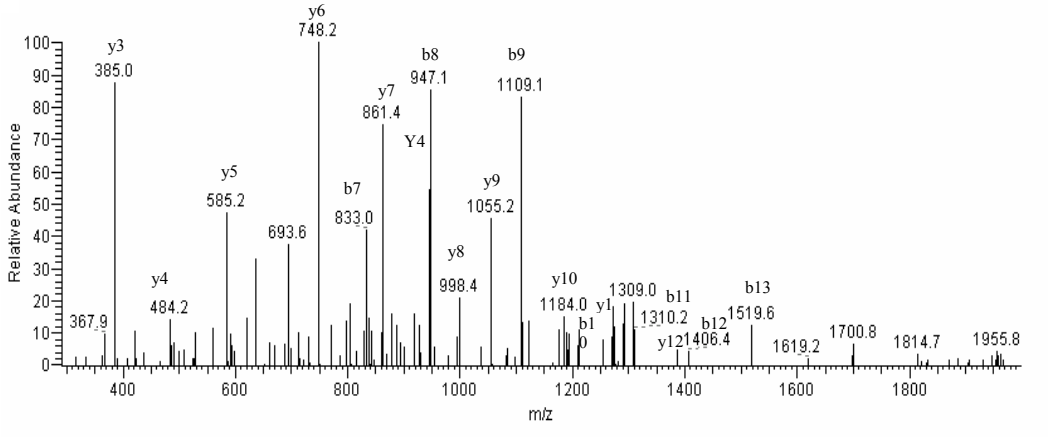

Figure 25. Peptide mass finger printing of caveolin-1 YVDSEGHLYTVPIR peptide from in-gel digestion of 22kDa (sample D, lane 05). Nitration of Y^6

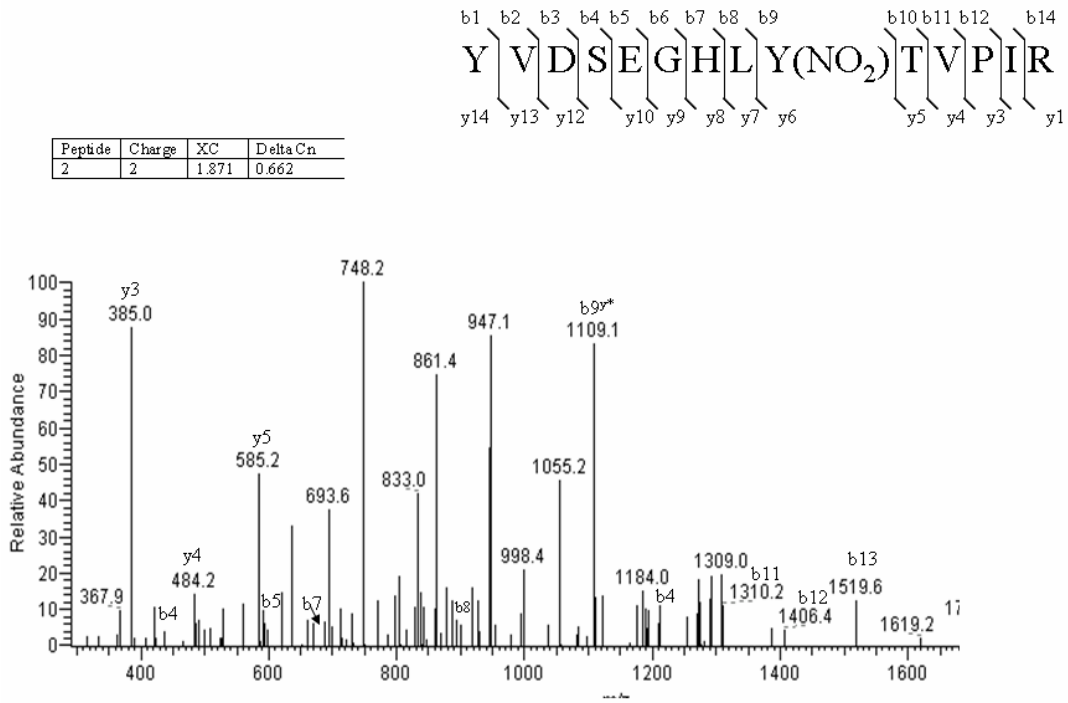

Figure 26. Peptide mass finger printing of caveolin-1 YVDSEGHLYTVPIR peptide from in-gel digestion of 22kDa (sample D, lane 05). Nitration of Y^{14}

Sample E, lane 6. Protein band at 44kDa

The band at 44kDa (dimer) (figure 19) is less dense in SDS-PAGE. The dimer showed at 44kDa in the western blot probed with anti caveolin mAb (Figure 20) as well as lane 5 in the western blot with anti 3NY mAb (Figure 21). These results suggested that either the nitration of the dimer with the increased peroxynitrite concentration of 300μM, or with increased peroxynitrite concentration, result in an increase in dimer concentration. The less dense bands at 44kDa at each lane were excised and combined (sample E) for ESI-MS analysis. Peptides isolated from sample E provided positive identification of canine caveolin-1 covering a total of 5 peptides corresponding to 43 amino acids or 25% of the canine caveolin sequence. Within this protein sequence coverage, 3 tyrosines from the total of 9 tyrosines were detected. The reason for the low protein sequence coverage could be the lower sample concentration and we could not detect any modifications within this sequence coverage.

Table 9. Peptides with reportable scores from MS analysis of sample E (44kDa, lanes 2, 3, 4 & 5)

Peptide	Charge	XC	Delta Cn	Sp
YVDSEGHLYTVPIR	2	3.095	0.493	1009.4
HLNDDVVK	2	2.837	0.552	1448.9

Summary of the results

Table 10. Reaction of different concentrations of peroxynitrite with caveolin 14μM in STE buffer (caveolin isolation buffer), pH 8.5. Results of western blotting probed with anti-caveolin monoclonal antibody (mAb)

Western blotting probed with anti-caveolin mAb				
Peroxynitrite	0μM	100μM	200μM	300μM
Presence of a band at 22kDa (monomer)	+	+	+	+
Presence of a band at 44kDa (dimer)	-	+	+	+
Presence of oligomer between 88-250kDa	-	+	+	+

Table 11. Reaction of different concentrations of peroxynitrite with caveolin 14μM in STE buffer (caveolin isolation buffer), pH 8.5. Results of western blotting probed with anti-nitrotyrosine monoclonal antibody

Western blotting probed with anti-nitrotyrosine mAb				
Peroxynitrite	0μM	100μM	200μM	300μM
Presence of a band at 22kDa (monomer)	-	+	+	+
Presence of a band at 44kDa (dimer)	-	-	-	+
Presence of the oligomer between 88-250kDa	-	+	+	+

Table 12. Reaction of different concentrations of peroxynitrite with caveolin (14μM) in STE buffer (caveolin isolation buffer), pH 8.5. Results of in-gel digestion of samples A, B, C and D from SDS-PAGE gel (figure 19)

Sample no.	Caveolin concentration	ONOO- concentration	Nitrated peptides	Nitrated Y residues
A	14μM	0μM	-	-
B	14μM	100μM	Y*VDSEGHLYTVPIR	Y6
C	14μM	200μM	Y*VDSEGHLYTVPIR YVDSEGHLY*TVPIR	Y6, Y14
D	14μM	300μM	Y*VDSEGHLYTVPIR YVDSEGHLY*TVPIR	Y6, Y14

4.c.2 Discussion

In the present study we investigated the *in vitro* reaction of peroxynitrite with caveolin-1 in STE buffer (caveolin isolation buffer) at pH 8.5. We have chosen a widely established proteomic approach i.e. SDS-PAGE for protein separation followed by peptide mass mapping by means of ESI-MS/MS. SDS-PAGE is robust and fairly reproducible, which makes it suitable for western blot analysis. Using this method we investigated peroxynitrite mediated post-translational modifications of caveolin-1 *in vitro*.

Excessive production of nitric oxide ($^{\cdot}NO$) and superoxide ($O_2^{\cdot -}$) free radicals is related to cell and tissue pathology.[46] One of the major injury mechanisms associated with the production of nitric oxide in vivo is due to its diffusion-limited reaction with superoxide to form peroxynitrite. Peroxynitrite modifies amino acids such as tyrosine, cysteine, tryptophan and methionine.[43] Superoxide rapidly combines with nitric oxide, with the energy release of 22kcal/mol.[92]

$$O_2^{\cdot -} + {}^{\cdot}NO \longrightarrow {}^{-}OONO$$

The larger Gibbs energy makes this reaction essentially irreversible. The second order reaction rate for the formation of peroxynitrite[92] is $6.7 \pm 0.9 \times 10^9$ $M^{-1}s^{-1}$.

Western blotting with anti-caveolin monoclonal antibody (figure 20) of the reaction of peroxynitrite with caveolin-1 in STE buffer pH 8.5 clearly showed that caveolin-1 forms a dimer and oligomer upon the addition of 100μM of peroxynitrite. The oligomer formation of caveolin-1 is increased as a function of increasing peroxynitrite concentration up to 300μM.

The nitration of caveolin-1 in the isolation buffer (STE pH 8.5) showed nitration of monomer as a dense band at 22kDa when reacted with peroxynitrite 100μM. This was increased as a function of increasing peroxynitrite concentration up to 300μM (figure 21). Also, lane 5 in figure 21 showed nitration of the dimer and lane 3, 4 & 5 showed nitration of the oligomer. Figure 21 clearly show that the nitration of oligomer is increasing as a function of increasing peroxynitrite concentration.

At pH 8.5 peroxynitrite exists as an anion and it can undergo the reactions[51] depicted below.

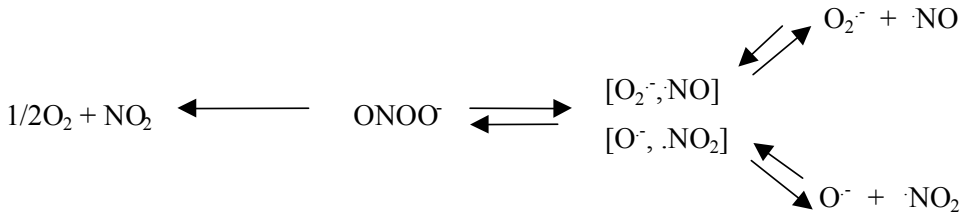

The rate constants for generation of $O_2^{\cdot -}$ and O^{-} from $ONOO^{-}$ have been shown to be 1.7 $x10^{-2}s^{-1}$ and $3x10^{-6}s^{-1}$ respectively.[51] $ONOO^{-}$ itself and also $O_2^{\cdot -}$,

$^{\cdot}NO$, O^{-} and $^{\cdot}NO_2$ radicals can act as oxidative and nitrative agents at alkaline pH.[51]

Peroxynitrite is a strong oxidant[52], which can directly oxidize sulfhydryl groups to disulfides (figure 06). Oxidative role of peroxynitrite is responsible for caveolin-1 oligomer formation (figure 28) upon peroxynitrite treatment. We added 200mM of dithiothreitol (DTT) in SDS-PAGE, which is able to reduce disulfide bonds. As we could observe caveolin-1 oligomer formation, it is obvious that peroxynitirite can cause formation of covalent bonds as SDS and DTT were not able to prevent caveolin-1 oligomer formation. The stability of caveolin-1 oligomers suggests that the coupling mechanism is most likely occurrs via a covalent bridge. A protein crosslink due to a covalent bond can occur due to cystein disulfide bond formation (figure 6) or formation of dityrosine (figure 5). In fact disulfide bonds can be reduced by DTT, but the steric restrictions due to caveolin-1 oligomer formation may limit the accessibility of DTT to reduce the disulfide bonds formed due to the reaction with peroxynitrite.[67] Dityrosine formation in caveolin-1 upon peroxynitrite treatment was investigated and detected the fluorescence signature of 3,3'-dityrosine at λ_{ex}=283nm and λ_{em}=410nm and will be described in section 4 f.

In gel tryptic digests of the samples A-E (figure 19) was analyzed by ESI-MS-MS analysis and searched the canine database from NCBI using TURBOSEQUEST algorithm. We searched these samples for post-translational modifications upon the reaction with peroxynitrite. The mass changes searched

were methionine +16kDa, cysteine +58kDa, cysteine +48kDa, and tyrosine +45kDa and methionine +32kDa. ESI-MS/MS revealed only the nitrative modifications of specific tyrosine residues of caveolin-1 from this analysis.

Tyrosine nitration is a convenient marker of reactive nitrogen centered oxidants being produced. Peroxynitrite is the most likely source in vivo for nitrotyrosine formation.[93] Protein tyrosine nitration is a fairly selective process. Most mammalian proteins contain approximately 4 mol% of tyrosines.[57] We could obtain about 60% of coverage from canine caveolin sequence. Caveolin-1 has 9 tyrosines and we were able to detect 8 tyrosines except Tyr 118. ESI-MS/MS analysis confirmed that only Tyr^6 showed selective nitration upon 100μM of peroxynitrite treatment in STE buffer pH 8.5. Tyr^6 and Tyr^{14} residues were nitrated with the increasing peroxynitrite concentration up to 300μM (table 13). These 2 tyrosine residues are located in a same peptide YVDSEGHLYTVPIR.

The residues Y^6, Y^{14}, Y^{25}, Y^{42} are located in the cytosolic N-terminal domain and Y^{148}, Y^{151} are in the C-terminal domain of caveolin-1. Although, all of these residues should be fairly accessible to reactive nitrogen species, it was shown that peroxynitrite 100μM concentration was selectively nitrated Y^6 and Y^{14}only. The Tyr residues, which are located in C-terminal domain, did not show nitration. Caveolin-1 cysteine residues C^{133}, C^{142} and C^{156} are located in C-terminal domain of caveolin-1. These cysteine residues can undergo modifications such as cysteine palmitoylation and disulfide bond formation,

which may cause steric interference with the nitration of tyrosine residues which are located at C-terminal domain.

The nitration of this peptide was observed with either nitration of Y^6, as shown in figure 23 or nitration of Y^{14}, as shown in figure 24 only. We repeated this experiment several times and this peptide did not show the nitrative modification on both Y^6 and Y^{14} residues simultaneously. The reason the nitration of a single tyrosine residue at one time could be if one tyrosine residue is nitrated it may cause steric hindrance of the nitration of the other tyrosine residue in the same peptide.

Tyr 118, which is located in the peptide, LLSALFGIPMALIWGIYFAILSFLHIWAVVPCIK (residues 102-147) was detected only in sample B which was nitrated caveolin-1 with 200μM of peroxynitrite from all the samples analyzed. This peptide is located in the hydrophobic domain of caveolin-1. As Y^{118} is in the hydrophobic trans-membrane domain of caveolin-1, the accessibility for oxidative agents also could be limited.

4.c.3 Conclusion

Peroxynitrite mediated *in-vitro* post-translational modifications of caveolin-1 upon the treatment of different concentrations of peroxynitrite was investigated in this study. The dimer and oligomer formation of caveolin-1 with the treatment of peroxynitrite 100μM was observed and this was increased as a function of increasing peroxynitrite up to 300μM. Oxidative role of peroxynitrite could be responsible for caveolin-1 oligomer formation. The stability of caveolin-1 oligomer suggests that the coupling mechanism most likely occurred via a covalent bond due to dityrosine formation or disulfide bond formation.

ESI-MS/MS analysis of caveolin-1 revealed that peroxynitrite can selectively nitrate Tyr^{6} and Tyr^{14} located in YVDSEGHLYTVPIR, at the concentration of 300μM peroxynitrite. These 2 tyrosine residues are located in the cytosolic N-terminal domain of caveolin-1, which could be fairly accessible to peroxynitrite. We report the selective nitration of Y^{6} and Y^{14} tyrosine residues of caveolin-1 at pH 8.5. This result is further investigated under the physiological conditions.

4.d Reaction of different concentrations of peroxynitrite with caveolin in phosphate buffer (physiological conditions) pH 7.5

4.d. 1 Results

Purified caveolin-1 (14μM) in phosphate buffer at physiological pH (pH 7.5)[45] was treated with 0, 100, 200, 300 and 400μM peroxynitrite in the presence of 25mM $NaHCO_3$. Carbonate is present in physiological fluids at a concentration of approximately 25mM[51]. SDS-PAGE and SDS-PAGE followed by western blotting with anti caveolin mAb (1:10,000 dilution in T-TBS), and anti 3-nitrotyrosine mAb (1:5,000 in T-TBS) were carried out to detect the reaction of peroxynitrite with caveolin. Also, visualized gel bands in SDS-PAGE was further analyzed by ESI-MS/MS to detect post-translational modifications.

Figure 27 shows the analysis of the above reaction using SDS-PAGE followed by Coomassie staining. Lane 01 is a protein molecular weight standard. Lanes 2,3,4 and 5 shows a band at 22 kDa, which is caveolin-1 monomer. Interestingly this gel shows that as a function of increasing peroxynitrite concentration, a significant decrease of the density of the band at 22 kDa. Caveolin-1 dimer is shown around 44kDa, as a less dense band in figure 27. The SDS-PAGE shown in figure 26 was further analyzed by western blotting with anti-caveolin monoclonal antibody (figure 28), and anti-nitrotyrosine monoclonal antibody (Figure 29). The samples F, G, H, I, J at 22kDa, sample K at 44kDa, and L, M at oligomer (125-175kDa), as shown in figure 27, were analyzed by mass spectrometry to detect post-translational modifications.

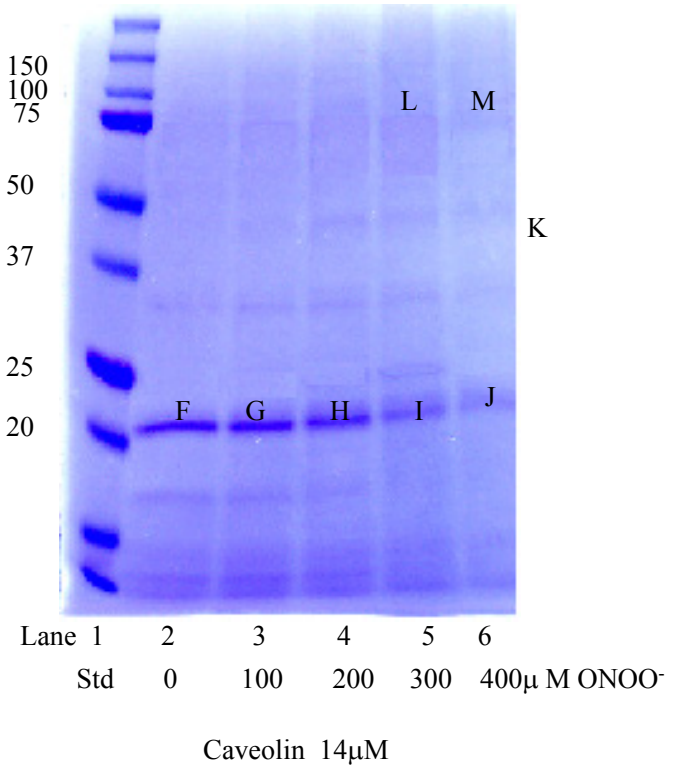

Figure 27. Reaction of different concentrations of peroxynitrite with caveolin-1 (14µM) in phosphate buffer pH 7.5 (physiological conditions), SDS-PAGE followed Coomassie staining. Lane 1- Protein standard, Lane 2- Caveolin-1 not treated with $ONOO^-$, Lane 3- Caveolin-1 treated with 100µM of $ONOO^-$, Lane 4- Caveolin-1 treated with 200µM of $ONOO^-$, Lane 5- Caveolin-1 treated with 300µM of $ONOO^-$, Lane 6- Caveolin-1 treated with 400µM $ONOO^-$.

Reaction Conditions: Phosphate buffer (25mM NaH_2PO_4, 150mM NaCl, 3mM EDTA), 25mM $NaHCO_3$

Figure 28 shows the western blotting with anti-caveolin monoclonal antibody (1:10,000) of caveolin-1 in phosphate buffer treated with peroxynitrite. Lane 1 is the protein molecular weight standard. Untreated caveolin-1 that was loaded in lane 2 shows caveolin-1 monomer. Lanes 3, 4, and 5 that were treated caveolin-1 with increasing concentrations of peroxynitrite showed 22kDa band as well as a band at 44 kDa. Also oligomerization of caveolin-1 was shown between 88kDa and 250 kDa in the lanes 3, 4 and 5 which were treated with peroxynitrite.

In the western blotting with anti-caveolin monoclonal antibody (figure 28) clearly shows that the density of the band at 22 kDa and 44kDa decreases as a function of increasing concentration of peroxynitrite. The reduction in the level of caveolin-1 monomer and dimer coincides with the appearance of caveolin-1 oligomer between the molecular weight range of 88kDa to 250kDa. Also, the density of the oligomer was increasing as a function of increasing peroxynitrite concentration. To detect possible post-translational modifications of caveolin-1 under physiological conditions, the visualized gel bands (F-M) in SDS-PAGE (figure 27) were further analyzed by ESI-MS/MS.

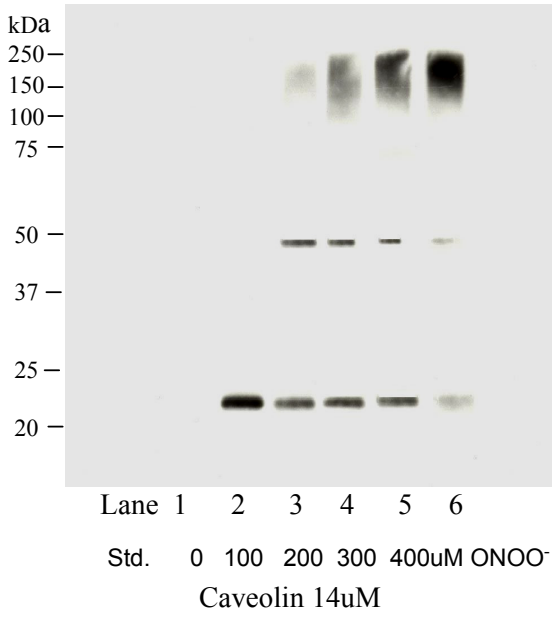

Figure 28. Reaction of different concentrations of peroxynitrite with caveolin-1 (14μM) in phosphate buffer pH 7.5 (physiological conditions), SDS-PAGE followed by western blotting probed with anti-caveolin antibody (1:10,000 dilution). Lane 1- Protein standard, Lane 2- Caveolin-1 not treated with $ONOO^-$, Lane 3- Caveolin-1 treated with 100μM of $ONOO^-$, Lane 4- Caveolin-1 treated with 200μM of $ONOO^-$, Lane 5- Caveolin-1 treated with 300μM of $ONOO^-$, Lane 6- Caveolin-1 treated with 400μM $ONOO^-$.

Reaction Conditions: Phosphate buffer (25mM NaH_2PO_4, 150mM NaCl, 3mM EDTA), 25mM $NaHCO_3$

To detect nitrotyrosine formation in caveolin-1 treated with peroxynitrite at physiological pH, and in the presence of carbonate, western blotting with anti-nitrotyrosine antibody was done as shown in figure 29. Lane 1 is the molecular weight standard (Bio Rad 161-0374). Lane 2 is untreated caveolin-1 and it didn't show any band at 22kDa. Lane 3, 4, 5 and 6 were treated with peroxynitrite 100, 200, 300 and 400μM respectively. Lanes 3 and 4, which were treated with peroxynitrite 100 and 200μM, didn't show any nitration. Lane 4, caveolin-1 treated with peroxynitrite 300μM, did not show any nitration at 22 kDa or 44kDa, but showed some extent of nitration in the oligomer. Lane 6, caveolin-1 treated with peroxynitrite 400μM showed a less dense band at 22kDa (monomer) and 44kDa (dimer). In this lane, nitration of the oligomer was observed between 88kDa and 250kDa.

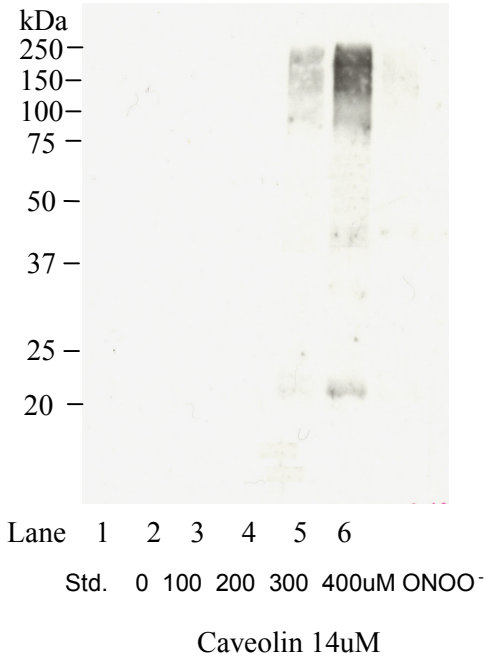

Figure 29. Reaction of different concentrations of peroxynitrite with caveolin-1 (14μM) in phosphate buffer pH 7.5 (physiological conditions), SDS-PAGE followed by western blotting probed with anti-nitrotyrosine antibody (1:5,000 dilution). Lane 1- Protein standard, Lane 2- Caveolin-1 not treated with $ONOO^-$, Lane 3- Caveolin-1 treated with 100μM of $ONOO^-$, Lane 4- Caveolin-1 treated with 200μM of $ONOO^-$, Lane 5- Caveolin-1 treated with 300μM of $ONOO^-$, Lane 6- Caveolin-1 treated with 400μM $ONOO^-$.

Reaction Conditions: Phosphate buffer p h 7.5 (25mM NaH_2PO_4, 150mM NaCl, 3mM EDTA), 25mM $NaHCO_3$

Summary of the results

Table 13. Reaction of different concentrations of peroxynitrite with caveolin (14μM) in phosphate buffer pH 7.5 (physiological conditions). Results of western blotting probed with anti-caveolin monoclonal antibody.

Western blotting with anti-caveolin mAb					
Peroxynitrite	0μM	100μM	200μM	300μM	400μM
Presence of a band at 22kDa (monomer)	+	+	+	+	+
Presence of a band at 44kDa (dimer)	-	+	+	+	+
Presence of the oligomer between 88-250kDa	-	+	+	+	+

Table 14. Reaction of different concentrations of peroxynitrite with caveolin (14μM) in phosphate buffer pH 7.5 (physiological conditions). Results of western blotting probed with anti-nitrotyrosine monoclonal antibody.

Western blotting probed with anti-nitrotyrosine mAb					
Peroxynitrite	0μM	100μM	200μM	300μM	400μM
Presence of a band at 22kDa (monomer)	-	-	-	-	+
Presence of a band at 44kDa (dimer)	-	-	-	-	+
Presence of the oligomer between 88-250kDa	-	-	-	+	+

MS Analysis of gel bands

ESI-MS analysis of the gel bands F to J (figure 27) at monomer 22kDa, gave positive identification of canine caveolin-1 but we could not detect any nitration of the monomer under physiological conditions. Also the sample K (the gel band at 44kDa) gave positive identification of canine caveolin-1 and the nitration was not detected by MS. For sample L and M gel bands were excised between 100-175kDa, which showed the oligomer in western blotting probed with anti-caveolin antibody (figure28) and could not detect clear bands in SDS-PAGE. Sample L revealed 44% sequence coverage with positive identification of canine caveolin-1. Sample M revealed the positive identification of canine caveolin-1 covering total of 12 peptides corresponding to 139 amino acids or 80% of canine caveolin-1 sequence confirming that caveolin-1 forms an oligomer upon peroxynitrite reaction. The reason for not detecting any modifications of caveolin-1 may be that the extent of nitration of the oligomer in SDS-PAGE gel is below the MS detection limits.

As the western blotting with anti-nitrotyrosine revealed some extent of nitration when caveolin-1 treated with peroxynitrite 300μM, 400μM, in-solution trypsin digestion was carried out to detect possible nitration of specific residues of caveolin-1.

Post-translational modifications of caveolin in physiological conditions-peroxynitrite reaction with caveolin-1, detection by in-solution trypsin digestion and ESI-MS/MS

Three samples were prepared by adding 0μM (sample A), 300μM (sample B) and 400μM (sample C) of peroxynitrite to 14μM 0f caveolin-1 in phosphate buffer as we could observe the nitration of caveolin-1 by adding peroxynitrite 300μM and 400μM in western blotting with anti-nitotyrosine monoclonal antibody (figure 29). These three samples were subjected to in-solution tryptic digestion to detect post-translational modifications using ESI-MS/MS.

In-solution trypsin digestion of sample A, which has no peroxynitrite gave positive identification of canine caveolin-1 with 34% of sequence coverage and did not show any nitrative modifications. Sample B, which has 300μM of peroxynitrite, gave positive identification of canine caveolin-1 with 36% sequence coverage and we could not detect any nitrated amino acid residues. Also when considering about the western blotting with anti-nitrotyrosine antibody (figure 29) lane 5, which was treated caveolin 14μM with peroxynitrite 300μM showed less nitration only at the oligomer (around 100-250kDa).

Peptides extracted from sample C that is caveolin-1 (14μM) treated with 400μM of peroxynitrite were analyzed by ESI-MS. This resulted in positive identification of canine caveolin-1 with a total of 6 peptides corresponding to 43% of the canine caveolin-1 sequence.

Table 15. Peptides with reportable scores from MS analysis of sample C (in-solution trypsin digestion)

Peptide	Charge	XC	Delta Cn
HLNDDVVK	2	3.151	0.564
EIDLVNRDPK	2	1.976	0.654
Y*VDSEGHLYTVPIR	2	3.250	0.392
YVDSEGHLY*TVPIR	2	1.824	0.259

Y* +45kDa (3-nitrotyrosine modification)

3NY formation at Tyr^6 and Tyr^{14} was located as shown in figures 30 and 31 (mass spectrum of Y*VDSEGHLYTVPIR and mass spectrum of YVDSEGHLY*TVPIR peptide respectively). The nitration of Y^6 showed 3 nitrotyrosine ion with 209.16, m/z correspond to an increased mass of 45 kDa in the Y*VDSEGHLYTVPIR peptide. In figure 31, which shows YVDSEGHLY*TVPIR peptide shows m/z 209.13 mass difference between y5 (584.17) and y6 (793.3) which shows increased mass of 45kDa in the YVDSEGHLY*TVPIR peptide. This result confirms that the reaction of peroxynitrite selectively formed 3NY at Tyr^6 and Tyr^{14}. The nitrated Tyr residues, Tyr^6 and Tyr^{14} are located in the cytosolic N-terminal domain of caveolin-1.

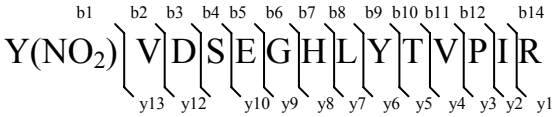

Charge	XC	Delta Cn
2	2.581	0.505

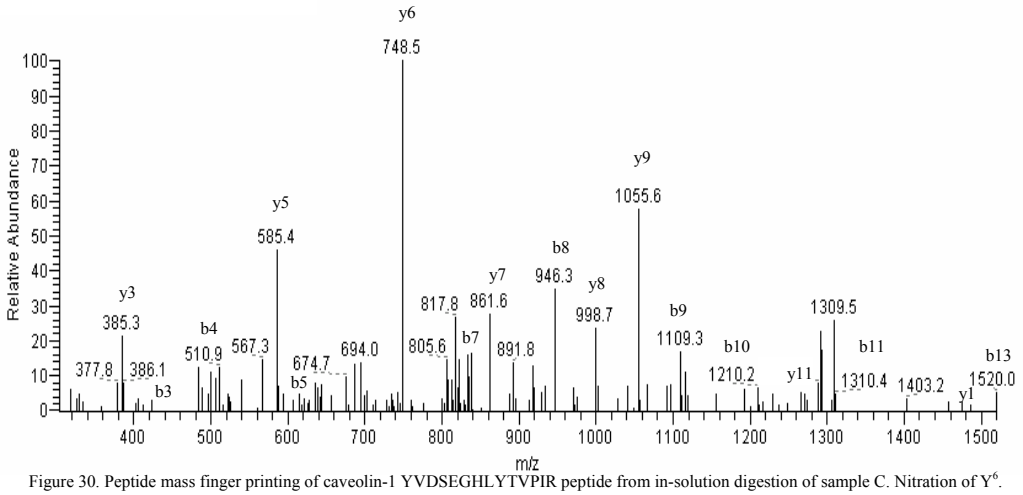

Figure 30. Peptide mass finger printing of caveolin-1 YVDSEGHLYTVPIR peptide from in-solution digestion of sample C. Nitration of Y^6. (caveolin-1 14μM in phosphate buffer treated with 400μM peroxynitrite).

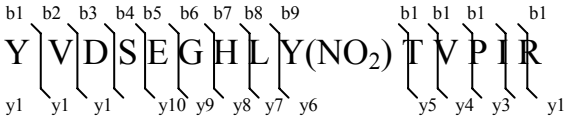

Charge	XC	Delta Cn
2	1.824	0.259

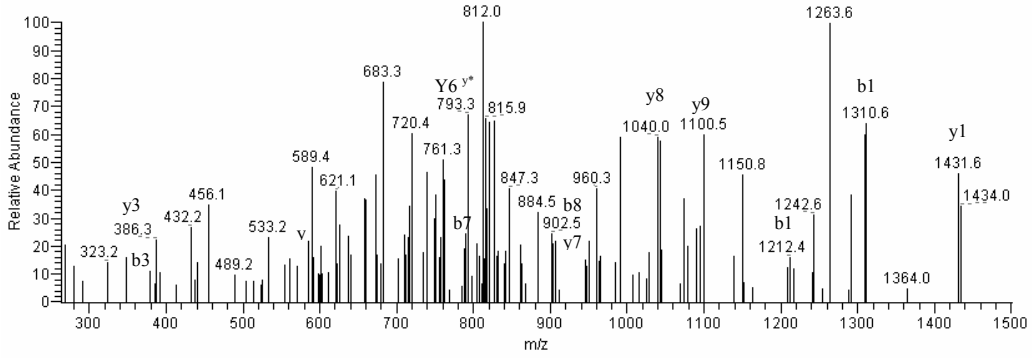

Figure 31. Peptide mass finger printing of caveolin-1 YVDSEGHLYTVPIR peptide from in-solution digestion of sample C

Summary of the results

Table 16. Reaction of different concentrations of peroxynitrite with caveolin in phosphate buffer pH 7.5 (physiological conditions). Results of in-solution trypsin digestion of samples A, B and C

Sample no.	Caveolin concentration	ONOO- concentration	Nitrated peptides	Nitrated Y residues
A	14μM	0μM	-	-
B	14μM	300μM	-	-
C	14μM	400μM	Y*VDSEGHLYTVPIR YVDSEGHLY*TVPIR	Y6, Y14

The reaction of peroxynitrite with caveolin-1 under physiological conditions showed that Tyr^{6} and Tyr^{14} residues are selectively nitrated when adding 400μM of peroxynitrite. This result is consistent with the MS analysis of nitration of caveolin by peroxynitrite (300μM) in caveolin isolation buffer (STE pH8.5) which showed the nitration of Tyr^{6} and Tyr^{14} residues.

4.d.2 Discussion

We investigated the *in vitro* reaction of peroxynitrite with caveolin-1 in phosphate buffer with the presence of 25mM carbonate at pH 7.5 (physiological conditions). At pH 7.5 peroxynitrite can be protonated and exists as peroxynitrous acid. Peroxynitrous acid is a strong oxidant that can react with biological molecules by a number of complex mechanisms. It is particularly efficient at oxidizing iron/sulfur centers, zinc fingers and protein thiols.[94] Augusto and coworkers studied peroxynitrite decompositions and they reported an electron spin resistance (ESR) spectrum that is characteristic of the hydroxyl radical spin abduct.[94]

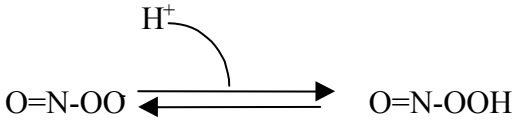

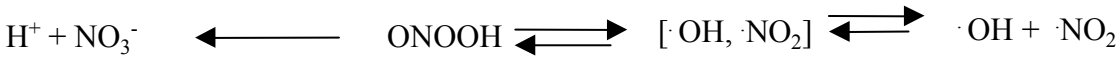

Caveolin-1 form dimer at 44kDa and oligomer between 88kDa and 250kDa upon the addition of peroxynitrite under the physiological conditions (figure 28, western blotting probed with anti-caveolin antibody). We could observe decrease of monomer and dimer concentrations with increasing concentration of peroxynitrite. The decrease of the caveolin-1 monomer and dimer coincides with the appearance of caveolin-1 oligomer (figure 28). The density of the oligomer was increasing as a function of increasing peroxynitrite concentration.

ONOOH-derived $^{\cdot}OH$ is a potent oxidant (reduction potential E= 2.3V)[44], which can oxidize amino acids such as tyrosine, methionine and cysteine. Nitrogen dioxide is an oxidant (E=0.99V) as well as a nitrating radical. After reacting caveolin-1 with peroxynitrite we added 200mM of DTT, which is able to reduce disulfide bonds. As we could observe caveolin-1 oligomer formation, it is obvious that peroxynitrite can cause formation of covalent bonds. DTT was not able to prevent caveolin-1 oligomer formation. The stability of caveolin-1 oligomers suggests that the coupling mechanism most likely occurred via a covalent bridge. A protein crosslink due to a covalent bond can occur due to cysteine disulfide bond formation (figure 6) or formation of dityrosine (figure 5). The disulfide bonds can be reduced by DTT, but the steric restrictions due to caveolin-1 oligomer formation may limit the accessibility of DTT to reduce the disulfide bonds formed due to the reaction with peroxynitrite.[67] Dityrosine formation in caveolin-1 upon peroxynitrite treatment was investigated and the

fluorescence signature of 3,3'-dityrosine at λ_{ex}=283nm and λ_{em}=410nm was detected. It will be described in section 4 f.

Under normal conditions, cholesterol moves directly to surface caveolae within minutes after being synthesized in the endoplasmic reticulum (ER) in human fibroblasts. Then cholesterol moves rapidly from caveolae to other regions of the plasma membrane and extracellular space.[96] The rapid transport of new cholesterol to the lymphocyte cell surface is dependent on the expression of caveolin-1.[97,98] Non palmitoylated caveolin-1 can be impaired in the transport of new cholesterol in lymphocyte cells.[98] Palmitoylation of caveolin-1 cysteine residues at positions 143 and 156 is required for cholesterol binding and transport from ER to plasma membrane. Cysteine residues of caveolin-1 may form oligomers as a result of disulfide bond formation with the reaction of peroxynitrite. This may lead to hinder palmitoylation of caveolin-1 cysteine residues and can impair cholesterol transport. However, this phenomenon should be further investigated to find out details such as which cysteine residues of caveolin-1 can form disulfide bonds with the reaction of peroxynitrite. If the caveolin-1 mediated cholesterol transport is impaired it may lead to diseases such as atherosclerosis and hypertension.[97,98]

Electron spin resistance (ESR) studies revealed the radical formation from peroxynitrous acid.[95] Oxidative attack of the polypeptide backbone is initiated by the hydroxyl radical dependent abstraction of the α-hydrogen atom of an amino acid residue. This can form a carbon-centered radical.[99] The carbon-centered

radical may react with another carbon-centered radical to form a protein – protein cross- link as shown below.

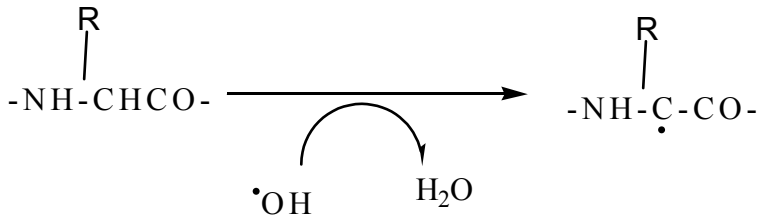

$$R^1C^{\bullet} + R^2C^{\bullet} \longrightarrow R^1C\text{-}CR^2$$

We could observe caveolin-1 dimer and oligomer formation upon the treatment of peroxynitrite. (figure 20) which suggests the formation of a protein-protein cross-link. The reaction of carbon-centered radical with another carbon-centered radical to form a protein-protein cross-linked derivative was reported previously.[99] Protein cross-link via carbon-centered radical formation could be the other reason for caveolin-1 oligomer formation except disulfide bond formation and the formation of dityrosine.

Nitrotyrosine formation in caveolin-1 treated with peroxynitrite at physiological conditions (phosphate buffer pH 7.5, 25mM carbonate) was investigated using western blotting with anti-nitrotyrosine antibody (figure 29). We could not detect any nitration when caveolin-1 reacted with peroxynitrite at

100μM or 200μM. Upon the addition of peroxynitrite 300μM, a faint band corresponding to the oligomer was observed (figure 29, lane 4). When caveolin-1 was exposed to peroxynitrite 400μM, nitration at the oligomer is observed (lane 6, figure 29). In this lane a less dense band at 22kDa and 44kDa was observed.

This result confirms that the nitration of caveolin-1 is much less under the physiological conditions at pH 7.5 (figure 29) than in the STE buffer at pH 8.5 (figure 21). Peroxynitrite has a pKa of 7.4 ± 0.06 at 37^0C.[48] At pH 8.5 peroxynitrite itself acts as a strong nitrative agent and oxidative agent. At pH 7.5 peroxynitrite rapidly converts to peroxynitrous acid which forms the hydroxyl radical, an oxidative agent and $^{\cdot}NO_2$ which is a nitrative agent (Figure 03, reaction 09).[51,52]

Carbonate 25mM is present when peroxynitrite reacted with caveolin-1 underphysiological conditions (pH 7.5). In this experiment, caveolin-1 showed less nitration compared to pH 8.5 in STE buffer. $ONOO^-$ is unstable in the presence of carbonate.[50]

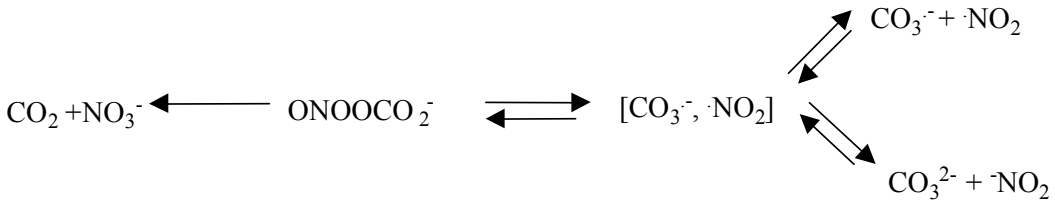

$ONOO^-$ reacts with CO_2 with the rate constant 3 x 10^4 M^{-1} s^{-1} forming the $ONO_2CO_2^-$ adduct.[52] This rate constant is sufficiently large that it could be the predominant pathway for peroxynitrite disappearance in normal physiological fluids. Carbonate concentration is approximately 25mM in physiological fluids.[50] CO_2 can effectively scavenge peroxynitrite generated in biological fluids. Therefore peroxynitrite is less damaging to cells under the physiological conditions.[50,51] This could be the reason for our observation of less nitration of caveolin-1 under physiological conditions in the western blotting with anti-nitrotyrosine antibody (figure 29).

To detect post-translational modifications of caveolin-1 upon the exposure to peroxynitrite under the physiological conditions, the in-gel tryptic digests of bands F to J in SDS-PAGE (figure 27) were subjected to ESI-MS/MS analysis. The mass changes searched were methionine +16kDa, cysteine +58kDa, cysteine +48kDa, and tyrosine +45kDa and methionine +32kDa. The in-gel digestion of the samples F-J (monomer) gave positive identification of canine caveolin-1 and nitration was not detected by MS. The sample K (gel band at 44kDa) gave positive identification of canine caveolin-1 and nitration was not observed. The samples L (lane 5, figure 27) and M (lane 6, figure 27) which were obtained from 100-175 kDa which showed oligomer in western blotting with anti-caveolin antibody revealed positive identification of canine caveolin-1 from the ESI-MS/MS analysis and did not show any nitration.

As the western blotting probed with anti-nitrotyrosine revealed some extent of nitration when caveolin-1 treated with peroxynitrite 300μM, 400μM, in-solution trypsin digestion was carried out to detect possible nitration of specific residues of caveolin-1.

In-solution trypsin digestion of sample A, which has no peroxynitrite gave positive identification of canine caveolin-1 with 34% of sequence coverage and did not show any nitrative modifications by ESI-MS/MS analysis. Sample B, which has 300μM of peroxynitrite, gave positive identification of canine caveolin-1 with 36% sequence coverage and we could not detect any nitrated amino acid residues. Also when considering about the western blot probed with anti-nitrotyrosine antibody (figure 29) lane 5, which was treated caveolin 14μM with peroxynitrite 300μM showed only a faint band at the oligomer (around 100-250kDa).

Peptides extracted from sample C, which is caveolin-1 (14μM) treated with 400μM of peroxynitrite were analyzed by ESI-MS. This was resulted positive identification of canine caveolin-1 with a total of 6 peptides corresponding to 43% of the canine caveolin-1 sequence. ESI-MS/MS analysis of in-solution trypsin digestion, confirmed that caveolin-1 is nitrated at the residues Y^{6} and Y^{14} upon the exposure to 400μM of peroxynitrite under the physiological conditions. If one considers dosage in terms of time x concentration, the bolus addition of 400μM (decaying only by proton-catalyzed decomposition) would be

equivalent to a physiologically relevant steady-state concentration of 11.2μM for 1min.[47]

ESI-MS/MS analysis showed the nitration of Tyr^6 and Tyr^{14} under physiological conditions (table 16). Several factors such as location of the tyrosine residue, nitrating agent and protein folding are expected to contribute to the nitration of specific tyrosine residues.[53,57] These two tyrosine residues are located in a same tryptic peptide YVDSEGHLYTVPIR, in the cytosolic N-terminal of caveolin-1, which should be fairly accessible to peroxynitrite. The schematic representation of nitration of caveolin-1 Tyr^6 and Tyr 14 is shown in figure 32.

Tyrosine nitration may interfere with tyrosine phosphorylation, which is an important regulator of signal transduction in cells. For example, Kong and coworkers showed that peroxynitrite mediated nitration of a single tyrosine residue in the cell cycle kinase cdc2 prevents tyrosine phosphorylation.[100] Gow and coworkers showed that formation of nitrotyrosine is responsible for the inhibition of tyrosine phosphorylation in endothelial cells exposed to peroxynitrite.[54] In this study, we found the selective nitration of Tyr^6 and Tyr^{14} of caveolin-1 exposed to peroxynitrite. Tyr^{14} is the only tyrosine residue within

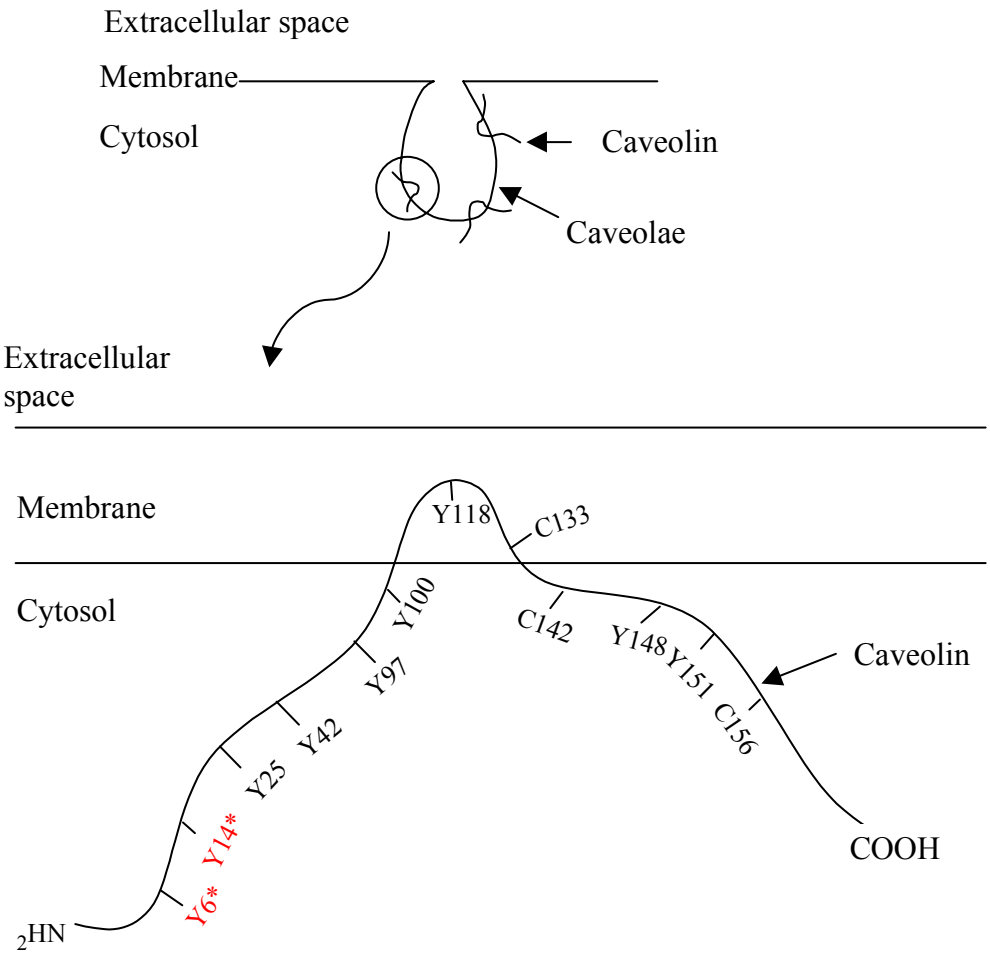

Figure 32. Tyrosine nitration (Y*) of caveolin-1. Y6 and Y14 residues in caveolin-1 is nitrated upon the treatment of $ONOO^-$ 400μM in physiological conditions (pH 7.5)

caveolin that bears resemblance to the known recognition motifs of v-Src and c-Abl tyrosine kinases.[38] Functional consequences of tyrosine phosphorylation of caveolin serving as a docking site for SH2 domain signaling molecules like activated growth factor receptors and recruit SH2 domain containing proteins to the cytoplasmic surface of the plasma membrane. This in turn leads to activation of down stream signaling cascades. If caveolin-1 Tyr^{14} is nitrated upon peroxynitrite treatment, it will interfere with phosphorylation of the same residue, which may therefore prevent recruiting SH2 domain containing proteins to the cytoplasmic surface of the plasma membrane.[38]

C-terminal Src kinase (Csk) negatively regulates the activities of Src family kinases by phosphorylating a conserved inhibitory tyrosine residue (527 in Src).[39] Csk is largely free in the cytosol while the Src family kinases are localized to lipid rafts in the plasma membrane. Csk is recruited to the plasma membrane by caveolin-1 phosphorylation. Csk binds specifically to phosphorylated caveolin-1. Activated Abl or Src tyrosine kinases phosphorylate caveolin-1 on tyrosine 14.[38] This leads to the recruitment of Csk and phosphorylation and inactivation of Src family kinases that are highly enriched in caveolae. The caveolin-1/Csk/Src kinase signaling complex involved in transmitting signals to the actin cytoskeleton.[39] We found that Tyr^{14} is nitrated when exposed to peroxynitrite. This could interfere with phosphorylation of caveolin-1 and this

may lead to inactivation of caveolin-1 function in the caveolin-1/Csk/Src kinase signaling complex.

4.d.3 Conclusion

In the present study, only the in-vitro reaction of caveolin-1 with peroxynitrite was investigated. We investigated the *in-vitro* reaction of peroxynitrite with caveolin-1 in phosphate buffer with the presence of 25mM carbonate at pH 7.5 (physiological conditions).

Caveolin-1 forms dimer and oligomer with the reaction of peroxynitrite under physiological conditions. Nitration and oxidation of caveolin-1 under physiolgical conditions (pH 7.5) is much less than at pH 8.5 as confirmed by the western blotting probed with anti-caveolin antibody (figure 20, figure 28) and anti-nitrotyrosine antibody (figure 21, figure 29).

Oxidative role of peroxynitrite is responsible for caveolin-1 oligomer formation upon peroxynitrite treatment. The stability of caveolin-1 oligomers suggests that the coupling mechanism most likely occurred via a covalent bridge such as dityrosine formation or via the formation of carbon-centered radicals.

In this study, we report nitration of specific tyrosine residues of caveolin-1 for the first time. Caveolin-1 has 9 tyrosines and ESI-MS/MS analysis confirmed that only selective nitration of Tyr6 and Tyr^{14} upon peroxynitrite treatment under the physiological conditions.

Under normal conditions tyrosine nitration may interfere with tyrosine phosphorylation, which is an important regulator of signal transduction in cells. Tyr^{14} is the only tyrosine residue within caveolin that bears resemblance to the known recognition motifs of v-Src and c-Abl tyrosine kinases[38]. If caveolin-1 Tyr^{14} is nitrated upon peroxynitrite treatment, it will interfere with phosphorylation of the same residue which may prevent recruiting SH2 domain containing proteins to the cytoplasmic surface of the plasma membrane[38].

C-terminal Src kinase (Csk) which negatively regulates the activities of Src family kinases binds specifically to phosphorylated caveolin-1 Tyr^{14}. We found that Tyr^{14} is nitrated when exposed to peroxynitrite. This could interfere with phosphorylation of caveolin-1 and in turn this may lead to inactivation of caveolin-1 function in caveolin-1/Csk/Src kinase signaling complex.

Oxidative and nitrative modifications due to reaction of peroxynitrite with caveolin-1 may lead to several pathological conditions in vivo. We were able to detect selective nitration of specific tyrosine residues of caveolin-1 and free radical damage to the protein with increased oxidative stress. Our study can provide authentic standards of modified proteins, which will be used to determine post-translational modifications of caveolin-1 in-vivo.

4.e Analysis of reducing effect of dithiothreitol (DTT) in caveolin-1 exposed to peroxynitrite by SDS-PAGE followed by western blotting with anti-caveolin monoclonal antibody

4.e.1 Results

Figure 33 shows analysis of the effect of dithiothreitol (DTT) in caveolin-1 exposed to peroxynitrite by SDS-PAGE followed by western blotting probed with anti-caveolin monoclonal antibody. Lane-1 is the protein molecular weight standard. $NaHCO_3$ 25mM was added to caveolin-1 (14μM) in phosphate buffer and this reaction was not exposed to peroxynitrite. 200mM of DTT was added after equilibration of the reaction mixture for 5 minutes (sample1). Lane 2 shows a dense band at 22kDa, which was recognized by anti-caveolin monoclonal antibody. In sample 2, 25mM $NaHCO_3$ was added to caveolin-1 (14μM) in phosphate buffer and this reaction was exposed to 200μM of peroxynitrite. 200mM of DTT was added after equilibration of the reaction mixture for 5 minutes. Lane 3 clearly shows that peroxynitrite reaction could form caveolin-1 dimer and oligomer. The density of the band at 22kDa (lane 3) is less than the density of the band at 22kDa in lane 2. No DTT was added to the 3rd sample, which is shown in lane 4. It shows dense oligomer and dimer. The density of the band at 22kDa, in lane 4 is much less than the 22kDa band in lane 2 and lane 3.

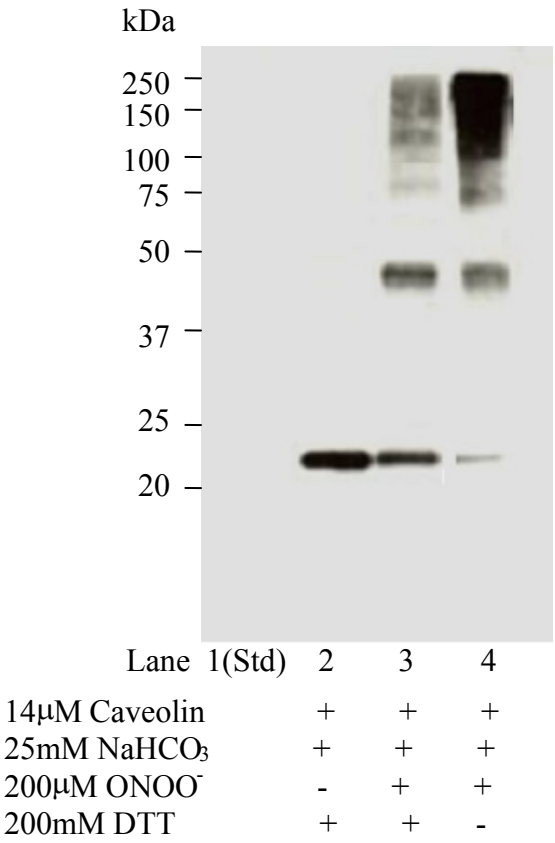

Figure 33. Analysis of the effect of dithiothreitol (DTT) in caveolin-1 exposed to peroxynitrite by SDS-PAGE followed by western blotting with anti-caveolin monoclonal antibody

4.e.2 Discussion

Peroxynitrite is a strong oxidant and can directly oxidize sulfhydryl groups to disulfides.[52] As we could observe the oligomer formation of caveolin-1 with the reaction of peroxynitrite, we analyzed the reducing effect of dithiothreitol using SDS-PAGE followed by western blotting probed with anti-caveolin monoclonal antibody.

Dithiothreitol-mediated reduction of oxidized thiols permitted determination of the reversibility of such oxidation processes.[47]

$$RSSR + \underset{DTT}{(CHOH\text{-}CH_2\text{-}SH)_2} \longrightarrow 2RSH + (CHOH\text{-}CH_2\text{-}S)_2$$

Figure 33, lane 2 shows that without any reaction with peroxynitrite caveolin-1 exists as a monomer at 22kDa. Lane 3 clearly shows that caveolin-1 forms dimer at 44kDa and oligomer between 88 to 250kDa upon the addition of peroxynitrite (200μM). The only difference in this sample from the sample in lane 2 is the exposure of caveolin-1 to 200μM of peroxynitrite. This result confirms that the peroxynitrite reaction with caveolin-1 forms covalent bonds, which cannot be reduced by DTT. The dimer and oligomer formation of caveolin-1 shows the oxidation of caveolin-1 with the reaction of peroxynitrite. Oxidation of caveolin may form protein crosslink due to disulfide bond formation. These disulfide bonds cannot be reduced by DTT due to steric interference, which could reduce the accessibility of DTT to reduce some disulfide bonds formed as a result of caveolin-1 exposure to peroxynitrite. DTT was not added to the sample loaded in

lane 4, which is caveolin-1 (14μM) exposed to 200μM of peroxynitrite. The density of the band at 22kDa in lane 4 is much less than that of lane 3 and this lane shows dense oligomer. This result confirmed that DTT could reduce about 70% of the disulfide bonds formed.

4.e.3 Conclusion

The effect of dithiothreitol in caveolin-1 exposed to peroxynitrite was investigated. This permits the determination of reversibility of peroxynitrite mediated oxidation processes. The result of this experiment confirmed that there are non-reversible bond formed upon the exposure of caveolin-1 to peroxynitrite. These covalent bonds could be disulfide bonds, which are formed as a result of oxidation of sulfydryl groups of caveolin-1 which are not accessible to DTT or dityrosine bond formation.

4.f Detection of dityrosine by fluorometry

4.f.1 Results

Three samples were prepared for detection of dityrosine using spectrofluorometer (Shimadzu RF5000U). Figure 34 shows the fluorescence spectrum of Sample A, which was prepared by adding 25mM $NaHCO_3$ and peroxynitrite 400μM to caveolin-1 14μM in phosphate buffer and equilibrated for 5 minutes. The fluorescence spectrum of dityrosine was obtained at excitation wavelength 283nm and emission wavelength 410nm.[63] Figure 34, graph A shows a peak at 410nm. Same experiment was done by adding 2% SDS to see whether there is any change of the spectrum by disrupting non-covalent bonds (Sample B). Figure 35 shows that there is no significant change of the excitation spectrum by the addition of 2% SDS. In sample C (control), peroxynitrite 200μM was added to phosphate buffer and equilibrated for 5 minutes followed by caveolin-1 (14μM) addition. Figure 34, graph B shows that there is no peak at 410nm in the excitation spectrum for the control experiment.

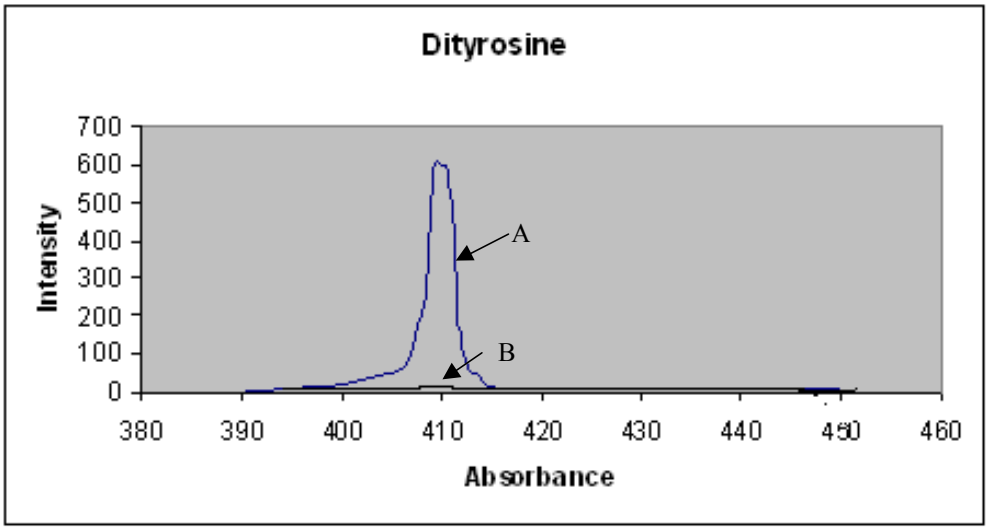

Figure 34. Detection of dityrosine by fluorometry. A. Caveolin (14μM) in phosphate buffer pH 7.5, $ONOO^-$ 400μM $NaHCO_3$ 25mM. B. $ONOO^-$ 400μM in phosphate buffer (pH 7.5) equilibrated for 5 minutes, Caveolin 14μM, $NaHCO_3$ 25mM, Fluorescence spectrum of dityrosine was obtained at excitation λ= 283nm and emission λ= 410nm.

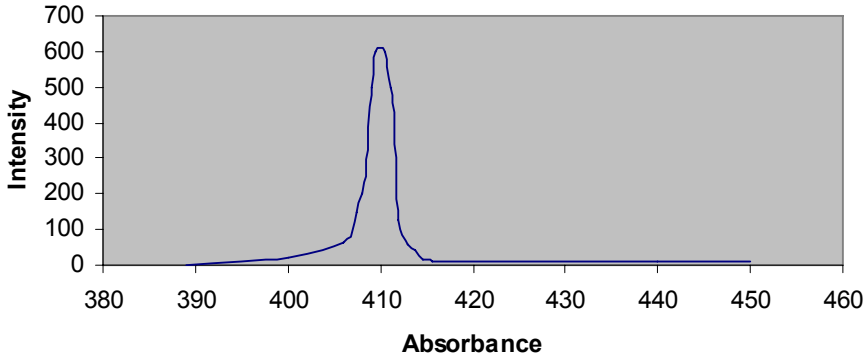

Figure 35. Detection of dityrosine by fluorometry. Caveolin 14μM in phosphate buffer pH 7.5, ONOO- 400μM $NaHCO_3$ 25mM and 2% SDS. Fluorescence spectrum of dityrosine was obtained at excitation λ= 283nm and emission λ= 410nm.

4.f.2 Discussion

Peroxynitrite reaction with tyrosine can form nitrotyrosine as well as dityrosines.[61] A covalent cross-link between two proximal tyrosines forms a dityrosine. Dityrosine cross-linking has been detected in human atherosclerotic plaques or Alzheimer diseased brains.[62,63] Caveolin-1 protein levels are up regulated by two-fold in AD brains, compared to age-matched control brains.[19] We investigated the dityrosine formation due to the exposure of caveolin-1 to peroxynitrite 400μM under the physiological conditions

Fluorescence spectrum of dityrosine was obtained at excitation wavelength 283nm and emission wavelength 410nm. Dityrosine peak was observed at 410nm (Figure 34, graph A), confirming the formation of dityrosine when exposing caveolin-1 to peroxynitrite. In the control experiment, peroxynitrite 200μM was added to phosphate buffer and equilibrated for 5 minutes followed by addition of caveolin-1 (14μM). No peak for dityrosine was observed at 410nm in the emission spectrum for control experiment.

This result confirmed dityrosine is formed as a result of peroxynitrite mediated oxidation of caveolin-1. Dityrosine linkage can occur intramolecularly (among two tyrosine residues in the same molecule) or intermolecularly (between two molecules). Intermolecular dityrosine bridging leads to a high molecular weight product, which could be one of the reasons for caveolin-1 oligomer formation.

4.f.3 Conclusion

This result confirms the formation of dityrosine when caveolin-1 is exposed to peroxynitrite. 3,3'-Dityrosine bond may facilitate the conversion of monomeric caveolin-1 into higher molecular mass oligomers. This covalent link would enhance the structural integrity of caveolin-1 oligomer and confer resistance to denaturing agents such as DTT and SDS. The dityrosine linkage is associated with insoluble and elastic properties of proteins that may lead to several pathological conditions.

4.g Prediction of caveolin-1 structure

4.g.1 Results

Figure 36 shows the front view of the predicted structure of caveolin-1. Locations of tyrosine residues in figure 36 are indicated by red color. Figure 37 shows the back view of the predicted structure of caveolin-1 and locations of tyrosine residues in figure 37 are indicated by red color.

Caveolin-1 consists of 178 amino acids, including 9 tyrosines, which are Tyr^{6}, Tyr^{14}, Tyr^{25}, Tyr^{42}, Tyr^{97}, Tyr^{100}, Tyr^{118}, Tyr^{148} and Tyr^{151}. Figure 36 shows that 8 tyrosine residues (Tyr^{6}, Tyr^{14}, Tyr^{25}, Tyr^{42}, Tyr^{97}, Tyr^{100}, Tyr^{148} and Tyr^{151}) are exposed to solvent phase in the front view. Figure 37 shows Tyr^{6}, Tyr^{14}, Tyr^{25}, Tyr^{42} and Tyr^{100} residues are exposed to solvent phase from the back view of the caveolin-1 structure. Interestingly, Tyr^{118} is not exposed to the solvent phase either from the front view or back view of the predicted caveolin structure as shown in figures 36 and figure 37.

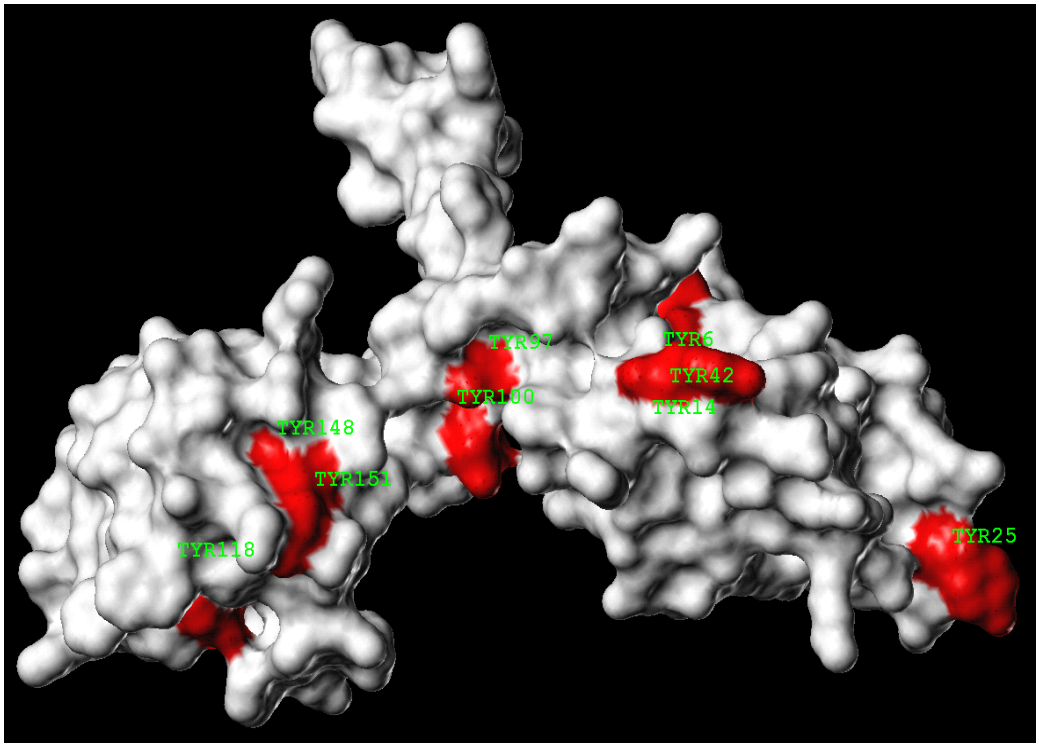

Figure 36. Predicted structure of caveolin-1 (front view). Locations of tyrosine residues are indicated by red color (courtesy of Dr. Gerald Lushington)

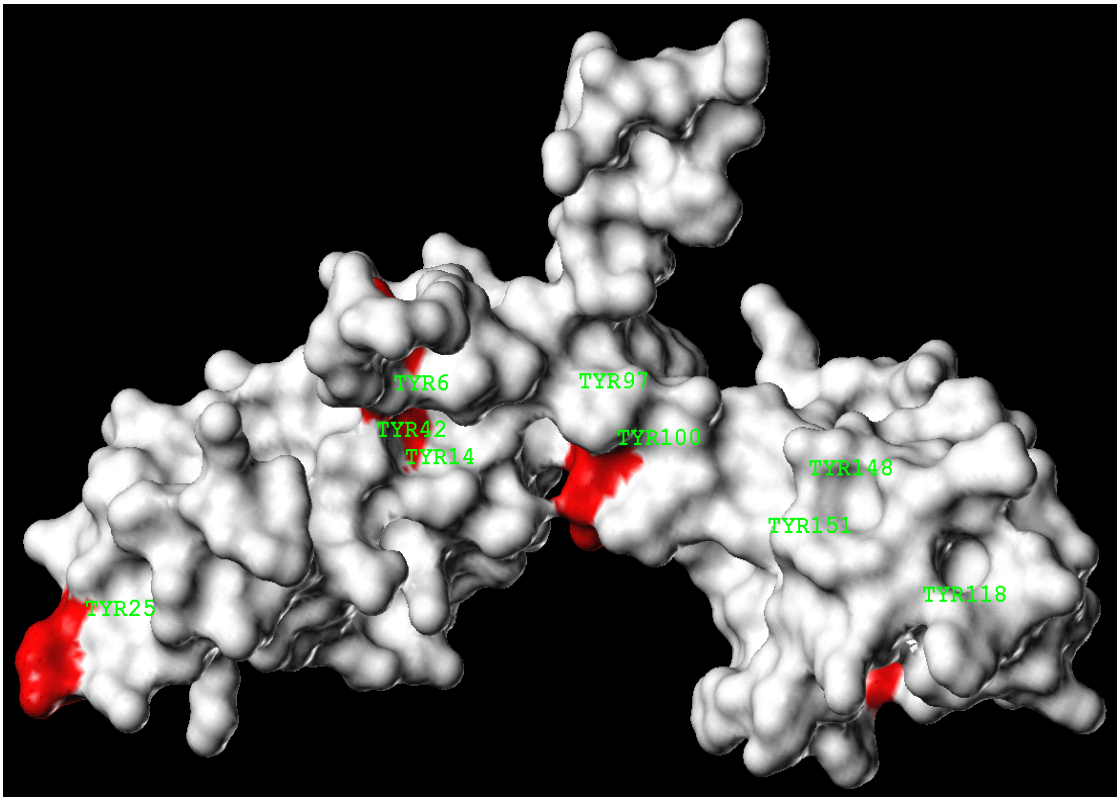

Figure 37. Predicted structure of caveolin-1 (back view). Locations of tyrosine residues are indicated by red color ((courtesy of Dr. Gerald Lushington)

4.g.2 Discussion

An understanding of the 3-D structure of a protein is required for successful interpretation of post-translational modifications. NMR based methods and X-ray diffraction have been successfully used to determine protein structure. However, the number of structurally characterized proteins is much less than the number of known protein sequences. The 3-D structure of caveolin-1 is unknown. To generate a 3-D model of caveolin-1 from its amino acid sequence comparative modeling is used.

We could obtain about 60% sequence coverage frequently when we analyze caveolin-1 for post-translational modifications using ESI-MS. It was difficult to recover the peptide LSALFGIPMALIWGIYFAILSFLHIWAVVPCIK (residues 142-147) which is located in the hydrophobic domain of caveolin-1 and contains Tyr^{118}.

Figures 36 and 37 show that 5 tyrosine residues (Tyr^{6}, Tyr^{14}, Tyr^{25}, Tyr^{42} and Tyr^{100}) are exposed to solvent phase from the front view and the back view, which could be easily accessible to reactive oxygen species or reactive nitrogen species such as peroxynitrite. However, ESI/MS/MS analysis in our study confirms that peroxynitrite was able to selectively nitrate only Tyr^{6} and Tyr^{14}.

4.g.3 Conclusion

Caveolin-1 is one of the vast majorities of proteins that has an amino acid sequence with unknown 3-D crystal structure. An experimentally solved template 3-D structure that has a significant amino acid sequence homology to the target sequence was used to predict unknown caveolin-1 structure. It is shown that peroxynitrite can selectively form 3-nitrotyrosine only at the residues Tyr^{6} and Tyr^{14} from the ESI/MS/MS analysis in this study. This result is consistent with the predicted caveolin-1 structure as it shows Tyr^{6} and Tyr^{14} residues are exposed to the solvent phase from both the front and back views of the predicted structure of caveolin-1.

References

1. Schelgel, A., Volonte, D., Engelman, J.A., Galbiati, F., Mehta, P., Zhang, X., Scherer, P.E., Lisanti, M.P.; Crowded little caves: Structure and function of caveolae, *Cell Signal.* **1998**, 10, 457-463
2. Okamoto, T., Schlegel, A., Scherer, P.E., Lisanti, M.P.; Caveolins, a family of scaffolding proteins for organizing " preassembled signaling complexes at the plasma membrane", *J. Biol. Chem.* **1998**, 273, 5419-5422
3. Glenny, G.R., Zokas, L.; Novel tyrosine kinase substrates from Rous Sarcoma virus transformed cells are present in the membrane skeleton, *J.Biol.Chem.* **1989,** 2401-2408
4. Parton, R.G.; Life without caveolae, *Science* **2001**, 293, 2404-2405
5. Scherer, P. E., Okamoto, T., Chun, M., Nishimoto, I., Lodish, H.F., Lisanti, M.P.; Identification, *sequence, and expression of caveolin-2 defines a caveolin gene family, Proc. Natl. Acad. Sci.* **1996**, 93, 131-135
6. Tang, Z., Scherer, P. E., Okamoto, T., Song,K., Chu, C., Kohtz, D.S., Nishimoto, I., Lodish, H.F., Lisanti, M.P.; Molecular cloning of caveolin-3, a novel member of the caveolin gene family expressed predominantly in muscle, *J. Biol. Chem.* **1996**, 271, 2255-2261
7. Schelgel, A., Lisanti, M.P.; The caveolin triad: caveolae biogenesis, cholesterol trafficking, and signal transduction, *Cytokine Growth F. R.* **2001,** 12, 41-51

8. Scherer, P.E., Tang, Z., Chun, M., Sargiacomo, M., Lodish, H.F., Lisanti, M.P.; Caveolin isoforms differ in their N-terminal protein sequence and subcellular distribution, *J. Biol. Chem*. **1995**, 270, 16395-16401
9. Murata, M., Peranene, J., Schreiner, R., Wieland, F., Kurzchalia, T.V., Simons, K.; VIP21/caveolin is a cholesterol-binding protein, *Proc. Natl. Acad. Sci.* **1995**, 92, 10339-10343
10. Sargiacomo, M., Scherer, P. E., Tang., Z., Kubler, E., Song, K.S., Sanders, M. C., Lisanti, M.P.; Oligomeric structure of caveolin: implications for caveolae membrane organization, *Proc. Natl. Acad. Sci.* **1995**, 92, 9407-9411
11. Li, S., Song, K.S., Koh, S.S., Kikuchi, A., Lisanti, M.P.; Baculovirus-based expression of mammalian caveolin in Sf21 insect cells, *J. Biol. Chem*. **1996,** 271, 28647-28654
12. Song, K.S., Li, S., Okamoto, T., Quilliam, L.A., Sargiacomo, M., Lisanti, M.P., Co-purification and direct interaction of Ras with caveolin, an integral membrane protein of caveolae microdomains, *J. Biol. Chem.* **1996**, 271, 9690-969740
13. Schengwen, L., Couet, J., Lisanti, M.P., Src Tyrosine Kinases, Gα subunits, and H-Ras share a common membrane-anchored scaffolding protein, caveolin, *J. Biol. Chem.* **1998,** 271, 29182-29190
14. Schelgel, A., Pestell, R.G., Lisanti, M.P.; Caveolins in cholesterol trafficking and signal transduction: implications for human disease, *Front. Biosci*. **2000**, 5, d929-937

15. Couet, J., Sargiacomo, M., Lisanti, M.P.; Interaction of a receptor tyrosine kinase, EGF-R, with caveolins, *J. Biol. Chem*. **1997**, 272, 30429-30438

16. Sprenger, R, Speijer, D., Back, J. W., Koster, Cg., Pannekoek, H., Horrevoets, A.J.G.; Comparative proteomics of human endothelial cell caveolae and rafts using two-dimensional gel electrophoresis and mass spectrometry, *Electrophoresis*, **2004**, 25, 156-172

17. Razani, B., Woodman, S.E., Lisanti, M.P.; Caveolae: from cell biology to animal physiology, *Pharmacol. Rev*. **2002**, 54, 431-467

18. Razani, B., Combs, T. P., Wang, X.B., Frank, P/G., Park, D.S., Russell, R.G., Li., M., Tang, B., Jelicks, L.A., Scherer, P.E., Lisanti, M.P.; Caveolin-1 deficient mice are lean, resistant to diet induced obesity, and show hypertriglyceridemia with adipocyte abnormalities, *J. Biol. Chem*. **2002**, 277, 8635-8647

19. Gaudreault, S.B., Dea, D., Poirier, J.; Increased caveolin-1 expression in Alzheimer's disease brain, *Neurol. Aging*, **2004**, 25, 753-779.

20. Ishiki, M., Anderson, R.G.W.; Function of caveolae in Ca^{2+}entry and Ca^{2+} dependent signal transduction, *Traffic* **2003**: 4: 717-723

21. Razani, B., Schlegel, A., Liu, J., Lisanti, M.P.; Caveolin-1, a putative tumour suppressor gene, *Biochem. Soc. T*. **2001**, 29, 494-499

22. Smart, E.J., Gregory, A.G., Mcniven, M.A., Sessa, W.C., Engleman, J.A., Scherer, P.E., Okamoto, T., Lisanti, M.P.; Caveolins, Liquid-ordered domains, and signal transduction, *Mol. Cell. Biol*.**1999**, 19, 7289-7304

23. Engleman, J.A., Zhang, X.L., Lisanti, M.P.; Genes encoding human caveolin-1 & 2 are co-localized to the D7S522 locus (7q31.1), a known fragile site (FRA7G) that is frequently deleted in human cancers, *FEBS Let*. **1998**, 436, 403-410

24. Campbell, L., Gumbleton, M., Ritchie, K., Caveolae and the caveolins in human disease, *Adv. Drug Deliver. Rev.,* **2001**, 49, 325-335

25. Razani, B., Schlegel, A., Lisanti, M.P.; Caveolin proteins in signaling, oncogenic transformation and muscular dystrophy, *J. Cell. Sci.* **2000,** 113, 2103-2109

26. Garcia-Gardena, G., Martasek, P., Masters, B.S.S., Skidd, P.M., Couet, J., Schengwen, L., Lisanti, M.P., Sessa, W. C.; Dissecting the interaction between Nitric oxide synthase (NOS) and caveolin, *J. Biol. Chem*. **1997**, 272, 25437-25440

27. Felley-Bosco, E., Bender, F., Quenst, A.F.G.; Caveolin-1 mediated post-transcriptional regulation of inducible nitric oxide synthase in human colon carcinoma cells, *Biol. Res.* **2002**, 35, 169-176

28. Sato, Y., Sagami, I, Shimizu, T.; Identification of caveolin-1 interacting sites in neuronal nitric-oxide synthase, *J. Biol. Chem*. **2004**, 279, 8827-8836

29. Razani, B., Engelman, J.A., Wang, X.B., Schubert, W., Zhang, X.L., Marks, C.B., Macaluso, F., Russell,R.G., Li, M., Pestell, T.G., Di Vizio, D., Hou, H., Kneitz, B., Lagaud, G., Christ, G.J., Edelmann, W., Lisanti, M.P.; Caveolin-1

null mice are viable but show evidence of hyperproliferative and vascular abnormalities, *J. Biol. Chem.* **2001**, 276, 38121-38178

30. Ferron, O., Dessy, C., Moniotte, S., Desager, J., Balligand L.; Hypercholesterolemia decreases nitric oxide production by promoting the interaction of caveolin and endothelial nitric oxide synthase, *J. Clin. Invest*. **1999**, 103, 897-905
31. Fulton, D., Gratton, J., Sessa, W.C.; Post-translational control of endothelial nitric oxide synthase: why isn't calcium/calmodulin enough, J. Pharmacol. Exp. Ther. **2002**, 299, 818-824
32. Couet, J., Li, S., Okamoto, T. Ikezu, T., Lisanti, M.P.; Identification of peptide and protein ligands for the caveolin-scaffolding domain, *J. Biol. Chem*. **1997**, 272, 6525-6533
33. Englemen, J.A., Zhang, X., Galbiati, F., Volonte, D., Sotgia, F., Pestell, R.G., Minett, C., Scherer, P.E., Okamoto, T., Lisanti, M.P.; Molecular genetics of the caveolin gene family: implications of human cancers, diabetes, Alzheimer disease, Muscular Dystrophy. *Am. J. Hum. Genet.* **1998**, 63, 1578-1587
34. Yan, S.B., Grinnell, B.W., Wold, F.; Post-translational modifications of proteins: some problems left to solve, *Trends Biochem. Sci.* **1989**, 264-268
35. Mann, M., Jensen, O.; Proteomic analysis of post-translational modifications, *Nat. Biotech.* **2003**, 21, 255-261

36. Schlegel, A., Arvan, P., Lisanti, M.P.; Caveolin-1 binding to endoplasmic reticulum membranes and entry into the regulated secretory pathway are regulated by serine phosphorylation, *J. Biol. Chem*. **2001,** 276, 4398-4408

37. Fielding, P.F., Chau, P., Liu, D., Spencer, T.A., Fielding, C.J.; Mechanism of platelet-derived growth factor dependent caveolin-1 phosphorylation: relationship to sterol binding and the role of serine-80, *Biochemistry,* **2004**, 43, 2578-2586

38. Schengwen, L., Seitz, R, Lisanti, M.P.; Phosphorylation of caveolin by Src tyrosine kinases, *J. Biol. Chem*. **1996**, 271, 3863-3868

39. Cao, H., Courchesne, W.E., Mastick, C.C.; A phosphotyrosine-dependent protein interaction screen reveals a role for phosphorylation of caveolin-1 on tyrosine-14, *J. Biol. Chem.* **2002**, 277, 8771-8774

40. Vainonen, J.P., Aboulaich, Turkina, M. V., Stralfors, P., Vener A.V.; N-terminal processing and modifications of caveolin-1 in caveolae from human adipocytes, *Bioch. Biophys. Res. Commun*. **2004**, 320, 480-486

41. Parat, M., Fox, P.L.; Palmitoylation of caveolin-1 in endothelial cells is post-translational but irreversible, *J. Biol. Chem*. **2001**, 276, 15776-15782

42. Uittenbogaard, E., Smart, E.J.; Palmitoylation of caveolin-1 is required for cholesterol binding, chaperone complex formation and rapid transport of cholesterol to caveolae, *J. Biol. Chem.* **2000**, 275, 25595-25599

43. Radi, R., Peluffo G., Alvarez, M.N., Naviliat, M., Cayota, A.; Unraveling peroxynitrite formation in biological systems, *Free Radic. Biol. Med*. 2001, 30, 463-488

44. Augusto, O., Bonini, M. G., Amanso, A.M., Linares, E., Santos, C.C., Menezes, S.L.; Nitrogen dioxide and carbonate radical anion: Two emerging radicals in Biology, *Free Rad. Biol. & Med*. **2002**, 32, 842-859

45. Ischiropoulos, H., Zhu, L., Beckman, J.S.; Peroxynitrite formation from macrophage-derived nitric oxide, *Arch. Biochem. Biophys*. **1992**, 298, 446-451

46. Denicola, A., Radi, R.; Peroxynitrite and drug-dependent toxicity, *Toxicology,* **2005**, 208, 273-288

47. Radi, R., Beckman, J.S., Bush, K.M., Freeman, B.A.; Peroxynitrite oxidation of sulfhydryls, *J. Biol. Chem*. **1991**, 266, 4244-4250

48. Beckman, J. S., Beckman, T.W., Chen, J., Marshall, P.A., Freeman, B.A.; Apparent hydroxyl radical production by peroxynitrite: implications for endothelial injury form nitric oxide and superoxide, *Proc. Natl. Acad. Sci*. **1990**, 87, 1620-1624

49. Radi, R.; Peroxynitrite reactions and diffusion in biology, *Chem. Res. Toxicol*. **1998**, 11, 720-721

50. Lymar, S.V., Hurst, J.K.; Rapid reaction between peroxynitrite ion and carbon dioxide: implications for biological activity, *J. Am. Chem. Soc.* **1995**, 117, 8867-8868

51. Tien, M., Berlett, B.S., Levine, R.L., Chock, P.B., Stadtman, E.R.; Peroxynitrite-mediated modification of proteins at physiological carbon dioxide concentration: pH dependence of carbonyl formation, tyrosine nitration, and methionine oxidation, *Proc. Natl. Acad. Sci*., **1999**, 96, 7809-781452.

52. Vesela, A., Wilhelm, J.; The role of carbon dioxide in free radical reactions of the organism, *Physiol. Res*. **2002**, 51, 335-339

53. Illarion V.T., Murad, F.; Protein nitration in cardiovascular diseases, *Pharmacol. Rev*. **2002**, 54, 619-634

54. Gow, A.J., Duran, D., Malcolm, S., Ischiropoulos, H.; Effects of peroxynitrite-induced protein modifications on throsine phosphorylation and degradation, *FEBS Lett*. **1996**, 385, 63-66

55. Mallozi, C., Di Stasi, A.M.M., Minetti, M.; Nitrotyrosine mimics phosphotyrosine binding to the SH2 domain of the src family tyrosine kinase lyn, *Febs Lett*. **2001**, 503, 189-195

56. Macmillan-Crow, L.A., Greendorfer, J.S., Vickers, S.M., Thompson, J. A.; Tyrosine nitration of c-SRC tyrosine kinase in human pancreatic ductal adenocarcinoma, *Arch. Biochem. Biophys.* **2000**, 377, 350-356

57. Ischiropoulos, H.; Biological tyrosine nitration: a pathophysiological function of nitric oxide and reactive oxygen speciens, *Arch. Biochem. Biophys*. **1998**, 356, 1-11

58. Viner, R.I., Ferrington, D.A., Williams, T.D., Bigelow, D.J., Schöneich, C.; Protein modification during biological aging: selective tyrosine nitration of the SERCA2a isoform of the sarcoplasmic reticulum Ca^{2+} ATPase in skeletal muscle, *Biochem. J*. **1999**, 340, 657-669

59. Vliet, A.V., Eiserich, J.P., Kaur, H., Cross, C.E., Halliwell, B.; Nitrotyrosine as a biomarker for reactive nitrogen species, *Methods Enzymol*. **1996**, 269, 175-194

60. Kanski, J., Alterman, M.A., Schöneich, C.; Proteomic identification of age-dependent protein nitration in rat skeletal muscle*, Free Rad. Biol. Med*. **2001**, 35, 1229-1239

61. Pfeiffer, S., Schmidt, K., Mayer, B.; Dityrosine formation outcompetes tyrosine nitration at low steady-state concentrations of peroxynitrite, *J. Biol. Chem*. **2000**, 275, 6346-6352

62. Balasubramanian, D., Kanwar, R.; Molecular pathology of dityrosine cross-links in proteins: structural and functional analysis of four proteins, *Mol. Cell. Biochem*. **2002**, 234/235, 27-38

63. Reynolds, M.R., Berry, R.W., Binder, L. I.; Site-specific nitration and oxidative dityrosine bridging of the τ protein by peroxynitrite: Implications of Alzheimer's disease, *Biochemistry*, **2005**, 44, 1690-1700

64. Stadtman, E.R., Moskovits, J., Levine, R.L.; Oxidation of methionine residues of proteins: biological consequences, *Antioxid. Redox signaling,* **2003**, 5, 577-582

65. Hoshi, T., Heinemann, S.H.; Regulation of cell function by methionine oxidation and reduction, *J. Physiol*. **2001**, 531, 1-11

66. Schöneich, C.; Methionine oxidation by reactive oxygen species: reaction mechanisms and relevance to Alzheimer's disease, *Biochim. Biiophys. Acta* **2005**, 1703, 111-119

67. Viner, R. I., Huhmer, A.F.R., Bigelow, D.J. Schöneich, C.; The oxidative inactivation of sarcoplasmic reticulum Ca^{2+}-ATPase by peroxynitrite, *Free Rad. Res* **1999**, 24, 243-259

68. Kuhn, D.M., Aretha, C.W., Geddes, T.J.; Peroxynitrite inactivation of tyrosine hydroxylase: mediation by sulfhydryl oxidation, not tyrosine nitration, *J. Neurosci*. **1999**, 19, 10289-10294

69. Sharov, V.S., Galeva, N.A., Knysushko, T, Bigelow, D.J., Williams, T.D., Schoneich, C.; Two-dimensional separation of the membrane protein sarcoplasmic reticulum Ca-ATPase for high performance liquid chromatography-tandem mass spectrometry analysis of posttranslational protein modifications, *Anal. Biochem*. **2002**, 308, 328-335

70. Yates, J.R.; Mass spectrometry and the age of the proteome, *J. Mass Spectrom*. **1998**, 33, 1-19

71. Gerber, S.A., Rush, J., Stemman, O., Kirshner, M., Gygi, S.P.; Absolute quantification of proteins and phosphoproteins from cell lysages by tandem ms, *Proc. Nat. Acad. Sci.* **2003**, 100, 6940-6945

72. Hoffmann, E., Stroobant, V.; Electrospray, *In Mass spectrometry principles and applications*, 2nd Ed. John Wiley, Chichester, **2001**, 33-44

73. Marina, A., Miguel, A.G., Alber, J.P., Yague, J., Castro, J.A.L., Vazquez, J.; High-sensitivity analysis and sequencing of peptides and proteins by quadrupole ion-trap mass spectrometry, *J. Mass Spectrom*. **1999**, 34, 17-27

74. Pryor, W.A., Cuerto, X.J., Koppenol, W.H., Ngu-Schwemlein, M., Squadrito, G.I., Uppu, P.L., Uppu, R.M.; A practical method for preparing peroxynitrite solutions of low ionic strength and free of hydrogen peroxide, *Free Radical Biol. Med*. **1995**, 18, 75-83

75. Eyber, F.; Structure determination using NMR data, *Analusis* **1993**, 21, M27-M28

76. Jardetzky, O., Wade-Jardetzky, N.G.; Comparison of protein structures by high-resolution solid state and solution NMR, *FEBS Lett.* **1980**, 110, 133-135

77. Schwede, T., Kopp, J., Guex, N., and Peitsch, M.C.; SWISS-MODEL: an automated protein homology-modeling server, *Nucleic Acids Research.* **2003**, 31**:** 3381-3385.

78. arti-Renom, M.A., Stuart, A., Fiser, A., Sánchez, R., Melo, F., Sali, A.; Comparative protein structure modeling of genes and genomes, *Annu. Rev. Biophys. Biomol. Struct.* **2000**, 29, 291-325.

79. Bateman, A., Coin, L., Durbin, R., Finn, R.D., Hollich, V., Griffiths-Jones, S.,

Khanna, A., Marshall, M., Moxon, S., Sonnhammer, E.L.L., Studholme, D.J., Yeats C., Eddy, S.R.; The Pfam Protein Families *Database, Nucl. Acids Res.* **2004**, Database Issue 32: D138-D141.

80. Jones, D.T.; THREADER : Protein Sequence Threading by Double Dynamic Programming, In: *Computational Methods in Molecular Biology*. Salzberg, S., Searls, D., and Kasif, S., Eds., Elsevier Science, New York, **1998**, Chapter 13.

81. McGuffin, L.J., Bryson, K., Jones, D.T.; The PSIPRED protein structure prediction server. *Bioinformatics*. **2000**; 16**,** 404-405.

82. Sahasrabudhe, P.V., Tejero, R., Kitao, S., Furuichi, Y., Montelione, G.T.; Homology modeling of an RNP domain from a human RNA-binding protein: homology-constrained energy optimization provides a criterion for distinguishing potential sequence alignments., *Proteins: Struct. Funct. Genetics*, **1998**, 33**:** 558-566.

83. Oubridge, C., Ito, N., Evans, P.R., Teo, C.H., Nagai, K.; Crystal structure at 1.92 Å resolution of the RNA-binding domain of the U1A spliceosomal protein complexed with an RNA hairpin, *Nature.* **1994**, 372, 432-438.

84. Sliz, P., Engelmann, R., Hengstenberg, W., Pai, E.F.; The structure of enzyme II Alactose from Lactococcus lactis reveals a new fold and points to possible interactions of a multicomponent system, *Structure* **1997,** 5**,** 775-788.

85. Lee, J.Y., Min, K., Cha, H., Shin, D.H., Hwang, K.Y., Suh, S.W.; Rice non-specific lipid transfer protein: the 1.6 Å crystal structure in the unliganded state reveals a small hydrophobic cavity, *J. Mol. Biol.* **1998**, 276**,** 437-448.

86. Story, R.M., Weber, I.T., Steitz, T.A.; The structure of the *E. coli* recA protein monomer and polymer, *Nature* **1992**, 355**,** 318-325.

87. MacKerell, A.D. Jr., Brooks, B., Brooks, C.L. III, Nilsson, L., Roux, B., Won, Y., and Karplus, M. CHARMM: The Energy Function and Its Parameterization with an Overview of the Program, In *The Encyclopedia of Computational Chemistry*, Schleyer, P.V.R., Schreiner, P.R., Allinger, N.L., Clark, T., Gasteiger, J., Kollman, P.A., Schaefer, H.F. III.; Eds. John Wiley & Sons, Chichester, **1998,** 1, 271-277.

88. Simons, K., Ikonen, E.; Functional rafts in cell membranes, *Nature* 1997, 387, 569-572.

89. SYBL 7.0, The Tripos Associates, St. Louis, MO, **2004**

90. Frangioni, J.V., Neel, B.G.; Solubilization and purification of enzymatically active glutathione S-transferase (pGEX) fusion proteins, *Anal. Biochem* **1993**,. 210, 179-187

91. Shevchenko, A., Wilm, M., Vorm, O., Mann, M.; Mass spectrometric sequencing of proteins from silver-stained polyactrylamide gels, **1996** *Anal. Chem.* 68, 850-858.

92. Beckman, J.S., Koppenol, W.H.; Nitric oxide, superoxide, and peroxynitrite: the good, the bad, and the ugly, *Am. J. Physiol*. **1996**, 271, C1424-1437.

93. Lymar, S.V, Jiang, Q., Hurst, J.K.; Mechanism of carbon dioxide-catalyzed oxidation of tyrosine by peroxynitrite, *Biochemistry*. **1996,** 35, 7855-7861

94. Pryor, W.A., Squadrito, G.L.; The chemistry of peroxynitrite: a product from the reaction of nitric oxide with superoxide, *Am. J. Physiol*. **1995**, 268, L697-L722

95. Augusto, O, Gatti, R.M., Radi, R.; Spin-trapping studies of peroxynitrite decompostion and of 3-morpholinosydnonimine N-ethylcarbamide autooxidation: direct evidence for metal independent formation of free radical intermediates, *Arch. Biochem. Biophys*. **1994**, 310, 118-25

96. Liu, P., Rudick, M., Anderson, G.W.; Multiple functions of caveolin-1, , *J. Biol. Chem.,* **2002** 277, 41295-41298

97. Smart, E.J., Ying, Y., Donzell, W.C., Anderson, R.G.W., A role for caveolin in transport of cholesterol from endoplasmic reticulum to plasma membrane, *J. Biol. Chem*. **1996**, 271, 29427-29435

98. Uittenbogaard, A., Smart, E.J.; Palmitoylation of caveolin-1 is required for cholesterol binding, chaperone complex formation, and rapid transport of cholesterol to caveolae, *J. Biol. Chem.* **2000**, 275, 25595-25599

99. Berlett, B.S., Stadtman, E.R.; Protein oxidation and aging, disease, and oxidative stress, , *J. Biol.Chem*. **1997**, 272, 20313-20316

100. Kong, S.K., Yim, M.B., Stadtman, E.R., Chock, P.B.; Peroxynitrite disables the tyrosine phosphorylation regulatory mechanism: lymphocyte-specific tyrosine kinase fails to phosphorylate nitrated cdc2 (6-2) NH2 peptide. *Proc. Natl. Acad. Sci*. **1996**, 93, 3377-3382